

**Numerical modelling of die filling and
compaction in pharmaceutical tableting process**

Ryoichi Furukawa

Doshisha University

2017

Contents

Chapter 1 Introduction.....	1
1.1 Motivation and objectives.....	2
1.2 Review of previous works.....	8
1.2.1 Numerical simulation of calcium carbonate.....	8
1.2.2 Modelling of granules.....	9
1.2.3 Die filling behaviour.....	10
1.2.4 Closed die compaction	11
1.3 Thesis structure	16
References	18
Chapter 2 Effect of surface properties of calcium carbonate on aggregation process ...	27
2.1 Introduction.....	28
2.2 Simulation details.....	30
2.3 Results and discussion	36
2.3.1 Density profile and orientational angle of water	36
2.3.2 Charge density on the crystal surface.....	42
2.3.3 Self-diffusion coefficient and dielectric constant.....	46
2.3.4 Grain boundary energy in aggregation process	49
2.4 Conclusion	51
References.....	52
Chapter 3 Formation mechanism of spindle-shaped calcium carbonate particles in the solution using cluster-moving Monte Carlo simulation	56
3.2 Simulation details.....	58
3.3 Results and discussion	62
3.3.1 Formation of spindle-shape CaCO ₃ by cluster-moving MC simulation.....	62
3.3.2 Analysis of point charges in the clusters	66
3.4 Conclusion	67
References.....	69
Chapter 4 DEM modelling of granule rearrangement and fracture behaviours during a closed-die compaction	71

4.1 Introduction.....	72
4.2 Materials and methods	74
4.2.1. Materials	74
4.2.2. Granulation procedure	74
4.2.3. Characterization of D-mannitol powder and granules.....	75
4.2.4. DEM simulation method	76
4.2.5. Simulation procedure of uniaxial compression and closed-die compaction .	78
4.3 Results and discussion	80
4.3.1 Characterization of the tested granule	80
4.3.2 Comparison between experimental and DEM simulated uniaxial compression tests of a granule	81
4.3.3 DEM modelling of granular bed compression	85
4.4 Conclusion	92
References.....	93

Chapter 5 Size-induced segregation during pharmaceutical particle die filling assessed by response surface methodology using discrete element method..... 96

5.1 Introduction.....	97
5.2 Materials and methods	99
5.2.1. Filling experiments	99
5.2.2. Calibration of DEM parameters	102
5.2.3. DEM simulations.....	103
5.2.4. Quantification of segregation of binary particle mixtures.....	105
5.3 Results and discussion	107
5.3.1 Material parameter calibration for DEM simulations	107
5.3.2 Comparison between experimental and simulated NONPAREIL [®] particle flow behaviours	109
5.3.3 Segregation of binary particle mixtures.....	113
5.4 Conclusion	122
References.....	123

Chapter 6 Numerical evaluation of the capping tendency of microcrystalline cellulose tablets during a diametrical compression test..... 126

6.1 Introduction.....	127
6.2 Materials and Methods.....	130
6.2.1. Materials	130

6.2.2. Tableting and diametrical compression testing.....	130
6.2.3. Evaluation of the capping tendency.....	131
6.2.4. Numerical simulation	133
6.3 Results and discussion	138
6.3.1. Compaction and strength test of microcrystalline cellulose tablets	138
6.3.2. Calibration of the material parameters of the DPC model	140
6.3.3. FEM results of the tablet thickness and the density distribution.....	142
6.3.4. Estimation of the capping tendency during the diametrical compression test via the actively yielding (AC YIELD) output of ABAQUS.....	146
6.4 Conclusion	154
References.....	155
Chapter 7 Concluding remarks	159
List of publications	164
Acknowledgements	166

Chapter 1 Introduction

1.1 Motivation and objectives

The pharmaceutical industry makes efforts to improve the efficiency of manufacturing processes and quality of drug products to provide reliable products to patients. Against the background of accelerating development of first-in-class and best-in-class drugs, gaining a comprehensive understanding of manufacturing processes assumed more importance than ever before. Developing the formulation of drug products and transferring a production process from the laboratory scale to the commercial scale are cost- and time-intensive processes; for example, conducting an adequate number of experimental runs involves the cost of active pharmaceutical ingredients (APIs) and manufacturing equipment. The average cost incurred by large companies to launch a new drug to the market is estimated to be approximately \$1.8 billion (Paul et al., 2010). Suresh and Basu (2008) showed that product development cost was about 30–35% of the total cost of developing new drug. Additionally, they reported that reduction of product development costs would potentially be required to prevent the total cost of developing a new drug from increasing. On the other hand, the pharmaceutical industry is subject to considerable regulatory requirements such as the International Conference on Harmonisation of Technical Requirements for Registration of Pharmaceuticals for Human Use (ICH) Q8 guideline. ICH Q8 describes the principles of quality by design (QbD), which focuses on both science-based and risk-based robust process designs to ensure the quality of pharmaceutical dosage forms. ICH Q8 states, “Quality cannot be tested into products; i.e., quality should be built in by design”; thus, it is important to describe how the quality of pharmaceutical dosage forms is ensured or how the quality should be established by covering information obtained from the early to late stages of clinical trials. QbD should be achieved by

linking the Critical Material Attributes (CMAs) and Critical Process Parameters (CPPs) to Critical Quality Attributes (CQAs) through a large number of experimental runs. Thus, understanding and optimising the manufacturing process are essential for reducing the development cost and responding to regulatory changes under the circumstances of pharmaceutical companies.

Against the background of increasing in computing power and the optimised coding, numerical simulations have gained attention as a means to identify the key process parameters and to reduce the time and cost for developing a robust manufacturing process. The use of numerical simulations has increased dramatically (Kremer and Hancock, 2006), and various numerical simulations are commonly performed to improve equipment design, process efficiency, and scale-up procedures (Ketterhagen et al., 2009). Numerical simulations such as molecular dynamics (MD) simulation, Monte Carlo simulation (MC), discrete element method (DEM), computational fluid dynamics (CFD), and finite element method (FEM) are useful for capturing the fundamental physical particle properties and thus for enhancing the understanding of a process (Yu, 2008; Gernaey et al., 2012; Rogers et al., 2013; Rogers and Ierapetritou, 2015). Numerical simulations were used to model the manufacturing processes of oral solid dosage forms, including granulation, drying, sieving, blending, tableting, and film coating, as shown in Figure 1-1.

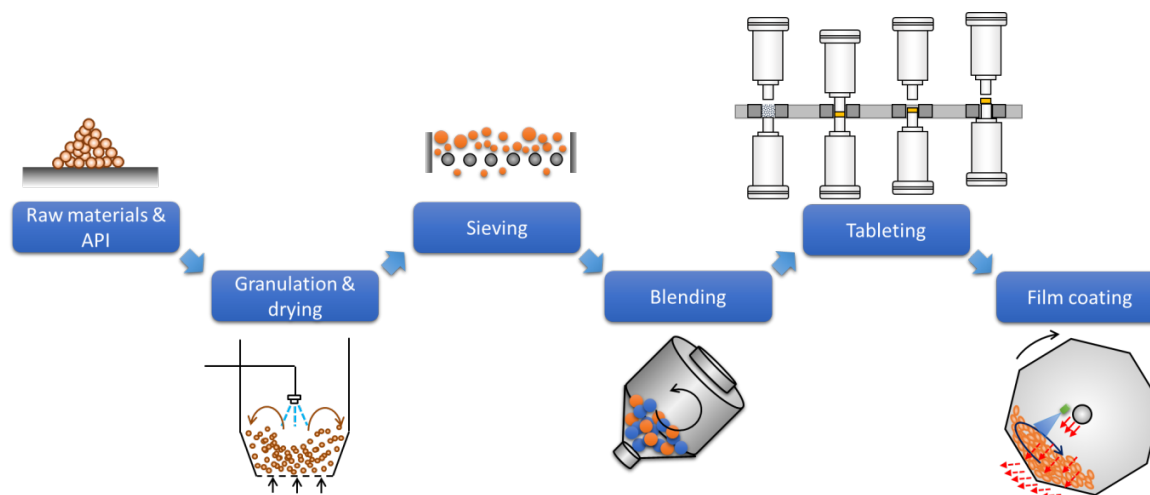


Figure 1-1 Typical manufacturing processes of film coating tablets.

High-shear granulation, fluidised-bed granulation, and roller compaction (dry granulation) are the commonly used granulation methods, and these granulation processes were modelled by numerical simulations. The DEM modelling of high-shear granulation (Terashita et al., 2002; Gantt and Gatzke, 2005; Gantt et al., 2006; Sato et al., 2008; Nakamura et al., 2013; Börner et al., 2016; Chan et al., 2016), fluidised bed granulation (Horio 2003; Deen et al., 2007), and roller compaction (Dec et al., 2003; Cunningham et al., 2010) were conducted using DEM, FEM, and combined CFD-DEM models. Blending and coating processes were also modelled by the DEM. These studies aimed to improve the mixing efficiency by investigating the particle behaviour in a blender (Moakher et al., 2000; Kuo, et al., 2002; Kuo et al., 2005; Lemieux et al., 2007; Lemieux et al. 2008; Alchikh-Sulaiman et al. 2015) and coating pan (Yamane et al., 1995; Kalbag et al., 2008; Dubey et al. 2011; Sahni and Chaudhuri, 2011; Ketterhagen, 2011; Just, et al., 2013; Toschkoff, et al., 2015). Recently, several pharmaceutical companies applied numerical simulations to construct the design space and conduct risk assessment within the QbD framework (Adams et al., 2011; Stocker et al., 2014) and to

gain an understanding of manufacturing processes (Kremer and Hancock, 2006; Ketterhagen et al., 2009; Rantanen and Khinast, 2015). Numerical simulations are being developed to characterise continuous manufacturing systems, which were actively developed in the pharmaceutical industry because of their low cost and scale-up advantage as compared to a batch process. Numerical simulations of continuous manufacturing were performed to understand process dynamics based on residence time distribution (RTD), which is important for determining a batch (Lee et al., 2015). DEM can calculate the RTD of blending process by capturing individual particles, and it is one of the techniques for batch definition (Rogers and Ierapetritou, 2014). Moreover, other continuous manufacturing systems, such as those with twin-screw granulator (Barrasso et al., 2015; Eitzlmayr and Khinast, 2015a, 2015b), sieve mill (Deng et al., 2015), blender (Boukouvala et al., 2013), tableting machine (Boukouvala et al., 2012), and pan coating (Suzzi et al., 2012), were also simulated. As described above, numerical simulations are commonly used for analysing and understanding pharmaceutical manufacturing processes, and they can be used to establish a robust manufacturing process.

Among the manufacturing process of a film coating tablet, the tableting process is considered as the critical or key step to control tablet qualities such as appearance, tensile strength, weight, thickness, content uniformity, assay, and dissolution. Tablets are commercially manufactured by using rotary tableting machines owing to their production efficiency. Tablet manufacture using such machines mainly involves the die filling of powders and granules and the compaction and ejection of the tablets (Figure 1-2). The mixture of granules and excipients in a feeder is supplied from a hopper positioned above the feeder. This mixture flows into the die and is compacted by upper

and lower punches. Following compaction, the upper punch is removed, and the formed tablets are ejected from the die by moving the lower punch. Because tableting parameters and granule properties strongly affect tablet quality, the manufacturing process must be accurately controlled to achieve the desired tablet properties and quality. Therefore, numerical approaches can play an important role in the development of a robust tableting process.

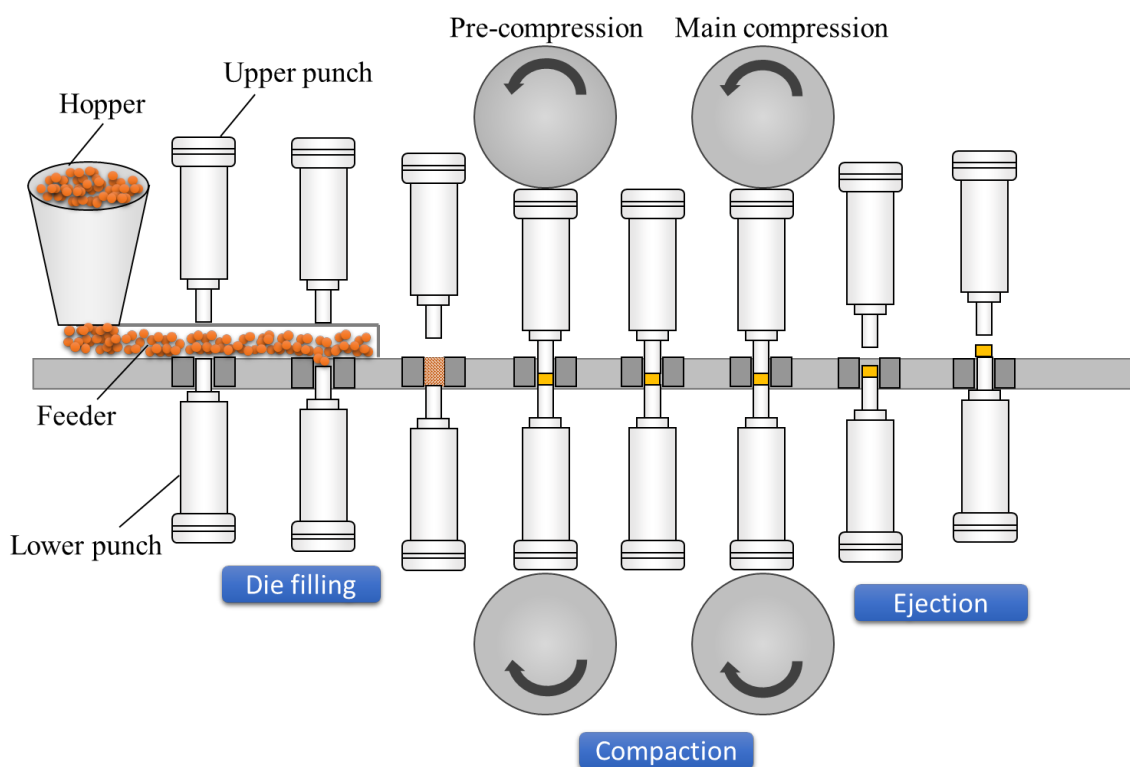


Figure 1-2 Schematic diagram of a rotary tableting machine.

The objective of this thesis is to model a pharmaceutical tableting process by numerical simulations, as illustrated in Figure 1-3. In particular, this thesis is devoted to

- Study the microscopic properties of calcium carbonate/water interfaces by MD
- Investigate the aggregation mechanism of spindle calcium carbonate as a model raw material by MC
- Model the granule and its compaction behaviour by DEM
- Investigate the segregation of binary particles during die filling by DEM
- Develop an evaluation method for the capping tendency observed during a diametrical compression test by FEM

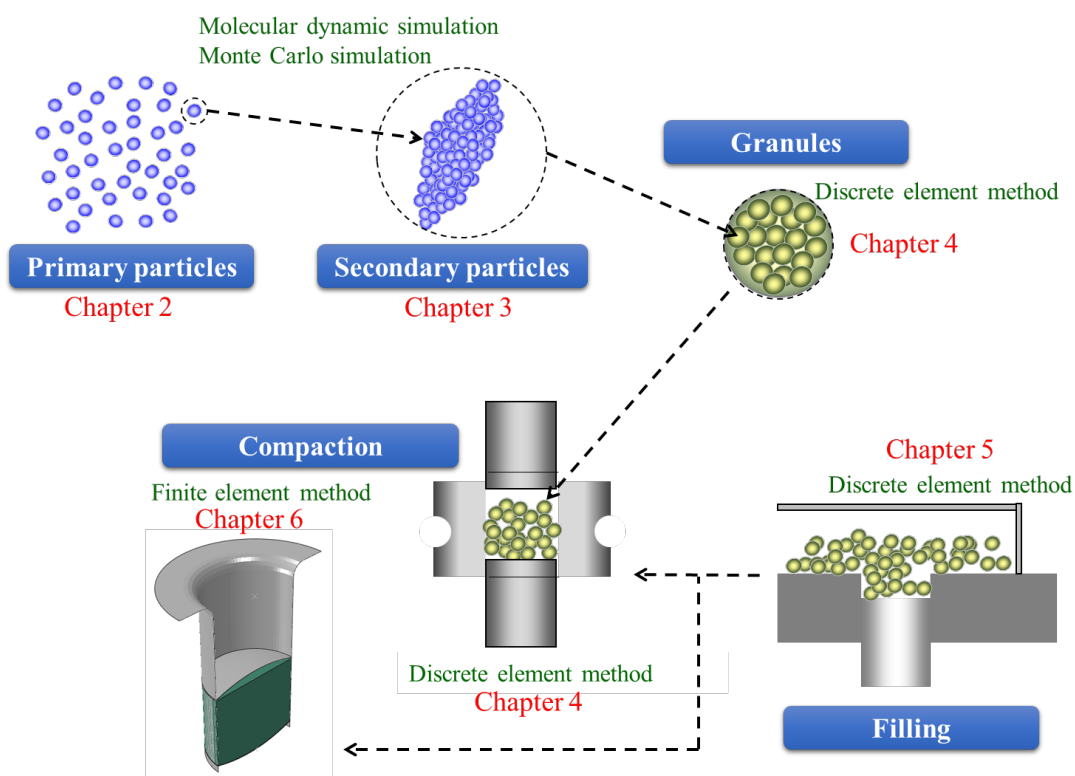


Figure 1-3 Schematic illustration of the structure of this thesis.

1.2 Review of previous works

1.2.1 Numerical simulation of calcium carbonate

Because the lot-to-lot variability of raw materials is an important matter with regard to tablet quality, variability of excipients has been well documented in previous works (Chamarthy, et al., 2009). Understanding the variation in APIs and excipient properties is very important for controlling the CQA and CMA (Fonteyne et al., 2014; Dave et al., 2015). The characteristics and variation of excipients must be controlled strictly to ensure constant quality throughout the lifecycle over the next few decades. Although excipients for pharmaceutical dosage forms are manufactured according to several specifications, some problems in quality and manufacturing still exist. Severe control of excipient properties is essential because the performance of pharmaceutical dosage forms depends on the excipient properties such as morphology, particle size, bulk density, flowability, and compactability. Calcium carbonate (CaCO_3) was chosen as a model excipient because of its particular formation mechanism.

MD simulation is a well-known tool used to investigate molecular behaviour. It enables simulation of nanometre-scale phenomena within nanoseconds by exposing specific crystal faces. In previous researches, MD simulations of solid-liquid interfaces were performed to discuss phenomena such as crystal growth, dehydration, and nucleation (Shinto et al., 1998; Zahn, 2004; Kadota et al., 2007, 2012; Yamanaka et al., 2010). Leeuw et al. (1997, 1998, 1999) simulated the interface between CaCO_3 and water. They investigated the stability of crystal surfaces, solubility, and effects of impurities on crystal growth. Duffy and Harding (2002, 2004a, 2004b) simulated the interfaces between calcite and organic monolayers to study nucleation on organic substrates. In order to identify the aggregation mechanism of spindle CaCO_3 ,

anisotropic phenomena at the molecular level CaCO_3 / water interfaces and solution structure should be considered.

The aggregation structures of colloidal particles with anisotropic properties such as heterogeneous surface charges (Striolo et al., 2002; Liang et al., 2006), various shapes (Qin and Fichthorn, 2003, 2006), dipole moment (Bratko et al., 2002; Sinyagin et al., 2006), and different surface charges (heteroaggregation; Puertas et al., 2001; Kim et al., 2003) were studied experimentally and numerically. Numerical simulations provide development solutions for understanding the microscopic aggregation structure of primary particles.

1.2.2 Modelling of granules

Granulation is one of the most important processes in the production of pharmaceutical tablets. Through granulation, the particle size is increased to improve flowability, prevent segregation, increase the uniformity of drug, and improve the compression properties. Fluidised bed granulation is the common manufacturing method for preparing granules for subsequent tableting process because the granules produced by the fluidised bed granulator have good compactability and plasticity owing to the porous granular structure achieved by spraying a binder solution. During uniaxial compression, a granule deforms elastically in the initial stage until its yield point, and thereafter, it undergoes elastic-plastic deformation until fracture. Detailed understanding of these mechanical properties is essential as these elastic-plastic behaviours play important roles in closed die compaction.

Agglomerates were modelled using DEM to understand how to deform and break granules by applying external forces such as diametrical compression and wall

impact (Subero et al., 1999; Thornton et al., 1999; Kafui and Thornton, 2000; Moreno et al., 2003; Golchert et al., 2004; Thornton et al., 2004; Antonyuk et al., 2006, 2011; Metzger and Glasser, 2012). Thornton et al. (1999, 2004) simulated the fracture of granules that were bonded by the surface force between primary particles. They also investigated the effect of interface energy (Subero et al., 1999), granule morphology (Golchert et al., 2004), and impact angle (Moreno et al., 2003) on granule fracture and impact strength. Antonyuk et al. (2006) modelled granules by connecting primary particles with a spring bond, and if either the normal stress or shear stress reached critical bond strength, the spring bond was broken. The model allowed them to study crack initiation and propagation, and simulate the impact breakage of spherical granules at different velocities. Although the fracture behaviour of the single granule was studied in the past decade, numerical modelling of compaction of dozens of granules consisting of primary particles is necessary to reveal compaction behaviour, including rearrangement and fracture. A detailed review of closed die compaction is provided in *section 1.2.4*.

1.2.3 Die filling behaviour

Die filling is considered a key process to control tablet qualities such as weight variation, content uniformity, and mixture homogeneity. These qualities are severely affected by factors such as the physical properties of powder, turret speed, and feed frame design. Although a comprehensive understanding of powder filling is very important to guarantee tablet qualities, fundamental knowledge of flow behaviour in feed frames is lacking. Numerical researches on die filling were reported in the past decade. Wu (2008a) simulated the simple die filling behaviour of pharmaceutical

particles flowing from a stationary shoe to a moving die. The effect of air on powder flow was investigated by DEM-CFD modelling by Guo et al. (2009). They actively conducted numerical modelling of die filling. With regard to the design of feed frames, Mateo-Ortiz et al. (2014, 2015) investigated particle size segregation inside a feed frame fitted with two paddle wheels and studied the relationship between residence time distribution and forces applied by a feed frame paddles by DEM. Ketterhagen (2015) researched the effect of paddle wheel shape and rotation speed on powder flow pattern, residence time distributions, and weight variability. More recently, Gopireddy (2016) simulated die filling within a lab-scale rotary tableting machine to investigate the effects of tableting conditions and particle properties on mass variation. Size-induced segregation sometimes occurs during long-term tableting because the pharmaceutical powder used for tableting is a mixture of several excipients and API with different size distributions. Such segregation will result in poor content uniformity and weight uniformity, which may lead to failure to meet product specification. Therefore, gaining a fundamental understanding of particle flow during die filling in the feed frame of a rotary tableting machine is essential.

1.2.4 Closed die compaction

Numerical simulation of closed die compaction can be performed using either the discrete approach or the continuum approach. Table 1-1 summarises previous research on the numerical simulation of closed die compaction. DEM, which is the discrete approach, is applied to closed die compaction by using a plastic contact model. DEM can account for the microscopic properties of particle beds and interactions between particles. Thonton and Ning (1998) applied an elastic-plastic deformation

model, and Kruggel-Emden et al. (2007) reviewed several contact models. The plastic contact model was used in numerical studies on pharmaceutical powder compaction to estimate the tensile strength based on the bonding strength between the particles (Koynov et al., 2011; Siiria et al., 2011). Persson and Frenning (2012) introduced a simple modification of the contact model for the elastic–perfectly plastic region in the DEM analysis of confined compression. Following along the lines of Walton and Braun (1986), Mehrotra et al. (2009) carried out the DEM simulation of closed die compaction by using two spring constants K_1 and K_2 for compression and recovery. Thus, there exist some published reports on closed die compaction by DEM. The compaction of granules, including failure, were simulated in a few studies (Martin and Bouvard, 2006; Balakrishnan et al., 2010), but they could not provide an understanding of the failure and rearrangement during compaction. The failure and rearrangement mechanisms are important to form tablets without compaction failure.

FEM, which is the continuum approach, is commonly used in the closed die compaction involving large deformations and strains to simulate the stress, strain, and density distributions inside a tablet. Several types of plasticity models were applied to analyse powder compaction. Among the plasticity models, the Drucker–Prager cap (DPC) model, which consists of a shear failure line and a cap surface, was widely used to study pharmaceutical powder compaction in the past 15 years, as presented in Table 1-1. Previous researches mainly focused on stress and density states inside tablets of various shapes during compaction process. Michrafy et al. (2002) investigated the stress distribution of lactose powder, and Sinka et al. (2003) modelled the density distribution of microcrystalline cellulose powder by using the DPC model. Numerical simulations were validated by comparison with the results obtained using the surface hardness

measurement method (Sinka et al., 2003; Sinha et al., 2010b), X-ray computed tomography (Wu et al., 2005, 2008b), and axial density analysis (Kadiri et al., 2005). Recently, Shang et al. (2013) and Podczeck et al. (2013) evaluated the tensile strength and development of a general equation by FEM. Despite the numerous FEM compaction studies, an evaluation method for capping is yet to be developed. Because capping causes severe quality problems, an evaluation method is essential to prevent it.

Table 1-1. Previous works on the numerical simulations of die compaction and ejection of pharmaceutical powders (1/2)

Authors and reference	Simulation method	Excipients	Summary
Michrafy et al. (2002)	FEM	LAC	Calibration of DPC parameters and modelling the compaction behaviour of LAC
Sinka et al. (2003)	FEM	MCC (Avicel PH-102)	Calibration of DPC parameters and validation of the model and investigation of the effect of wall friction on tablet density
Sinka et al. (2004)	FEM	MCC (Avicel PH-102)	Examination of the relative density distribution of curved-faced tablet under lubricated and unlubricated conditions.
Hassanpour et al. (2004)	DEM	–	Evaluation of the Heckel analysis of bulk powder compression
Wu et al. (2005)	FEM	LAC	Calibration of DPC parameters and simulation of stress distribution during compaction
Kadiri et al. (2005)	FEM	MCC (Vivapur 102)	Investigation of the axial density distribution during uniaxial compaction using FEM and experimental data
Lewis et al. (2005)	FEM, DEM	Starch etc.	Simulations using combined finite and discrete element methods for particle types with irregular shape, sizes, and size distributions
Wu et al. (2008b)	FEM	LAC	Simulation of the stress inside tablets to investigate the capping mechanism
Han et al. (2008)	FEM	MCC (Avicel PH-101)	Compaction simulation of pharmaceutical powder modelled using a density-dependent DPC model
Zavaliangos et al. (2008)	FEM	MCC (Avicel PH-102)	Prediction of temperature evolution in tablet compaction
Mehrotra et al. (2009)	DEM	–	Examination of the effect of cohesion and compression speed on the outcome of the compression process
Sinha et al. (2010a)	FEM	MCC (Avicel PH-102), LAC	Investigation of the sensitivity of DPC model parameters
Sinha et al. (2010b)	FEM	MCC (Avicel PH-102)	Comparison of FEM model predictions with the results of the surface hardness measurement method
Klinzing et al. (2010)	FEM	MCC (Avicel PH-102)	Prediction of the internal distribution of porosity and temperature and comparison of numerical and experimental results (microCT and IR).
Koynov et al. (2011)	DEM	MCC (Avicel PH-102)	Investigation of the bonding in compressed granular assemblies by adopting a hybrid quasi-continuum approach.
Siiria et al. (2011)	DEM	Pellets composed of theophylline anhydrate and MCC (Avicel PH-101)	Development of a model for simulating bond formation during compaction and estimation of the strength of tablets

MCC: Microcrystalline cellulose, LAC: Lactose, L-HPC: Low-substituted hydroxypropyl cellulose, Mg-St: Magnesium-stearate, DPC: Drucker-Prager Cap

Table 1-1. Previous works on the numerical simulations of die compaction and ejection of pharmaceutical powders (2/2)

Authors and reference	Simulation method	Excipients	Summary
Persson and Frenning (2012)	DEM	MCC granules	Analysis of granule rearrangement and plastic deformation by utilizing the truncated Hertzian contact model for elastic–perfectly plastic material
Diarra et al. (2013)	FEM	Mixture of MCC (Avicel PH-200) and Mg-St	Investigation of the influence of visco-elastic phenomena
Kadiri et al. (2013)	FEM	MCC (Vivapur 102)	Compaction simulations of punches of different shapes
Hayashi et al. (2013)	FEM	Mixture of LAC, cornstarch, MCC (Ceolus PH-101), and Mg-St	Analysis of the relation of stress with tensile strength and with disintegration time
Krok et al. (2014)	FEM	Mixture of MCC (Avicel PH-101) and Mg-St	Study of the influence of punch shape on the stress of tablets
Otoguro et al. (2015)	FEM	Mixture of acetoaminophen, LAC, cornstarch, MCC (Ceolus PH-101), L-HPC and Mg-St	Investigation of the effect of residual stress on tensile strength, dissolution, and disintegration time

MCC: Microcrystalline cellulose, LAC: Lactose, L-HPC: Low-substituted hydroxypropyl cellulose, Mg-St: Magnesium-stearate, DPC: Drucker-Prager Cap

1.3 Thesis structure

This thesis consists of seven chapters and a brief summary of the contents is as follows:

Chapter 1 describes the introduction, including the objectives and literature review.

Because a tablet contains several excipients, the control of material properties is an important problem for manufacturing high-quality products. MD and MC simulations can be used for studying material properties at nanometre and micrometre scales. CaCO₃ is chosen as the model excipient, as described in chapters 2 and 3, because it is frequently added to tablet formulations. Chapter 2 describes the MD simulations of calcium carbonate/water interface. These simulations were performed to investigate the electric charge of calcium carbonate surface and the dielectric property of water between different crystal surfaces. The effects of surface properties on an aggregation of primary particles were studied by considering the charge distribution of the CaCO₃ surface. Chapter 3 presents the formation mechanism of non-spherical CaCO₃ determined by introducing the surface charge densities obtained from MD simulation into MC simulation. The primary particles of CaCO₃ were modelled by cubic particles with surface charge densities as obtained from MD simulations. The aggregated structure was analysed using the cluster-moving MC simulation to investigate the mechanism of formation of spindle-shaped clusters from primary particles.

Chapter 4 describes the modelling of single granules consisting of primary particles and the closed die compaction of these granules using DEM. A uniaxial compression test was conducted for single granules to validate the proposed granule

model by comparing the fracture behaviour and force with the experimental results. Then, the validated granule model was used for simulating the closed die compaction behaviour of several granules to understand the rearrangement and fragmentation during compaction.

Chapter 5 presents studies that attempted to gain a fundamental understanding of particle flow and segregation of binary particles during die filling by using DEM. Purified sucrose spherical granules were selected as the model particles, and DEM parameters were calibrated by laboratory experiments. The segregation of binary particle mixtures during a simple filling process with a moving bottom punch was simulated and analysed by using the calibrated DEM parameters with response surface methodology (RSM). The horizontal and vertical position, small particle size, and die velocity were chosen as the input factors of RSM, and their effects on the segregation index were investigated.

Chapter 6 describes the application of FEM based on the density-dependent Drucker–Prager Cap (DPC) model to evaluate the capping tendency of microcrystalline cellulose tablets. DPC parameters were measured in uniaxial compression and diametrical compression tests as functions of relative density. The capping tendency is defined as the lamination occurring during a diametrical compression test. An attempt was made to predict the lamination by using FEM. Variations in the plastic strain of tablets during a diametrical compression test were observed, and a method to predict capping tendency was developed.

Finally, chapter 7 summarizes the conclusions obtained based on the results of this thesis.

References

- Adam, S., Suzzi, D., Radeke, C., Khinast, J. G., 2011. An integrated Quality by Design (QbD) approach towards design space definition of a blending unit operation by Discrete Element Method (DEM) simulation. *Euro J Pharm Sci.* 42, 106-115.
- Akseli, I., Stecula, A., He, X., Ladyzhynsky, N., 2014. Quantitative correlation of the effect of process conditions on the capping tendencies of tablet formulations. *J Pharm Sci.* 103, 1652-1663.
- Alchikh-Sulaiman, B., Ein-Mozaffari, F., Lohi, A., 2015. Evaluation of poly-disperse solid particles mixing in a slant cone mixer using discrete element method. *Chem Eng Res Design.* 96, 196-213.
- Antonyuk, S., Khanal, M., Tomas, J., Heinrich, S., Morl, L., 2006. Impact breakage of spherical granules: Experimental study and DEM simulation, *Chem Eng Process.* 45, 838-856.
- Antonyuk, S., Palis, S., Heinrich, S., 2011. Breakage behaviour of agglomerates and crystals by static loading and impact, *Powder Technol.* 206, 88-98.
- Balakrishnan, A., Pizette, P., Martin, C.L., Joshi, S.V., Saha, B.P., 2010. Effect of particle size in aggregated and agglomerated ceramic powders. *Acta Materialia.* 58, 802-812.
- Barrasso, D., Eppinger, T., Pereira, F.E., Aglave, R., Debus, K., Bermingham, S.K., Ramachandran, R., 2015. A multi-scale, mechanistic model of a wet granulation process using a novel bi-directional PBM–DEM coupling algorithm. *Chem Eng Sci.* 123, 500-513.
- Börner, M., Michaelis, M., Siegmann, E., Radeke, C., Schmidt, U., 2016. Impact of impeller design on high-shear wet granulation. *Powder Technol.* 295, 261-271.
- Boukouvala, F., Gao, Y., Muzzio, F., Ierapetritou, M.G., 2013. Reduced-order discrete element method modeling. *Chem Eng Sci.* 95, 12-26.
- Boukouvala, F., Niotis, V., Ramachandran, R., Muzzio, F.J., Ierapetritou, M.G., 2012. An integrated approach for dynamic flowsheet modeling and sensitivity analysis of a continuous tablet manufacturing process. *Comput Chem Eng.* 42, 30-47.
- Bratko, D., Striolo, A., Wu, J. Z., Blanch, H. W., Prausnitz, J. M., 2002. Orientation-Averaged Pair Potentials between Dipolar Proteins or Colloids. *J Phys Chem B.* 106, 2714-2720.
- Celik, M., 1992. Overview of compaction data analysis techniques, *Drug Dev Ind Pharm.* 18, 767-810
- Chamarthy, S.P., Pinal, R., Carvajal, M.T., 2009. Elucidating Raw Material Variability—Importance of Surface Properties and Functionality in

- Pharmaceutical Powders. *AAPS PharmSciTech.* 10, 780-788.
- Chan, E.L., Washino, K., Reynolds, G.K., Gururajan, B., Hounslow, M.J., Salman, A.D., 2016. Blade-granule bed stress in a cylindrical high shear granulator: Further characterisation using DEM. *Powder Technol.* 300, 92-106.
- Cundell, P.A., Strack, O.D.L., 1979. A discrete numerical model for granular assemblies. *Geotechnique.* 29, 47-65.
- Cunningham, J.C., Winstead, D., Zavaliangos, A., 2010. Understanding variation in roller compaction through finite element-based process modeling. *Comput Chem Eng.* 34, 1058-1071.
- Dave, V.S., Saoji, S.D., Raut, N.A., Haware, R.V., 2015. Excipient Variability and Its Impact on Dosage Form Functionality. *J Pharm Sci.* 104, 906-915.
- Dec, R.T., Zavaliangos, A., Cunningham, J.C., 2003. Comparison of various modeling methods for analysis of powder compaction in roller press. *Powder Technol.* 130, 265-271.
- Deen, N.G., Annaland, M.V.S., Van der Hoef, M.A., Kuipers, J.A.M., 2007. Review of discrete particle modeling of fluidized beds. *Chem Eng Sci.* 62, 28-44.
- Deng, X., Scicolone, J., Han, X., Dave, R.N., 2015. Discrete element method simulation of a conical screen mill: A continuous dry coating device. *Chem Eng Sci.* 125, 58-74.
- Diarra, H., Mazel, V., Busignies, V., Tchoreloff, P., 2013. FEM simulation of the die compaction of pharmaceutical products: Influence of visco-elastic phenomena and comparison with experiments. *Int. J. Pharm.* 453, 389-394.
- Dubey, A., Hsia, R., Saranteas, K., Brone, D., Misra, T., Muzzio, F.J., 2011. Effect of speed, loading and spray pattern on coating variability in a pan coater. *Chem Eng Sci.* 66, 5107-5115.
- Duffy, D.M., Harding, J.H., 2002. Modeling the interfaces between calcite crystals and Langmuir monolayers. *J Mater Chem.* 12, 3419-3425.
- Duffy, D.M., Harding, J.H., 2004a. Simulation of Organic Monolayers as Templates for the Nucleation of Calcite Crystals. *Langmuir.* 20, 7630-7636.
- Duffy, D.M., Harding, J.H., 2004b. Growth of polar crystal surfaces on ionized organic substrates. *Langmuir.* 20, 7637-7642.
- Eitzlmayr, A., Khinast, J., 2015a. Co-rotating twin-screw extruders: Detailed analysis of conveying elements based on smoothed particle hydrodynamics. Part1: Hydrodynamics. *Chem Eng Sci.* 134, 861-879.
- Eitzlmayr, A., Khinast, J., 2015b. Co-rotating twin-screw extruders: Detailed analysis of conveying elements based on smoothed particle hydrodynamics. Part2: Mixing.

- Chem Eng Sci. 134, 880-886.
- Fonteyne, M., Wickstrom, H., Peeters, E., Vercruyssen, J., Ehlers, H., Peters, B-H., Remon, J.P., Vervaet, C., Ketolainen, J., Sandler, N., Rantanen, J., Naelapaa, K., Beer, T.D., 2014. Influence of raw material properties upon critical quality attributes of continuously produced granules and tablets. *Euro J Pharm Biopharm.* 87, 252-263.
- Gantt, J.A., Gatzke, E.P., 2005. High-shear granulation modeling using a discrete element simulation approach. *Powder Technol.* 156, 195-212.
- Gantt, J.A., Cameron, I.T., Litster, J.D., Gatzke, E.P., 2006. Determination of coalescence kernels for high-shear granulation using DEM simulations. *Powder Technol.* 170, 53-63.
- Gernaey, K.V., Cervera-Padrell, A.E., Woodley, J.M., 2012. A perspective on PSE in pharmaceutical process development and innovation. *Comput Chem Eng.* 42, 15-29.
- Golchert, D., Moreno, R., Ghadiri, M., Litster, J., 2004. Effect of granule morphology on breakage behaviour during compression, *Powder Technol.* 144, 84-96.
- Gopireddy, S.R., Hildebrandt, C., Urbanetz, N.A., 2016. Numerical simulation of powder flow in a pharmaceutical tablet press lab-scale gravity feeder. *Powder Technol.* 302, 309-327.
- Guo, Y., Kafui, K.D., Wu, C.Y., Thornton, C., Seville, J.P.K., 2009. A coupled DEM/CFD Analysis of the Effect of Air on Powder Flow During Die Filling. *AIChE J.* 55, 49-62.
- Han, L.H., Elliot, J.A., Bentham, A.C., Mills, A., Amidon, G.E., Hancock, B.C., 2008. A modified Drucker-Prager Cap model for die compaction simulation of pharmaceutical powders. *Int J Solids Struct.* 45, 3088-3106.
- Hassanpour, A., Ghadiri, M., 2004. Distinct element analysis and experimental evaluation of the Heckel analysis of bulk powder compression. *Powder Technol.* 141, 251-261.
- Hayashi, Y., Miura, T., Shimada, T., Onuki, Y., Obata, Y., Takayama, K., 2013. Prediction of Tablet Characteristics from Residual Stress Distribution Estimated by the Finite Element Method. *Chem Pharm Bull.* 102, 3678-3686.
- Heckel, R.W., 1961a. Density-pressure relationships in powder compaction, *Trans Metall Soc AIME.* 221, 671-675
- Heckel, R.W., 1961b. An analysis of powder compaction phenomena, *Trans Metal Soc AIME.* 221, 1001-1008
- Horio, M., 2003. Binderless granulation—its potential, achievements and future issues.

- Powder Technol. 130, 1-7.
- ICH Harmonised tripartite guideline pharmaceutical development Q8(R2), step 4 version dated August 2009. http://www.ich.org/fileadmin/Public_Web_Site/ICH_Products/Guidelines/Quality/Q8_R1/Step4/Q8_R2_Guideline.pdf
- Just, S., Toschkoff, G., Funke, A., Djuric, D., Scharrer, G., Khinast, J., Knop, K., Kleinebudde, P., 2013. Experimental Analysis of Tablet Properties for Discrete Element Modeling of an Active Coating Process. *AAPS PharmSciTech.* 14, 402-411.
- Kadiri, M.S., Michrafy, A., Dodds, J.A., 2005. Pharmaceutical powders compaction: Experimental and numerical analysis of the density distribution. *Powder Technol.* 157, 176-182.
- Kadiri, M.S., Michrafy, A., 2013. The effect of punch's shape on die compaction of pharmaceutical powders. *Powder Technol.* 239, 467-477.
- Kadota, K., Shimosaka, A., Shirakawa, Y., Hidaka, J., 2007. Dehydration process in NaCl solutions under various external electric fields. *J Nanoparticle Res.* 9, 377-387.
- Kadota, K., Shirakawa, Y., Wada, Mayuko. Shimosaka, A., Hidaka, J., 2012. Influence of clusters on the crystal surface of NaCl at initial growth stage investigated by molecular dynamics simulations. *J Molecular Liq.* 166,31-39.
- Kafui, K.D., Thornton, C., 2000. Numerical simulation of impact breakage of a spherical crystalline agglomerate, *Powder Technol.* 109, 113-132.
- Kalbag, A., Wassgren, C., Penumetcha, S.S., Pérez-Ramos, J.D., 2008. Inter-tablet coating variability: Residence times in a horizontal pan coater. *Chem Eng Sci.* 63, 2881-2894.
- Ketterhagen, W.R., Ende, M.T., Hancock, B.C., 2009. Process Modeling in the Pharmaceutical Industry using the Discrete Element Method. *J. Pharm. Sci.* 98, 442-470.
- Ketterhagen, W.R., 2011. Modeling the motion and orientation of various pharmaceutical tablet shapes in a film coating pan using DEM. *Int J Pharm.* 409, 137-149.
- Ketterhagen, W.R., 2015. Simulation of powder flow in a lab-scale tablet press feed frame: Effects of design and operating parameters on measures of tablet quality. *Powder Technol.* 275, 361-374.
- Kim, A. Y., Hauch, K. D., Berg, J. C., Martin, J. E., Anderson, R. A., 2003. Linear chains and chain-like fractals from electrostatic heteroaggregation. *J Colloid Interface Sci.* 260, 149-159.

- Klinzing, G.R., Zavaliangos, A., Cunningham, J., Mascaro, T., Winstead, D., 2010. Temperature and density evolution during compaction of a capsule shaped tablet. *Comput Chem Eng.* 34, 1082-1091.
- Koynov, A., Akseli, I., Cuitino, A. M., 2011. Modeling and simulation of compact strength due to particle bonding using a hybrid discrete-continuum approach. *Int. J. Pharm.* 418, 273-285.
- Kremer, D.M., Hancock, B.C., 2006. Process Simulation in the Pharmaceutical Industry: A Review of Some Basic Physical Models. *J Phama Sci.* 95, 517-529.
- Krok, A., Peciar, M., Fekete, R., 2014. Numerical investigation into the influence of the punch shape on the mechanical behavior of pharmaceutical powders during compaction. *Particuology.* 16, 116-131.
- Kuo, H.P., Knight, P.C., Parker, D.J., Tsuji, Y., Adams, M.J., Seville, J.P.K., 2002. The influence of DEM simulation parameters on the particle behaviour in a V-mixer. *Chem Eng Sci.* 57, 3621-3638.
- Kuo, H.P., Knight, P.C., Parker, D.J., Seville, J.P.K., 2005. Solids circulation and axial dispersion of cohesionless particles in a V-mixer. *Powder Technol.* 152, 133-140.
- Lee, S.L., O'Connor, T.F., Yang, X., Cruz, C.N., Chatterjee, S., Madurawe, R.D., Moore, C.M.V., Yu, L.X., Woodcock, J., 2015. Modernizing Pharmaceutical Manufacturing: from Batch to Continuous Production. *J Pham Innov.* 10, 191-199.
- Leeuw, N.H., Parker, S.C., 1997. Atomistic simulation of the effect of molecular adsorption of water on the surface structure and energies of calcite surfaces. *J Chem Soc Faraday Trans.* 93, 467-475.
- Leeuw, N.H., Parker, S.C., 1998. Surface structure and morphology of calcium carbonate polymorphs calcite, aragonite, and vaterite: An atomistic approach. *The J Phys Chem B.* 102, 2914-2922.
- Leeuw, N.H., Parker, S.C., Harding, J.H., 1999. Molecular dynamics simulation of crystal dissolution from calcite steps. *Phys Rev B.* 60, 13792-13799.
- Lemieux, M., Bertrand, F., Chaouki, J., Gosselin, P., 2007. Comparative study of the mixing of free-flowing particles in a V-blender and a bin-blender. *Chem Eng Sci.* 62, 1783-1802.
- Lemieux, M., Léonard, G., Doucet, J., Leclaire, L.A., Viens, F., Chaouki, J., Bertrand, F., 2008. Large-scale numerical investigation of solids mixing in a V-blender using the discrete element method. *Powder Technol.* 181, 205-216.
- Lewis, R.W., Gethin, D.T., Yang, X.S., Rowe, R.C., 2005. A combined finite-discrete element method for simulating pharmaceutical powder tableting. *Int. J. Numer. Meth. Engng.* 62, 853-869.

- Liang, H., Angelo, C., Eric, L., Steve, G., 2006. Clusters of Charged Janus Spheres. *NANO Lett.* 6, 2510-2514.
- Martin, C.L., Bouvard, D., 2006. Discrete Element Simulations of the Compaction of Aggregated Ceramic Powders. *J. Am. Ceram. Soc.* 89, 3379-3387.
- Mateo-Ortiz, D., Muzzio, F.J., Mendez, R., 2015. Particle size segregation promoted by powder flow in confined space: The die filling process case. *Powder Technol.* 262, 215-222.
- Mateo-Ortiz, D., Mendez, R., 2015. Relationship between residence time distribution and forces applied by paddles on powder attrition during the die filling process. *Powder Technol.* 278, 111-117.
- Mehrotra, A., Chaudhuri, B., Faqih, A., Tomassone, M.S., Muzzio, F.J., 2009. A modeling approach for understanding effects of powder flow properties on tablet weight variability. *Powder Technol.* 188, 295-300.
- Metzger, M.J., Glasser, B.J., 2012. Numerical investigation of the breakage of bonded agglomerates during impact, *Powder Technol.* 217, 304-314.
- Michrafy, A., Ringenbacher, D., Tchoreloff, P., 2002. Modelling the compaction behavior of powders: application to pharmaceutical powders. *Powder Technol.* 127, 257-266.
- Moakher, M., Shinbrot, T., Muzzio, F.J., 2000. Experimentally validated computations of flow, mixing and segregation of non-cohesive grains in 3D tumbling blenders. *Powder Technol.* 109, 58-71.
- Moreno, R., Ghadiri, M., Antony, S.J., 2003. Effect of the impact angle on the breakage of agglomerates: a numerical study using DEM, *Powder Technol.* 130, 132-137.
- Nakamura, H., Fujii, H., Watano, S., 2013. Scale-up of high shear mixer-granulator based on discrete element analysis. *Powder Technol.* 236, 149-156.
- Otoguro, S., Hayashi, Y., Miura, T., Uehara, N., Utsumi, S., Onuki, Y., Obata, Y., Takayama, K., 2015. Numerical Investigation of the Residual Stress Distribution of Flat-Faced and Convexly Curved Tablets Using the Finite Element Method. *Chem Pharm Bull.* 63, 890-900.
- Paul, S.M., Mytelka, D.S, Dunwiddie, C.T., Persinger, C.C., Munos, B.H., Lindborg, S.R., Schacht, A.L., 2010. How to improve R&D productivity: the pharmaceutical industry's grand challenge. *Nature Rev.* 9, 203-214.
- Persson, A.S., Frenning, G., 2012. An experimental evaluation of the accuracy to simulate granule bed compression using the discrete element method. *Powder Technol.* 219, 249-256.
- Podczec, F., Drake, K.R., Newton, J.M., 2013. Investigations into the tensile failure of

- doubly-convex cylindrical tablets under diametral loading using finite element methodology. *Int J Pharm.* 454, 412-424.
- Puertas, A. M., Fernández-Barbero, A., de las Nieves, F. J., 2001. Kinetics of charge heteroaggregation by Brownian dynamics simulation: role of the interaction potential profile. *Colloids and Surf A*, 195, 189-195.
- Qin, Y.; Fichthorn, K. A., 2003. Molecular-dynamics simulation of forces between nanoparticles in a Lennard-Jones liquid. *J Chem Phys*, 119, 9745-9754.
- Qin, Y.; Fichthorn, K. A., 2006. Solvophobic solvation at large and intermediate length scales: Size, shape, and solvent effects. *Phys Rev E*, 73, 020401-1-020401-4.
- Rantanen, J., Khinast, J., 2015. The Future of Pharmaceutical Manufacturing Sciences. *J. Pharm. Sci.* 104, 3612-3638.
- Rogers, A.J., Hashemi, A., Ierapetritou, M.G., 2013. Modeling of Particulate Processes for the Continuous Manufacture of Solid-Based Pharmaceutical Dosage Forms. *Processes*. 1, 67-127.
- Rogers, A., Ierapetritou, M.G., 2014. Discrete Element Reduced-Order Modeling of Dynamics Particulate Systems. *AIChE J.* 60, 3184-3194.
- Rogers, A., Ierapetritou, M., 2015. Challenges and opportunities in modeling pharmaceutical manufacturing processes. *Comput Chem Eng.* 81, 32-39.
- Sahni, E., Chaudhuri, B., 2011. Experiments and numerical modeling to estimate the coating variability in a pan coater. *Int J Pharm.* 418, 286-296.
- Sato, Y., Nakamura, H., Watano, S., 2008. Numerical analysis of agitation torque and particle motion in a high shear mixer. *Powder Technol.* 186, 130-136.
- Shang, C., Sinka, I. C., Pan, J., 2013. Modelling of the break force of tablets under diametrical compression. *Int. J. Pharm.* 445, 99-107.
- Shinto, H., Sakakibara, T., Higashitani, K., 1998. Molecular Dynamics Simulations of Water at NaCl(001) and NaCl(011) Surfaces. *J Phys Chem B.* 102, 1974-1981.
- Siiria, S. M., Antikainen, O., Heinamaki, J., Yliruusi, J., 2011. 3D simulation of Internal Tablet Strength During Tableting. *AAPS PharmSciTech.* 12, 593-603.
- Sinha, T., Curtis, J.S., Hancock, B.C., Wassgren, C., 2010a. A study on the sensitivity of Drucker-Prager Cap model parameters during the decompression phase of powder compaction simulations. *Powder Technol.* 198, 315-324.
- Sinha, T., Bharadwaj, R., Curtis, J.S., Hancock, B.C., Wassgren, C., 2010b. Finite element analysis of pharmaceutical tablet compaction using a density dependent material plasticity model. *Powder Technol.* 202, 46-54.
- Sinka, I. C., Cunningham, J. C., Zavaliangos, A., 2003. The effect of wall friction in the compaction of pharmaceutical tablets with curved faces: a validation study of the

- Drucker-Prager Cap model. *Powder Technol.* 133, 33-43.
- Sinka, I.C., Cunningham, J.C., Zavaliangos, A., 2004. Analysis of Tablet Compaction. II. Finite Element Analysis of Density Distributions in Convex Tablets. *J Pharm Sci.* 93, 2040-2053.
- Sinyagin, A. Y.; Belov, A.; Tang, Z.; Kotov, N. A. 2006. Monte Carlo Computer Simulation of Chain Formation from Nanoparticles *J Phys Chem B.* 110, 7500-7507.
- Stocker, E., Toschkoff, G., Sacher, S., Khinast, J.G., 2014. Use of mechanistic simulations as a quantitative risk-ranking tool within the quality by design framework. *Int J Pharm.* 475, 245-255.
- Striolo, A., Bratko, D., Wu, J. Z., Elvassore, N., Blanch, H. W., Prausnitz, J. M., 2002. Forces between aqueous nonuniformly charged colloids from molecular simulation. *J Chem Phys.* 116, 7733-7743.
- Subero, J., Ning, Z., Ghadiri, M., Thornton, C., 1999. Effect of interface energy on the impact strength of agglomerates, *Powder Technol.* 105, 66-73.
- Suresh, P., Basu, P.K., 2008. Improving Pharmaceutical Product Development and Manufacturing: Impact on Cost of Drug Development and Cost of Goods Sold of Pharmaceuticals. *J Pham Innov.* 3, 175-187.
- Suzzi, D., Toschkoff, G., Radl, S., Machold, D., Fraser, S.D., Glasser, B.J., Khinast, J.G., 2012. DEM simulation of continuous tablet coating: Effects of tablet shape and fill level on inter-tablet coating variability. *Chem Eng Sci.* 69, 107-121.
- Terashita, K., Nishimura, T., Natsuyama, S., 2002. Optimization of Operating Conditions in a High-Shear Mixer Using DEM Model: Determination of Optimal Fill Level. *Chem Pharm Bull.* 50, 1550-1557.
- Thornton, C., Ciomocos, M.T., Adams, M.J., 1999. Numerical simulation of agglomerate impact breakage, *Powder Technol.* 105, 74-82.
- Thornton, C., Ciomocos, M.T., Adams, M.J., 2004. Numerical simulations of diametrical compression tests on agglomerates, *Powder Technol.* 258-267.
- Toschkoff, G., Just, S., Knop, K., Kleinebudde, P., Funke, A., Djuric, D., Scharrer, G., Khinast, J.G., 2015. Modeling of an Active Tablet Coating Process. *J Pharm Sci.* 104, 4082-4092.
- Walton, O.R., Braun, R.L., 1986. Viscosity, granular temperature and stress calculations for shearing assemblies of inelastic, frictional disks. *J Rheology.* 30, 949-980.
- Wu, C. Y., Ruddy, O. M., Bentham, A. C., Hancock, B. C., Best, S. M., Elliott, J. A., 2005. Modelling the mechanical behavior of pharmaceutical powders during compaction. *Powder Technol.* 152, 107-117.

- Wu, C-Y., 2008a. DEM simulations of die filling during pharmaceutical tableting, *Particuology*, 6, 412-418.
- Wu, C. Y., Hancock, B. C., Mills, A., Bentham, A. C., Best, S. M., Elliott, J. A., 2008b. Numerical and experimental investigation of capping mechanisms during pharmaceutical tablet compaction. *Powder Technol.* 181, 121-129.
- Yamanaka, S., Shimosaka, A., Shirakawa, Y., Hidaka, J., 2010. Molecular dynamics simulations of the formation for NaCl cluster at the interface between the supersaturated solution and the substrate. *J Nanoparticle Res.* 12, 831-839.
- Yamane, K., Sato, T., Tanaka, T., Tsuji, Y., 1995. Computer simulation of tablet motion in coating drum. *Pharm Res.* 12, 1264-1268.
- Yu, L.X., 2008. Pharmaceutical quality by design: product and process development, understanding, and control. *Pharm Res.* 25, 781-791.
- Zahn, D., 2004. Atomistic mechanism of NaCl nucleation from an aqueous solution. *Phys Rev Lett.* 92, 040801.1-040801.4.
- Zavaliangos, A., Galen, S., Cunningham, J., Winstead, D., 2008. Temperature Evolution during Compaction of Pharmaceutical Powders. *J Pharm Sci.* 97, 3291-3304.

Chapter 2
Effect of surface properties of calcium carbonate
on aggregation process

2.1 Introduction

CaCO₃ has been intensely studied as an important material used for industrial products such as plastics, rubber, papers inks and pharmaceutical materials over the past century (Chikazawa and Fuji, 2001). CaCO₃ is employed as a pharmaceutical excipient and it is used in solid dosage forms as a diluent, a buffering agent and a dissolution aid (Rowe, et al., 2009). The studies of CaCO₃ focused on compaction (Serra and Robles., 2003; Bacher et al., 2007), crystallisation (Preisig et al., 2014), and granulation (Kristensen and Hansen, 2006; Li, et al., 2011) were recently conducted. Because the properties of the products are dependent on particulate characteristics of CaCO₃, the control of morphology and polymorphs of CaCO₃ is required (Kojima, et al., 1994; Cheng, et al., 2004; Yu, et al., 2004; Zhang, et al., 2010a).

Carbonation process of Ca(OH)₂ aqueous slurry is widely used for producing CaCO₃ in industrial fields. The crystallisation of CaCO₃ is carried out with dehydration of Ca(OH)₂ aqueous slurry by bubbling of CO₂. The CaCO₃ crystallised in the carbonation process is nanosized particles and has a narrow particle size distribution (Kim and Hirasawa, 2004). The particle characteristics of CaCO₃ have been controlled by the empirically determined operations such as changing temperature, CO₂ gas volume and CO₂ gas flow rate. Some researchers have succeeded in controlling the morphology and polymorphism of CaCO₃ particles by operating the reaction conditions (Reddy and Nancollas, 1976; Arai and Yasue, 1989; Park and Choi, 2004). Kitamura et al. (2002) clarified the relation between operation parameters and CaCO₃ polymorphism change. Among the CaCO₃ polymorphs, which have three types of calcite, aragonite and vaterite, the calcite is the most popular and utilised as the most stable crystals. The calcite of CaCO₃ is classified into two morphologies depending on the carbonation

conditions. Fine particles with rhombic shape can be obtained from the temperature below 291K, while large spindle particles can be made at higher temperature of 300K. It was commonly reported that the spindle shape was formed by the aggregation of primary particles with some sort of anisotropy in a preferential direction (Juvekar and Shama, 1943; Arai and Yasue, 1990; Arakawa, 2004) as shown in Figure 2-1 (Kadota, et al., 2011). Arakawa (2004) found how the large spindle particles generated from the supersaturated CaCO_3 solutions by their inventive electron microscope technique. This research indicated that the aggregation mechanism was related with characteristics of the primary CaCO_3 particles in the carbonation process. The spindle particles formed by the aggregation of CaCO_3 crystals with the transformation from the amorphous to calcite crystals in the carbonation process. Yamada and Hara (1985) proved that amorphous CaCO_3 was deposited in the early period of the crystallisation as a precursor of the final particles. In the research article, they discussed the morphology of the primary particle in relation with the ionic property of the suspension. It is difficult to clarify the formation mechanism of CaCO_3 polymorphs only by the experimental approaches because the nucleation and crystal growth of CaCO_3 occurred at nano scale and the aggregation of CaCO_3 was related to specific crystal faces. The knowledge of aggregation phenomena for anisotropic particles at nano scale is indispensable for morphology control in aggregation processes.

In this section, MD simulations were performed to study the effect of surface charge density and dielectric constant of water on aggregation process. The validity of MD simulation was justified to compare the results of the density profile of water calculated by MD simulation with the previous experimental results. The charge density from ionic structure on each crystal surface was calculated by MD simulations. The

charge density map was calculated from the existence of ion on the crystal surface using rigid model of MD simulations. The orientation of water to each crystal surface was estimated for the dielectric constant of water. The self-diffusion coefficients of water were calculated to investigate the mobility of water molecular. In addition, formation energy of grain boundary was calculated for the change of energy in the aggregation process of primary particles.

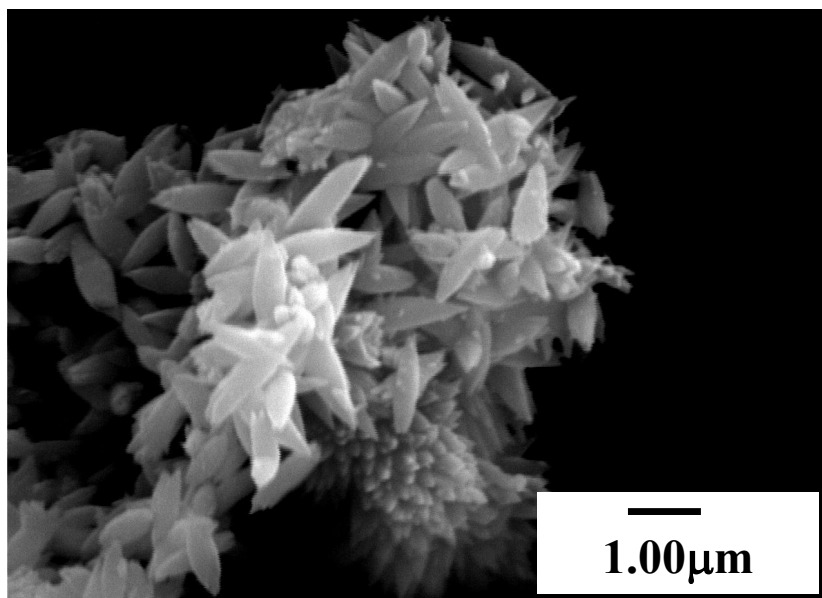


Figure 2-1 SEM photograph of spindle-shaped CaCO₃. (Kadota, et al., 2011)

2.2 Simulation details

In the aggregation process of CaCO₃ particles, a surface of primary CaCO₃ particle approaches that of another primary particle through water. A simulation model cell of CaCO₃/water/CaCO₃ was adopted. The change of distance between two CaCO₃ surfaces corresponds to an approach of the two primary particles. A schematic representation of simulation box for interface of water/CaCO₃ is depicted in Figure. 2-2. The interface is chosen to be perpendicular to the z axis.

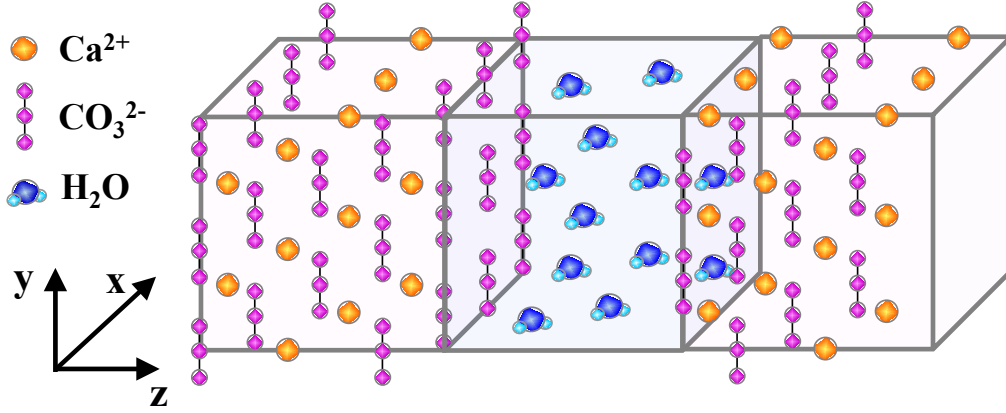


Figure 2-2. Basic cell of CaCO₃/water interface used in MD simulation.

A crystal of CaCO₃ consists of 576 Ca atoms, 576 C atoms and 1728 O atoms in a rectangular simulation cell with linear dimensions of $2.9928 \times 3.4560 \times 3.4122$ nm. Interatomic potential for CaCO₃ used in this section is based on a rigid-ion-model derived by Pavese et al. (1992).

$$U_T = \sum_i \sum_j U_{ij}^e + \sum_i \sum_j U_{ij}^{sr} + \sum_{CO_3^{2-}} (U^b + U^t) \quad (2-1)$$

where U_{ij}^e , U_{ij}^{sr} , U^b and U^t are the coulombic potential, Buckingham potential, Harmonic potential and Torsional potential, respectively, for the pair of atoms i and j .

Furthermore, each potential is shown in below:

$$U_{ij}^e = e^2 \frac{Z_i Z_j}{r_{ij}} \quad (2-2)$$

$$U_{ij}^{sr} = A_{ij} \exp(-r_{ij}/\rho_{ij}) - c_{ij}/r_{ij}^6 \quad (2-3)$$

$$U^b = \frac{1}{2} k_b (\theta_b - \theta_0)^2 \quad (2-4)$$

$$U^t = k_t (1 - \cos 2\theta_t) \quad (2-5)$$

where e is the elementary charge (1.602×10^{-19} C), Z is the Valence of ion, r is the distance between particles, A_{ij} and C_{ij} are the constant of Buckingham potential, ρ is the number of density, k_b is the constant of Harmonic potential, θ_b is Harmonic angle, k_t is the constant of Torsional potential, θ_t is Torsional angle, and the values of these parameters are listed in Table 2-1. U^b adjusts the angle formed by O-C-O and U^t adjusts the torsional angle formed by O-C-O-O. Water was modelled using the Extended Simple Point Charge (SPC/E) rigid water model and charges of H-atom and O-atom were $+0.4238(e)$ and $-0.8476(e)$, respectively (Berendsen, et al., 1987). The potential parameters between water and CaCO_3 were shown in Table 2-2, which were calculated by Leeuw et al. (Leeuw, et al., 1997). One part of the CaCO_3 crystal was kept fixed as well as some works (Duffy and Harding, 2002; Leeuw and Parker, 1998). The long-range Coulombic forces were calculated using Ewald summation (Ewald, 1921). The equation of transitional motions was solved using the velocity Verlet integration algorithm and the rotational motion of water molecules was integrated by a leap-frog algorithm. *NVT* simulations were used following adjustment with periodic boundary conditions. Temperature was kept fixed at 300 K using velocity scaling method and the time step was 1 fs for all MD simulations. First, only water molecules were allowed to relax for thermal equilibrium and a connected cell of CaCO_3 and water was constructed. The cell can be established an equilibrium state for less than 500 ps under the similar condition.

There are four types in calcium carbonate (calcite) structure consisting of alternate planes of Ca ions and CO_3 ions (Figure 2-3). MD simulation was performed to investigate the differences of surface properties among four surfaces of CaCO_3 , (001)Ca, (001) CO_3 , (100) and (104) surfaces. (001)Ca represents the surface with terminated Ca

ions and (001)CO₃ with terminated CO₃ ions, respectively. MD simulation was carried out in four different separation distance of 3.3, 2.3, 1.5 and 0.7 nm between the surfaces of CaCO₃. The number of water is calculated using water density of 0.998 g/cm³ and is shown in Table 2-3. The number of water was not same value because separation distances were slightly different at each surface.

Table 2-1 Parameters for CaCO₃

Interaction		Coefficients		
Coulomb	Atom	Charge (e)		
	C	0.985		
	O	-0.995		
	Ca	2.000		
Buckingham	Bond	A_{ij} (eV)	ρ_{ij} (Å)	C_{ij} (eV Å⁶)
	Ca-O	1870.29	0.2893	0
	O-O	14683.52	0.2107	3.47
	O-C	54129.49×10 ⁸	0.0402	0
Three-body	Bond	k_b (eV rad⁻²)	θ_0 (°)	
	O-C-O	2.5500	120	
Torsional	Bond	k_t (eV)	θ_t (°)	
	O-C-O-O	0.0917	±180	

Table 2-2 Parameters for CaCO₃/Water interactions

Interaction		Coefficients		
Buckingham	Bond	A_{ij} (eV)	ρ_{ij} (Å)	C_{ij} (eV Å⁶)
	Ca _{latt} -O _{water}	1186.8	0.297	0
	O _{latt} -O _{water}	12533.6	0.213	12.09
	O _{latt} -H _{water}	311.97	0.230	0

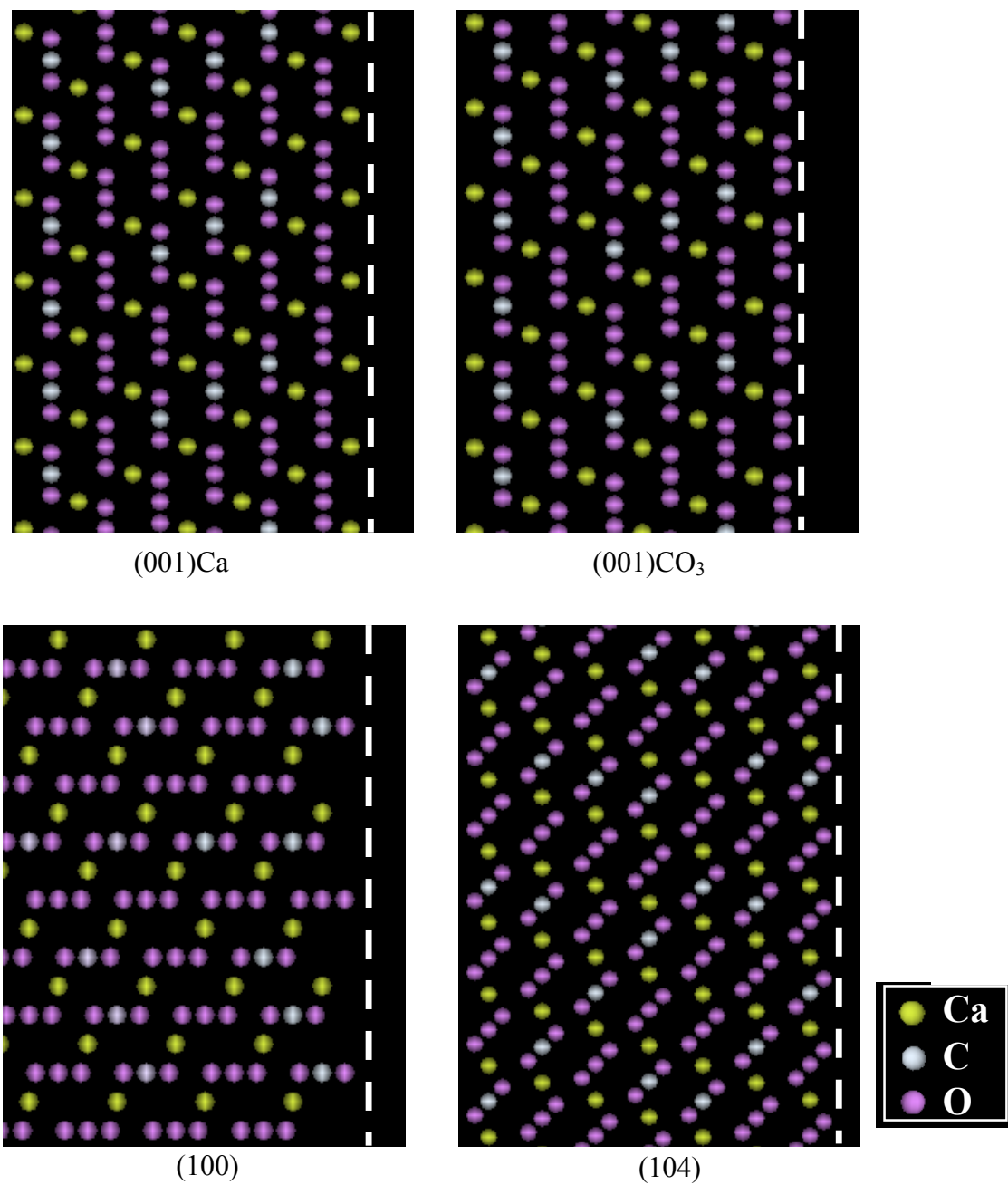


Figure 2-3 Four types of CaCO₃ crystal surfaces.

Table 2-3 Number of water changed interface gap against each CaCO₃ interface

Interface gap (nm)	Number of water (-)			
	(001)Ca	(001)CO ₃	(100)	(104)
0.7	242	242	238	228
1.5	513	513	511	489
2.3	799	799	783	750
3.3	1138	1138	1138	1138

2.3 Results and discussion

2.3.1 Density profile and orientational angle of water

Structures of water molecules between CaCO₃ primary particles are directly connected with the aggregation process. Figure 2-4 shows the density profiles of water between CaCO₃ crystals along the *z* direction. Distance from (104) surface to the first peak and to the second peak of water density represents d_1 and d_2 , respectively (Table 2-4). This result is in good agreement with that of Geissbühler et al. (2004) obtained by surface X-ray scattering and of Kerisit et al. (2005) obtained by MD simulation. In all cases, water molecules adsorbed to CaCO₃ surface and formed layer structure. Especially, water molecules with its high density adsorbed to the (001)Ca surface as seen from Figure 2-4. It seems that the adsorbed water molecules on CaCO₃ surfaces have a rigid structure because d_1 and d_2 did not change in small separation distance.

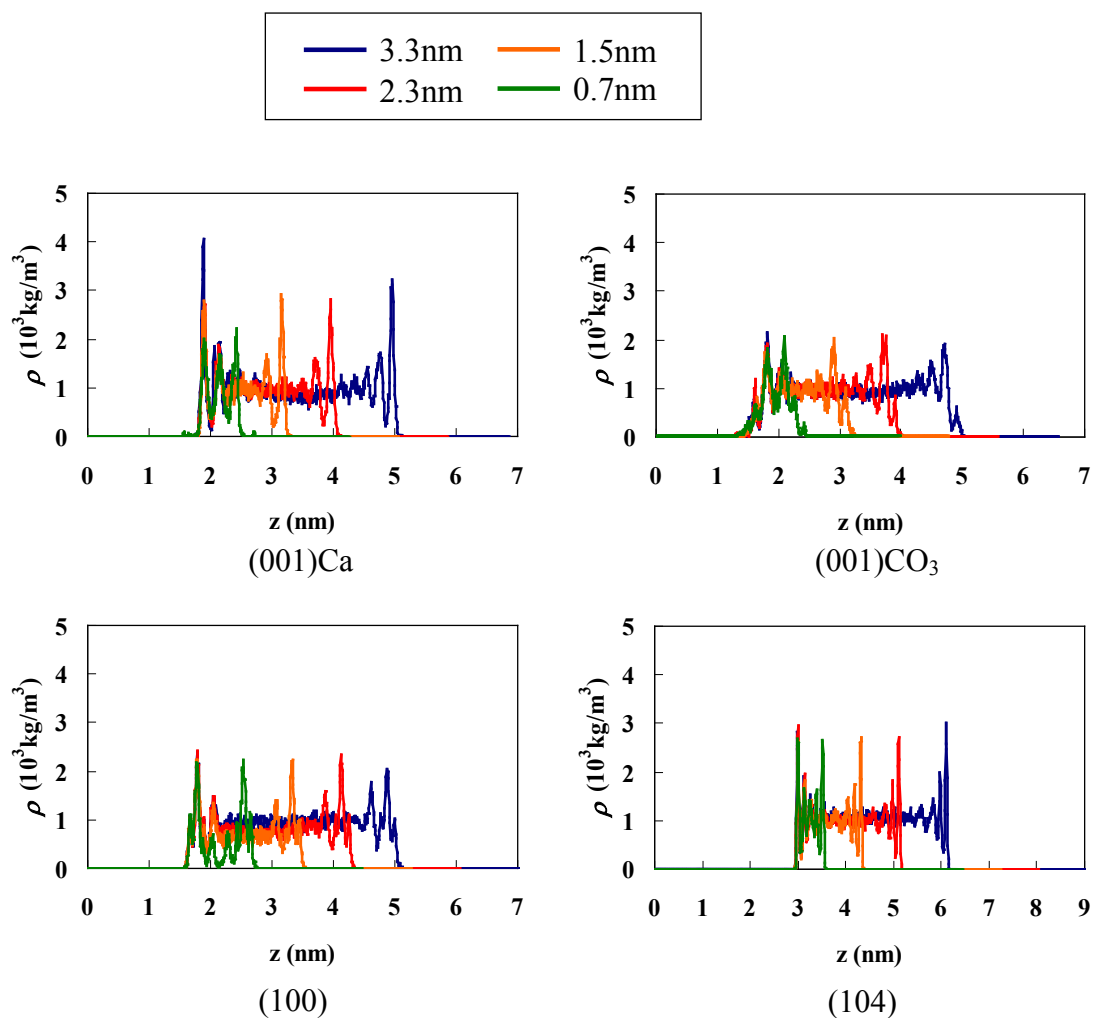


Figure 2-4 Density profiles of water along the z direction changing the distance between each crystal.

Table 2-4 Distance from surface to 1st water layer(d_1) and 2nd water layer(d_2) on different distance between surfaces

Distance between surfaces (nm)	d_1 (nm)	d_2 (nm)
0.7	0.199	0.340
1.5	0.209	0.347
2.3	0.216	0.352
3.3	0.216	0.343
Exp.	0.229	0.345

For detailed evaluation of the rigid structure of water molecules, the distribution of $\cos\theta$ was calculated, where θ was defined as angle between water dipole moment μ and unit vector in the z direction z_u as illustrated in Figure 2-5. In other words, oxygen atoms of water oriented towards the surface when $\cos\theta$ equaled to 1. O-atoms of water pointed towards (001)Ca surface with Ca ions terminated and charged positively as shown in Figure 2-6. The results of water orientations were illustrated and summarised in Figure 2-7. This result was caused by electric field from the (001)Ca surface and hydrogen bond network between water molecules. This interaction of the surface charge kept up fifth layer as shown in Figure 2-8. In contrast, on (001)CO₃ surface charged negatively, H-atoms of water pointed towards the surface and this interaction extended to fifth layer as well as (001)Ca. It indicated that the water molecules were influenced from the force by polar surface made from ionic

configuration and adsorbed strongly to the surface. The force was decreasing with increase in the distance from surface or was screened, and the water molecules behaved as bulk-like water in region remote from the surface. In case of (100) surface, waters were broadly distributed; it indicated that water did not order. As for the (104) surface, O-atoms of water in first layer pointed towards the surface, however, H-atoms of water in second layer pointed towards the surface. This result suggests that water molecules in first layer were drawn to Ca ions and hydrogen bond networks were formed between H-atom of water in first layer and O-atom of water in second layer, H-atom of water in first layer and O-atom in CaCO_3 surface, and H-atom of water in second layer and O-atom in CaCO_3 surface. Consequently, it was found that orientation of water molecules strongly depended on charge and structure of adsorbing surface.

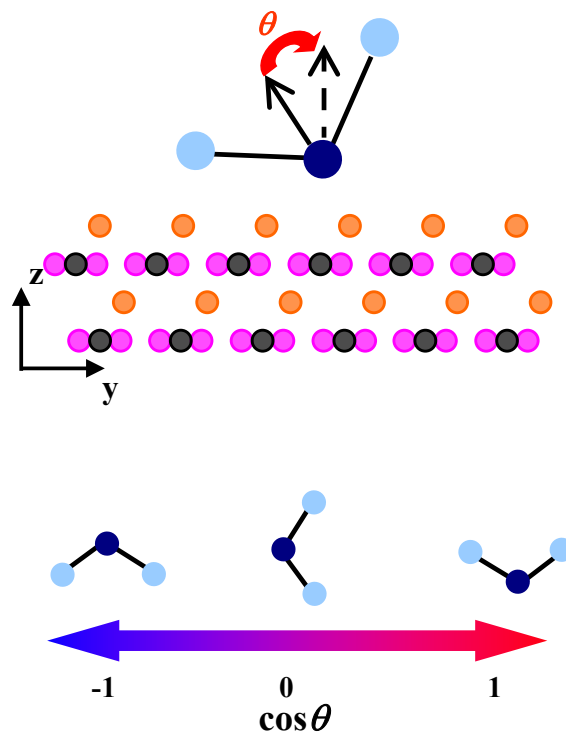


Figure 2-5 Orientation of a water molecule on the surface.

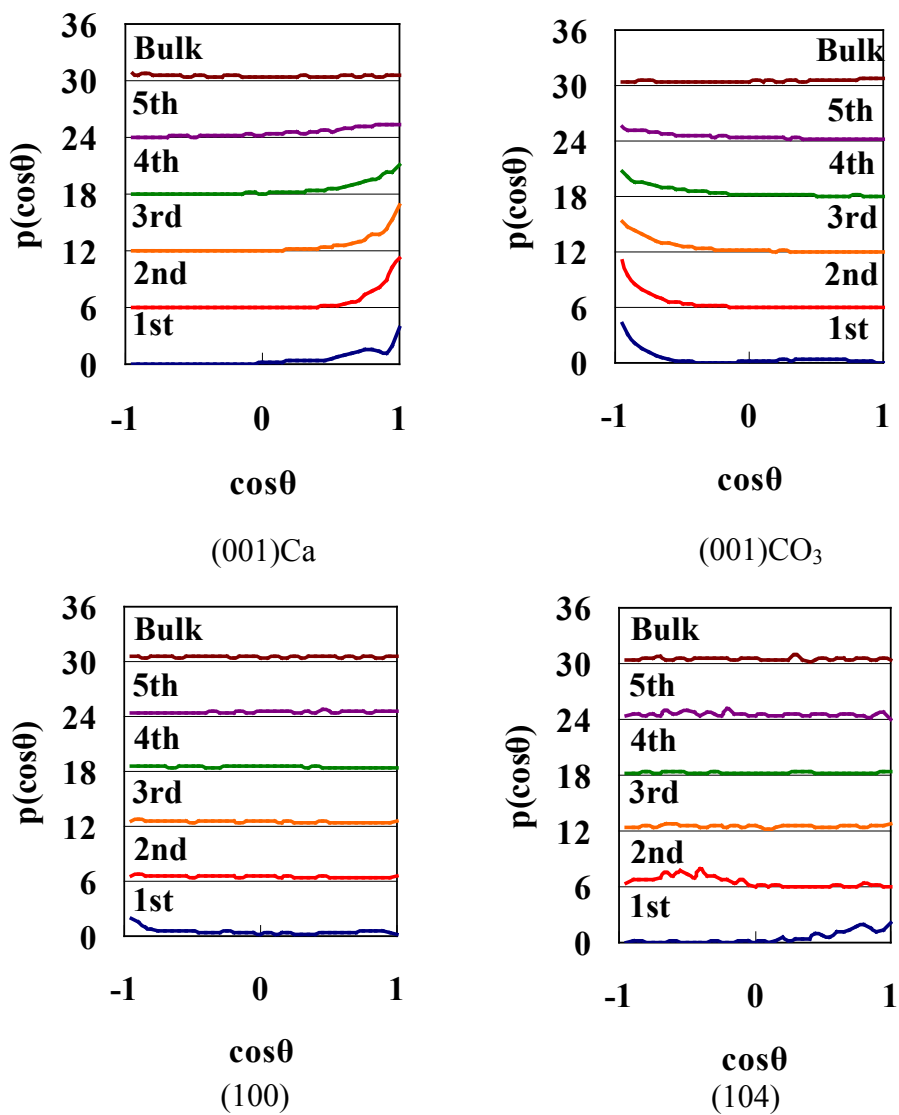


Figure 2-6 Orientational probability distribution of water dipole moment on several CaCO₃ surfaces. (distance is 3.3 nm)

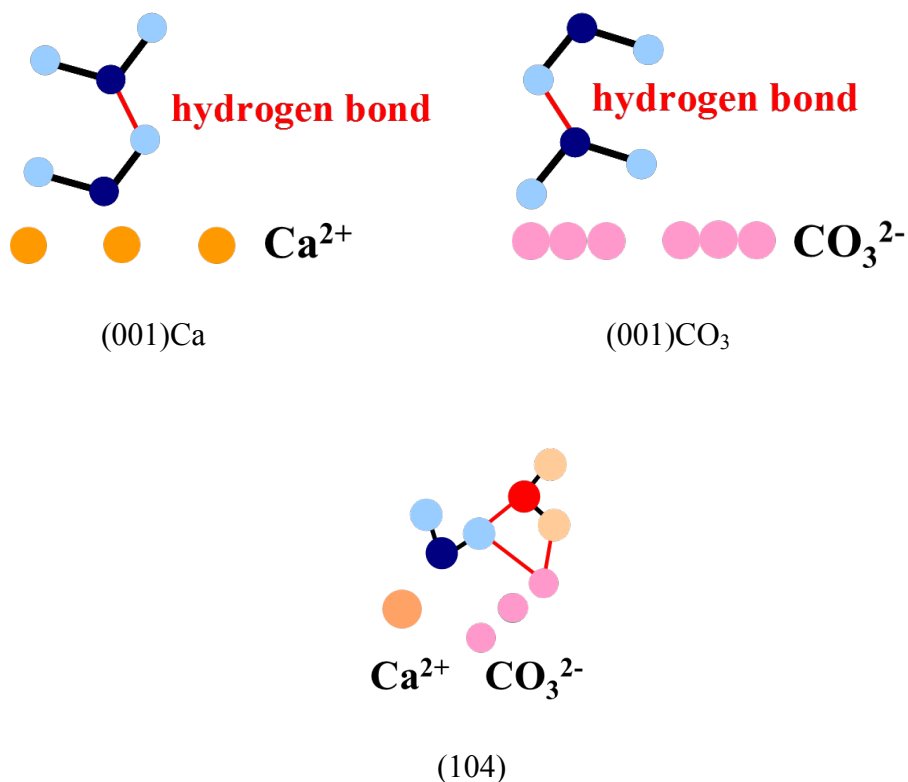


Figure 2-7 Orientation of water molecules on (001)Ca, (001)CO₃ and (104) surfaces.

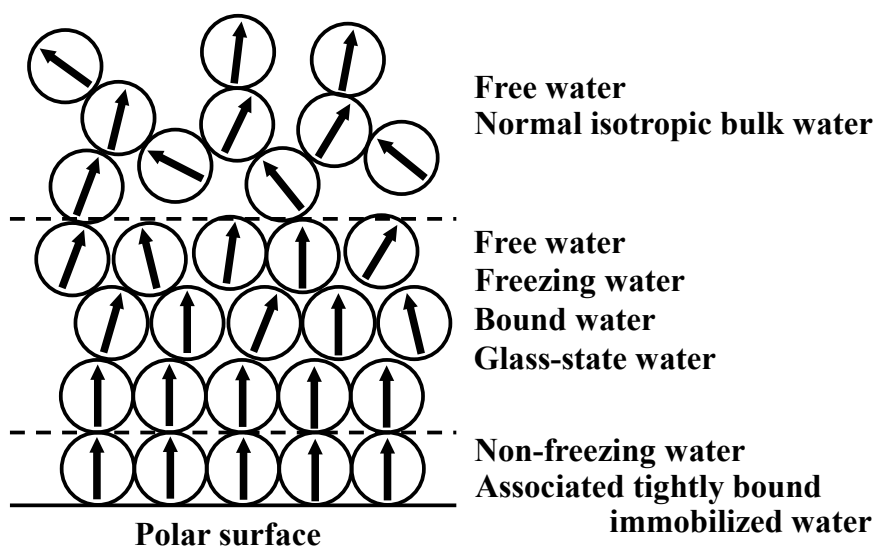


Figure 2-8 Model of the water structure on the polar surfaced.

2.3.2 Charge density on the crystal surface

Charge density map on the surface can be calculated from ionic structures given in MD simulations (Wang, et al., 2004). Valences of ion or ionic charges for all ions are tabulated in Table 2-1 as potential parameters. For instance, charge density maps of each CaCO_3 surface contacted with water are shown in Figure 2-9. Figure 2-9 shows the cross-section of the interface between CaCO_3 and water. The color of red and blue expresses respectively the positive charge and negative charge calculated from the total ion and ionic charge on the crystal surface. The origination of the first layer was illustrated by the atomic density contour maps for the valences of ion or ionic charges for all ions, located in the first maximum for the atomic density profile. The charge transfer between atoms is not treated in this simulation although it might be affected on the aggregation process. The prediction of aggregation could be expected without treating the charge transfer between atoms (Zhang et al. 2010b). According to Figure 2-10, Ca ions exist near the interface of (001) Ca/water and CO_3 ions near the interface of (001) CO_3 /water. In (100) and (104), the surface consists of Ca and CO_3 ions. The charge densities of CaCO_3 and water along z-axis for four interfaces of water/ CaCO_3 are shown in Figure 2-10. This showed that (001)Ca surface charged positively and (001) CO_3 surface charged negatively. In contrast, the surface of (100) and (104) has a small effective charge. It is well known that small CaCO_3 particles tend to form chain-like aggregates and some groups have reported the formation mechanism of chain-like aggregates (Matsushita et al., 1993; Fuji et al., 2000; Carmona et al., 2003). Carmona et al. (2003) reported that small amorphous CaCO_3 were generated in the early stage of reaction and they aggregated in the same direction because of their polarisation, and furthermore the amorphous CaCO_3 covered on $\text{Ca}(\text{OH})_2$ surface influenced the

aggregation of primary CaCO_3 particles. Some researchers experimentally discussed the reason why the primary particles of CaCO_3 aggregate in the same direction. For example, Arakawa experimentally demonstrated that larger spindle particles were composed of fine particle primary ones by their inventive electron microscopic investigation (Arakawa, 2004). This research indicates that the primary particles of CaCO_3 aggregate in the same direction due to the existence of high population of (001)Ca and (001)CO₃ in the primary particles. However, the study used electron diffraction and X-ray diffraction from Matsushita et al. (1993) showed that small particles generated in the early stage of reaction were amorphous, and chain-like particles were calcite polymorphs. These results indicate that calcite particles, not amorphous particles, tend to aggregate in the same direction. The X-ray diffraction study of Fuji et al. (2000) showed that colloidal CaCO_3 particles exposed (001) surface. It means that the spindle CaCO_3 is formed by aggregation of colloidal CaCO_3 , and (001) surface has significant role in forming spindle shape. Thus, the primary particles of spindle CaCO_3 have layer structure of alternate planes of (001)Ca and (001)CO₃, as a result they have heterogeneous surface charge. This heterogeneous surface charge might influence the aggregation of primary particle.

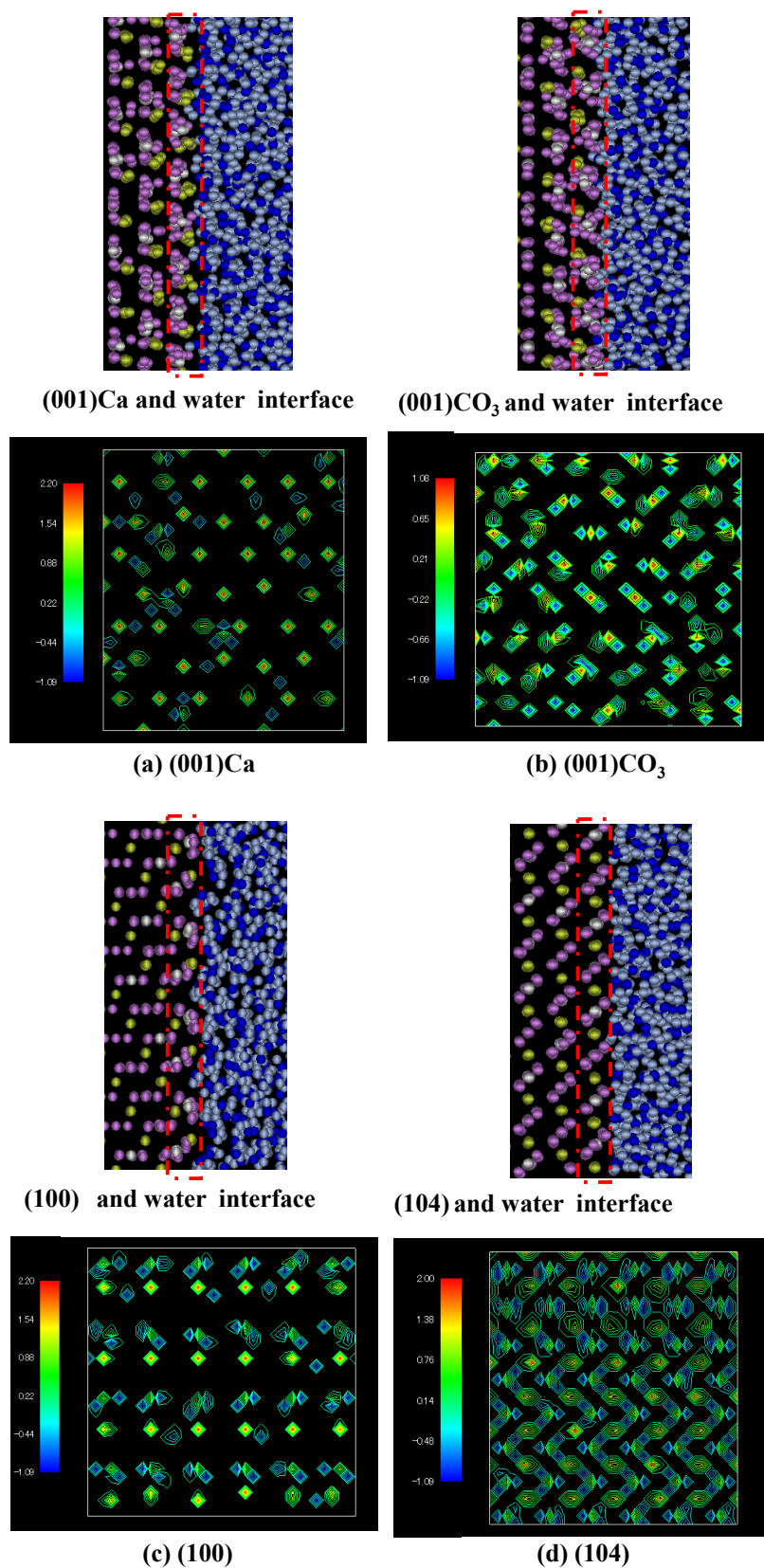


Figure 2-9 Charge density profiles on CaCO₃ crystal surface contacted with water

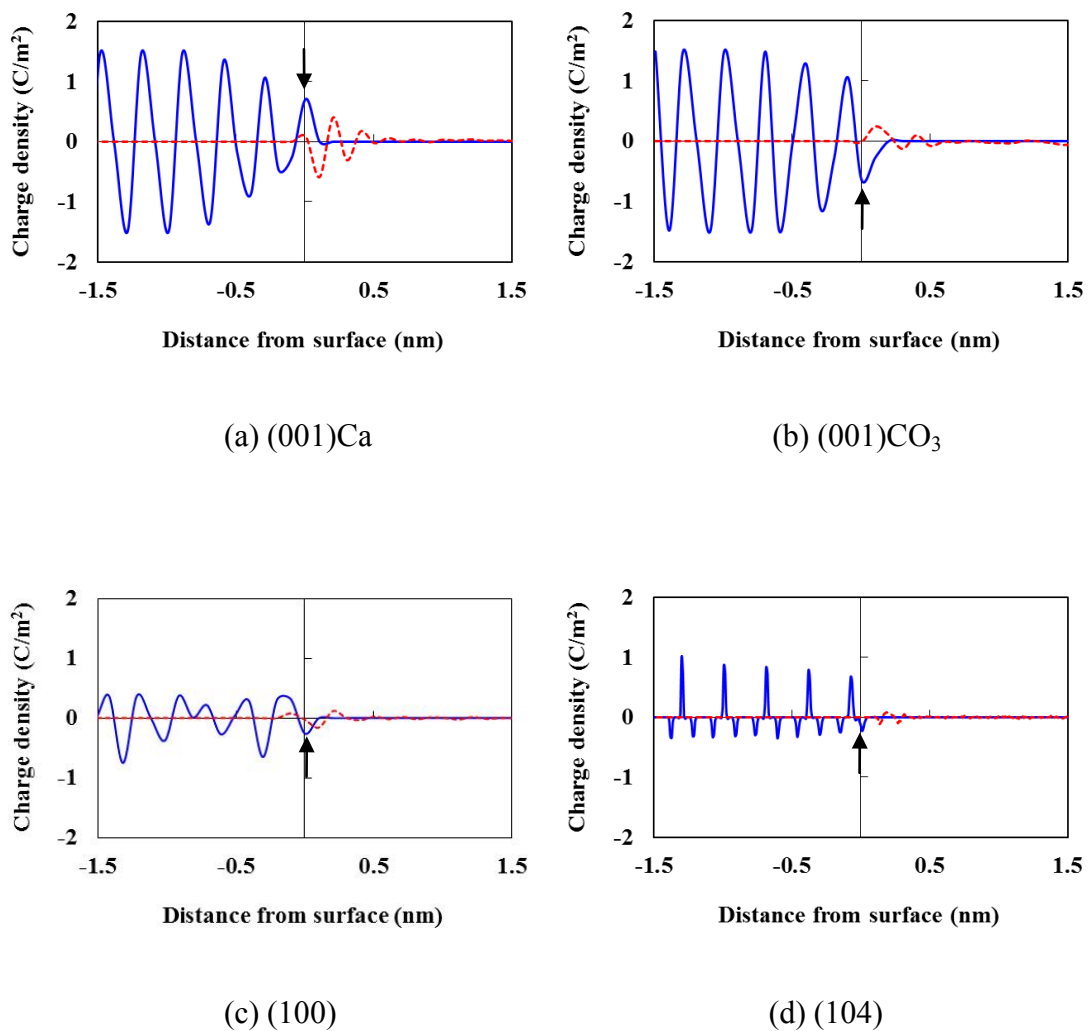


Figure 2-10 Charge densities of CaCO₃ and water. Blue solid line and red dashed line indicates CaCO₃ and water, respectively. Charge densities in arrow point were used in section 3.2 (Table 3-1).

2.3.3 Self-diffusion coefficient and dielectric constant

Water molecules are more strained and structured with being smaller inter particle distance because the force from crystal surface becomes stronger. Self-diffusion coefficient D is calculated by

$$D = \lim_{t \rightarrow \infty} \frac{1}{6t} \langle |\mathbf{r}(t) - \mathbf{r}(0)|^2 \rangle \quad (2-6)$$

where $\mathbf{r}(t)$ is the position vector at t and the bracket $\langle \rangle$ expresses statistical average. The self-diffusion coefficients of water between surface distances shown in Figure 2-11 were calculated to discuss their mobility as a function of separation distance from the surface. The water molecules were constrained with decreasing in the distance between surfaces, resulting the decrease of the self-diffusion coefficients in all surfaces. The water molecules were structured with keeping their orientation near the crystal interface. Although water molecular structures have large difference as mentioned in section 2.3.1, there is no significant difference of the mobility of water molecules in all surfaces. Consequently, it has a cause to change the dielectric constant of water and to affect the aggregation structure.

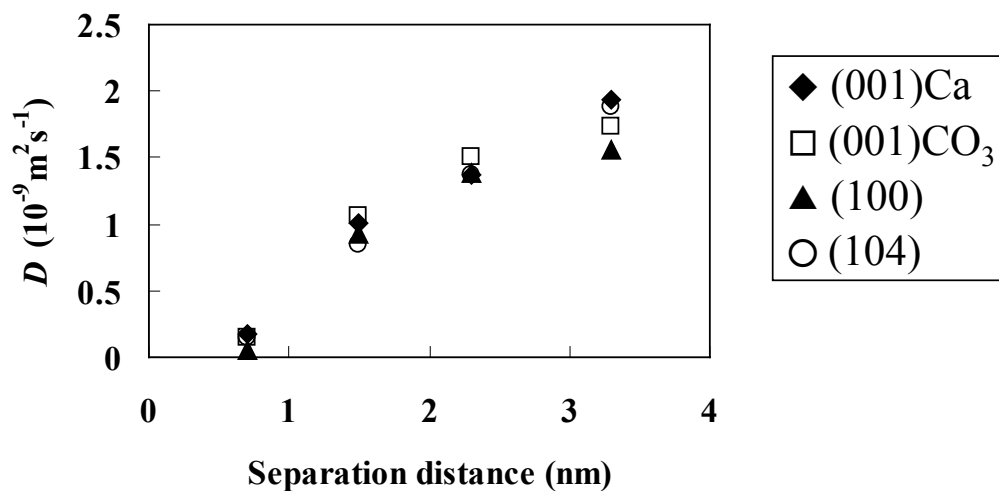


Figure 2-11 Diffusion coefficient on the conditions of different separations. Diffusion coefficient of SPC/E water model is $2.5 \times 10^{-9} \text{ m}^2 \text{ s}^{-1}$ (Berendsen, et al., 1987).

Electrostatic potential and Hamaker constant are a function of dielectric constants. Variation of dielectric constants changes total potential and it affects aggregation structure. Investigation of the variation in dielectric constant as a function of distance between CaCO_3 surfaces was carried out. Dielectric constants were calculated from fluctuations in total dipole moment $\langle M^2 \rangle$ of a system (Neumann, 1983)

$$M = \sum_{i=1}^N \mu_i \quad (2-7)$$

$$\varepsilon = 1 + \frac{4\pi}{3} \frac{\langle M^2 \rangle}{VkT} \quad (2-8)$$

where μ is dipole of a water molecule and V is volume of the system. The dielectric constant as a function of distance between CaCO_3 surfaces is displayed in Figure 2-12. The dielectric constants were gradually increasing with the increase of distance between the surfaces in the case of (001)Ca, (100) and (104) surfaces. However, the value of

dielectric constant rapidly increased when distance between surfaces became long from 0.7nm to 1.5 and 2.3nm in the case of (001)CO₃ and more than 2.3 nm the dielectric constant of SPC/E approached 70, which was similar to the previous simulation results (Reddy and Berkowitz, 1989; Martí et al., 2006). Their results showed that the dielectric constants changed 85, 71 and 232 with decreasing the distance between graphite surfaces, 3.1, 1.5 and 1.2 nm, respectively. When the distance between graphite surfaces was 1.2 nm, the dielectric constant became abnormally large value. They concluded that this result was attributed to the strong orientational order of water molecules. Thus, the simulation result of the dielectric constants for (001)CO₃ was also caused by strong orientational order of water molecules.

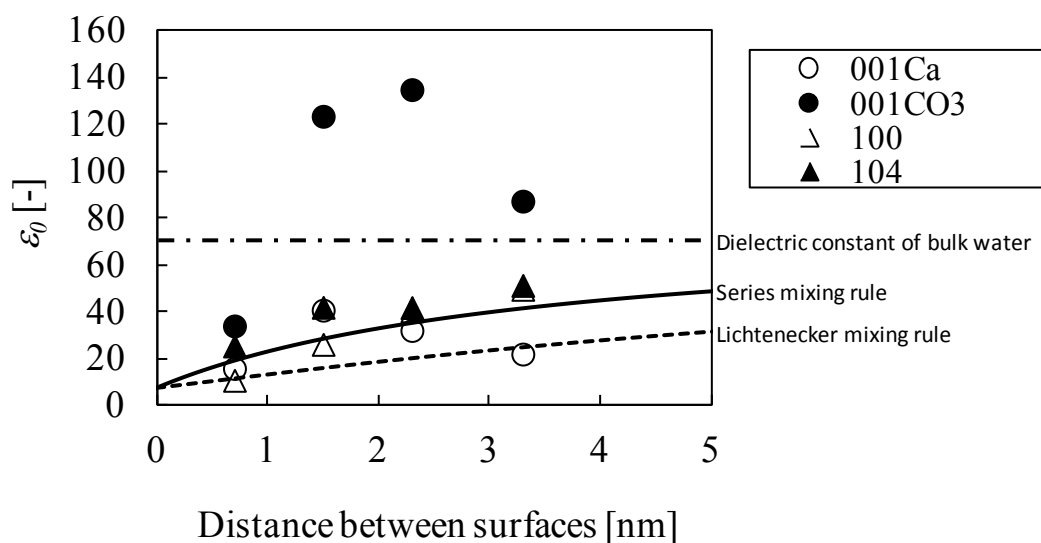


Figure 2-12 Lichtenecker and Series mixing rules fit to dielectric constant calculated by MD simulation.

The dielectric constants were estimated using Lichtenecker and series mixing rules, it was compared with the value calculated by MD simulation (Figure 2-12). The mixing rules are given by follows (Habeger et al., 1997):

$$\log(\varepsilon) = \nu_1 \log(\varepsilon_1) + \nu_2 \log(\varepsilon_2) \quad \text{Lichtenecker mixing rule} \quad (2-9)$$

$$\varepsilon = \nu_1 \varepsilon_1 + \nu_2 \varepsilon_2 \quad \text{Series mixing rule} \quad (2-10)$$

where ε and ν represent dielectric constant and volume fraction, and subscript 1 and 2 denote CaCO_3 and water, respectively. The variation in dielectric constants of water against (001)Ca, (100) and (104) calculated by MD simulation was in good agreement with the series mixing rule, while dielectric constant of (001) CO_3 had a specific behaviour and it seemed that extraordinary change of the dielectric constant caused the anisotropic aggregation process of CaCO_3 particles. Sinyagin et al. (2006) have investigated the effect of dielectric constant using a distance-dependent model predicted by the Lichtenecker mixing rule on aggregation of nano particles. Therefore, it is concluded that the variation of dielectric constant may have an important role to determine the aggregation structure of CaCO_3 particles.

2.3.4 Grain boundary energy in aggregation process

Grain boundary energy can be calculated to investigate change of energy in an aggregation process of primary particles. The grain boundary energy (γ_b) of interface between CaCO_3 particles was calculated using;

$$\gamma_b = \frac{U_{gb} - U_0}{2A_{gb}} \quad (2-11)$$

where U_{gb} is total energy including grain boundary, U_0 is total energy of monocrystal structure without grain boundary, A_{gb} is cross section area of interface (Suzuki and

Matsubara, 1999). The grain boundary energy for each interface was shown in Figure 2-13 as a function of gap between the surfaces. Five boundary types in pairs of crystal surfaces were calculated. The change of energy was evaluated by changing the surface gap from 0.5 nm to 0.1 nm. The energy of interface between (001)Ca and (001)Ca surface was the highest among five types of interface. On the other hand, that of interface between (001)Ca and (001)CO₃ was the lowest among five types of interfaces. With considering above these results, it indicates that the aggregation of (001)Ca and (001)CO₃ surface can stabilise aggregated particles among all types of interfaces.

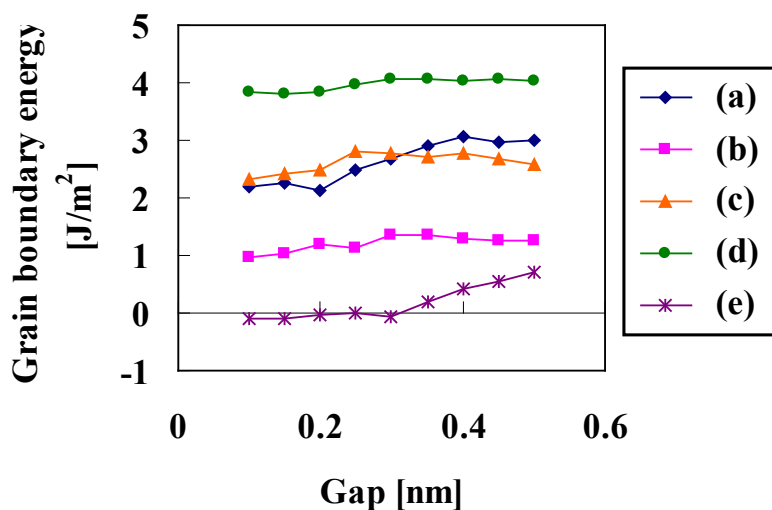


Figure 2-13 Grain boundary energy of crystal interface. (a) (001)Ca-(104), (b) (100)-(104), (c) (001)Ca-(100), (d) (001)Ca-(001)Ca, (e) (001)Ca-(001)CO₃

2.4 Conclusion

The formation mechanism of spindle CaCO_3 has been investigated by molecular dynamics simulation. MD simulation was performed to investigate the differences of surface properties among four main crystal surfaces of CaCO_3 , (001)Ca, (001) CO_3 , (100) and (104) surfaces. In consequence, (001)Ca and (001) CO_3 charged positively and negatively. On the other hand, (100) and (104) charged neutrally. From the result of the dynamics of water molecules, the water molecules were more confined with decreasing the separation distance because water molecules were structured by the force from the crystal surface. The structured water molecules influenced the dielectric constant of water. When distance between surfaces was small, dielectric constant of water became small except (001) CO_3 and it was increased in the case of (001) CO_3 . The boundary energy was calculated to investigate the change of energy in an aggregation process of primary particles. The boundary energy of interface between (001)Ca and (001) CO_3 was the lowest among five types of interfaces. It indicates that the aggregation of (001)Ca and (001) CO_3 surface is easiest among all types of interfaces.

References

- Arai, Y., Yasue, T., 1989. Synthesis and shape control of powder material by liquid phase reaction. *Powder sci eng.* 4, 62-71.
- Arai, Y., Yasue, T., 1990. Controls of crystal shape and modification in preparation of calcium carbonate. *Gypsum & Lime.* 228, 291-301.
- Arakawa, M., 2004. Nanotechnology in taisho age and characterization in showa age-preparation of nanoparticles of CaCO_3 . *J Soc Powder Technol, Jpn.* 41, 25-33.
- Bacher, C., Olsen, P.M., Bertelsen, P., Kristensen, J., Sonnergaard, J.M., 2007. Improving the compaction properties of roller compacted calcium carbonate. *Int J Pharm.* 342, 115-123.
- Berendsen, H.J.C., Grigera, J.R., Straatsma, T.P., 1987. The missing term in effective pair potentials. *J Phys Chem.* 91, 6269-6271.
- Carmona, J.G., Morales, J.G., Clemente, R.R., 2003. Morphological control of the precipitated calcite obtained by adjusting the electrical conductivity in the $\text{Ca}(\text{OH})_2\text{-H}_2\text{O-CO}_2$ system. *J Cryst Growth.* 249, 561-571.
- Cheng, B., Lei, M., Yu, J., Zhao, X., 2004. Preparation of monodispersed cubic carbonate particles via preparation reaction. *Mater Lett.* 58, 1565.
- Chikazawa, M., Fuji M., 2001. Nano particles of lime and calcium carbonate. *J Soc Inorg Mater, Jpn.* 8, 507-514.
- Duffy, D.M., Harding, J.H., 2002. Modeling the interfaces between calcite crystals and Langmuir monolayers. *J Mater Chem.* 12, 3419-3425.
- Ewald, P.P., 1921. Die berechnung optischer und elektrostatischer gitterpotentiale. *Annalen der Physik.* 64, 253-287.
- Fuji, M., Kobayashi, H., Takei, T., Watanabe, T., Chikazawa, M., Watanabe, T., Tanabe, K., 2000. Characteristic Surface Properties of Colloidal Calcium Carbonate. Existing Surface Hydroxide Ion and Its Properties. *J Soc Inorg Mater, Jpn.* 7, 13-18.
- Geissbühler, P., Fenter, P., DiMasi, E., Srajer, G., Sorensen, L.B., Sturchio, N.C., 2004. Three-dimensional structure of the calcite–water interface by surface X-ray scattering. *Surf Sci.* 573, 191-203.
- Habeger, C.F., Condon, C.E., Khan, S.R., Adair, J.H., 1997 Evaluation of the calcium oxalate monohydrate Hamaker constant based on static dielectric constant determination and electronic polarization. *Colloids Surf B.* 10, 13-21.
- Juvekar, V.A., Sharma, M.M., 1943. Absorption of CO_2 in a suspension of lime. *Chem Eng Sci.* 28, 825-837.
- Kadota, K., Yamamoto, T., Shimosaka, A., Shirakawa, Y., Hidaka, J., Kouzu, M., 2011.

- Aggregation modeling of calcium carbonate particles by Monte Carlo Simulation. *J Nanoparticle Res.* 13, 7209-7218.
- Kerisit, S., Cooke, D.J., Spagnoli, D., Parker, S.C., 2005 Molecular dynamics simulations of the interactions between water and inorganic solids. *J Mater Chem.* 15, 1454-1462.
- Kim, W.S., Hirasawa, I., 2004. Polymorphic change of calcium carbonate during reaction crystallization in a batch reactor. *Ind Eng Chem Res.* 43, 2650-2657.
- Kitamura, M., Konno, H., Yasui, A., Matsuoka, H., 2002. Controlling factors and mechanism of reactive crystallization of calcium carbonate polymorphs from calcium hydroxide suspensions. *J Cryst Growth.* 236, 323-332.
- Kojima, Y., Kawanobe, A., Yasue, T., Arai, Y., 1994. Controls of polymorphism and morphology of calcium carbonate compounds formed by crystallizing amorphous. *J Ceram Soc Jpn.* 102, 1128-1136.
- Kristensen, J., Hansen, V.W., 2006. Wet Granulation in Rotary Processor and Fluid Bed: Comparison of Granule and Tablet Properties. *AAPS PharmSciTech.* 7, Article 22.
- Leeuw, N.H., Parker, S.C., 1997. Atomistic simulation of the effect of molecular adsorption of water on the surface structure and energies of calcite surfaces. *J Chem Soc, Faraday Trans.* 93, 467-475.
- Leeuw, N.H., Parker, S.C., 1998 Surface structure and morphology of calcium carbonate polymorphs calcite, aragonite, and vaterite: An atomistic approach. *J Phys Chem B.* 102, 2914-2922.
- Leeuw, N.H., Parker, S.C., Harding, J.H., 1999. Molecular dynamics simulation of crystal dissolution from calcite steps. *Phys Rev B.* 60, 13792-13799.
- Li, J., Tao, L., Dali, M., Buckley, D., Gao, J., Hubert, M., The Effect of the Physical States of Binders on High-Shear Wet Granulation and Granule Properties: A Mechanistic Approach Toward Understanding High-Shear Wet Granulation Process. Part II. Granulation and Granule Properties. *J Pharm Sci.* 100, 294-310.
- Martí, J., Nagy, G., Guàrdia, E., Gordillo, M.C., 2006. Molecular dynamics simulation of liquid water confined inside graphite channels: Dielectric and dynamical properties. *J Phys Chem B.* 110, 23987-23994.
- Matsushita, I., Seikita, T., Suzuki, T., Moriga, T., Ashida, T., Nakabayashi, I., 1993. Effects of Ca^{2+} and OH^- ions on the process of calcium carbonate synthesis and its crystallization. *J Soc Mater Sci, Jpn.* 42, 195-201.
- Neumann, M., 1983. Dipole moment fluctuation formulas in computer simulations of polar systems. *Molecular Physics.* 50, 841-858.

- Park, S., Choi, W.S., 2004. Effects of operating factors on the particle size distribution and particle shape of synthesized precipitated CaCO_3 : effect of reaction temperature, blowing rate of CO_2 gas and initial slurry concentration of $\text{Ca}(\text{OH})_2$ on reaction completion time. *Adv Powder Technol.* 15, 1-12.
- Pavese, A., Catti, M., Price, G.B., Jackson, R.A., 1992. Interatomic potentials for CaCO_3 polymorphs (calcite and aragonite), fitted to elastic and vibrational data. *Phys Chem Miner.* 19, 80-87.
- Preisig, D., Haid, D., Varum, F.J.O., Bravo, R., Alles, R., Huwyler, J., Puchkov, M., 2014. Drug loading into porous calcium carbonate microparticles by solvent evaporation. *Euro J Pharm Biopharm.* 87, 548-558.
- Reddy, M.M., Nancollas, G.H., 1976. The crystallization of calcium carbonate: IV. The effect of magnesium, strontium and sulfate ions. *J Cryst Growth.* 35, 33-38.
- Reddy, M.R., Berkowitz, M., 1989. The dielectric constant of DPC/E water. *Chem Phys Lett.* 155, 173-176.
- Rowe, R.C., Sheskey, P.J., Quinn, M.E., (Eds.) 2009. *Handbook of Pharmaceutical Excipients*. Sixth Edition. RPS Publishing, pp.86-89.
- Serra, M.D., Robles, L.V., 2003. Compaction of agglomerated mixtures of calcium carbonate and microcrystalline cellulose. *Int J Pharm.* 258, 153-164.
- Sinyagin, A.Y., Belov, A., Tang, Z., Kotov, N.A., 2006. Monte carlo computer simulation of chain formation from nanoparticles. *J Phys Chem B.* 110, 7500-7507.
- Suzuki, H., Matsubara, H., 1999. Molecular dynamics simulation on Al_2O_3 grain boundaries with Mg, Ca and Si segregation. *J Ceram Soc Japan.* 107, 727-732.
- Wang, J., Kalinichev, A.G., Kirkpatrick, R.J., 2004. Molecular modeling of water structure in nano-pores between brucite (001) surfaces. *Geochimica et Cosmochimica Acta.* 68, 3351-3365.
- Yamada, H., Hara, N., 1985. Formation process of colloidal calcium carbonate in the reaction of the synthesis of $\text{Ca}(\text{OH})_2\text{-H}_2\text{O-CO}_2$. *Gypsum & Lime.* 194, 3-12.
- Yu, S.H., Colfen, H., Xu, A.W., Dong, W.F., 2004. Complex spherical BaCO_3 superstructures self-assembled by a facile mineralization process under control of simple polyelectrolytes. *Crystal Growth & Design.* 4, 33-37.
- Zhang, Q., Ren, L., Sheng, Y., Ji, Y., Fu, J., 2010a. Control of morphologies and polymorphs of CaCO_3 via multi-additives system. *Mater Chem Phys.* 122, 156-163.
- Zhang, L., Bai, S., Sun, Y., 2010b. Molecular dynamics simulation of the effect of ligand homogeneity on protein behavior in hydrophobic charge induction

chromatography. *Journal of Molecular Graphics and Modelling*. 28, 863-869.

Chapter 3

Formation mechanism of spindle-shaped calcium carbonate particles in the solution using cluster-moving Monte Carlo simulation

3.1 Introduction

As described in *Chapter 2*, MD simulations make it possible to simulate nano-scale phenomena in nano-seconds and to expose specific crystal faces. The effect of surface properties including the charge density and the dielectric constant of water on the aggregation process was investigated using MD simulations. In addition to MD simulations, MC simulations have advantages of removing particles overlapping and preventing calculation from diverging. These advantages are useful for understanding aggregation in colloidal or suspension systems (Satoh et al., 1996a, 1996b; Kristof and Szalai, 2003; Aoshima and Satoh, 2004). A conventional metropolis MC simulation is difficult to calculate the aggregation phenomena when the interaction between particles is strong for forming chain-like structure. The chain-like cluster formation was not observed by the conventional MC simulation since it was not suitable for the strongly interactions between particles. It is difficult to form larger clusters because the conventional MC simulation prevents particles from separating the cluster (Coverdale et al., 1993, 1994). The development of algorithm, which a cluster is moving as a particle, is indispensable for realizing the aggregation phenomena. Aoshima and Satoh (2004, 2006) proposed a cluster-moving MC algorithm to capture aggregation structures of ferromagnetic particles. Their results provided that the thicker chain-like clusters formed in the applied magnetic field with increasing strength of magnetic interactions between particles. Simulation results showed that clusters possess a complicated internal structure as network.

The objective of this chapter is to elucidate the aggregation mechanism of the primary CaCO_3 particles at micro-level. A cluster-moving MC simulation has been carried out to investigate the dispersion and aggregation state of primary particles using

the surface charge density determined by the results of *Chapter 2*.

3.2 Simulation details

Table 3-1 shows the surface charge density calculated by the previous MD simulations. These results of charge density on the crystal surface were utilised to perform the cluster-moving MC simulation. The conventional MC simulation as mentioned above is difficult to duplicate the aggregation phenomena where particles formed chain-like structure owing to the strong interaction between particles. The clusters are slow to grow because the algorithm prevents particles from separating from the cluster. The cluster-moving MC algorithm was applied to calculate the aggregation structure of CaCO₃ particles. Satoh (1992) proposed this algorithm to capture aggregate structures of particles. This algorithm has been successful in simulating the aggregation of ferromagnetic particles (Aoshima and Satoh, 2004, 2006). The clusters defined by a separation distance is attempted to move randomly every 10 MC steps. The clusters move with a transition probability as well as Metropolis's method. Aggregated particles are regarded as a cluster in this algorithm. The potential function in this algorithm is

Table 3-1 Charge density at each surface calculated by MD simulation. Charge densities were calculated using arrow point in Figure 2-10.

Surface	Charge density (C/m ²)
(001)Ca	0.711
(001)CO ₃	-0.637
(100)	-0.258
(104)	-0.190

based on the DLVO theory which took into account van der Waals and electrostatic interaction (Deraguin and Landau, 1993; Verwey and Overbeek, 1948). Thus, the dispersion and aggregation state of particles were determined by the sum of two interactions. Van der Waals interaction V_A between two particles is given by (Israelachivili, 1991):

$$V_A = -\frac{A}{6} \left\{ \frac{2a^2}{r^2 - 4a^2} + \frac{2a^2}{r^2} + \ln \frac{r^2 + 4a^2}{r^2} \right\} \quad (3-1)$$

where a is particle radius and r is centre-to-centre particle distance. A is the Hamaker constant calculated using Lifshitz's theory (Dzyaloshinskii et al., 1961)

$$A = \frac{3kT}{4} \left(\frac{\varepsilon_1 - \varepsilon_2}{\varepsilon_1 + \varepsilon_2} \right)^2 (2\kappa s) \exp(-2\kappa s) + \frac{3h\nu_e}{16\sqrt{2}} \frac{(n_{R1}^2 - n_{R2}^2)^2}{(n_{R1}^2 + n_{R2}^2)^{3/2}} \quad (3-2)$$

where s is the separation distance, k is Boltzmann constant, T is absolute temperature, h is Planck's constant, n_R is refractive index, ε is dielectric constant, ν_e is the main electronic absorption frequency in ultraviolet region. Subscripts 1 and 2 denote CaCO_3 and water, respectively. The first term in equation (3-2) is the screening effect of the electrolytes on van der Waals interaction and the second term in equation (3-2) is dispersion energy contribution. $3 \times 10^{15} \text{ s}^{-1}$ is used as a typical value of ν_e (Davis et al., 1999; Sinyagin et al., 2006). According to the DLVO theory, the electrostatic interaction with low surface charge ($\psi_0 < 100 \text{ mV}$) is given by:

$$V_C = 4\pi\varepsilon\varepsilon_0 a \psi_0^2 \exp(-\kappa s) / r \quad (\kappa a < 10) \quad (3-3a)$$

$$V_C = 2\pi\varepsilon\varepsilon_0 a \psi_0^2 \ln[1 + \exp(-\kappa s)] \quad (\kappa a > 10) \quad (3-3b)$$

where ε_r is permittivity of vacuum, Ψ_0 is surface potential, and κ is Debye screening factor. In the present calculation, it was assumed the primary particle as cubic model

with the heterogeneously charged surfaces from surface charge density determined by Chapter 2. It is necessary to state how to decide the value of surface charge density in the cluster-moving MC simulation. Because positive ions have negative ions nearby, the electric field becomes screened and decays rapidly with distance from ions compared with an isolated ion (Mahanty and Ninham, 1976). The force from ions in the bulk is screened and it does not influence the interaction between particles. The surface charge density at the first layer of CaCO₃ crystal was used to calculate the MC simulation, assuming that the interactions from ions at position larger than second layer are negligible since the calcite model particle has layer structure of positive and negative ions. Figure 3-1 shows the crystalline structure of calcite. The surface charge distribution was provided for the unit particles in accordance with the layered structure of calcite crystalline in the hexagonal system as shown in Figure 3-1. Figure 3-2 shows heterogeneous charge distribution of the cubic primary particles: (a) surface charge density of (001)Ca on upper and lower surfaces, (b) surface charge density of (001)CO₃ on upper and lower surfaces and surface charge density of (100) was applied on four side surfaces. The (104) surface is the most stable surface of calcite. It consists of layers of calcium, carbon and one oxygen atom in a plane with the other two oxygen atoms above and below this plane as illustrated in Figure 3-1. However, the spindle CaCO₃ particles generated by the aggregation of primary CaCO₃ particles in the process of transformation from amorphous to calcite crystals (Arakawa, 2004; Yamada and Hara, 1985). The point charge varies depending on the surface area of particles. The point charges put on the centre of the surface. The energy arising from point charge – point charge is calculated by screening Coulomb potential:

$$V_c = \frac{q_i q_j e^2}{4\pi\epsilon_0 \epsilon r} e^{-r\kappa} \quad (3-4)$$

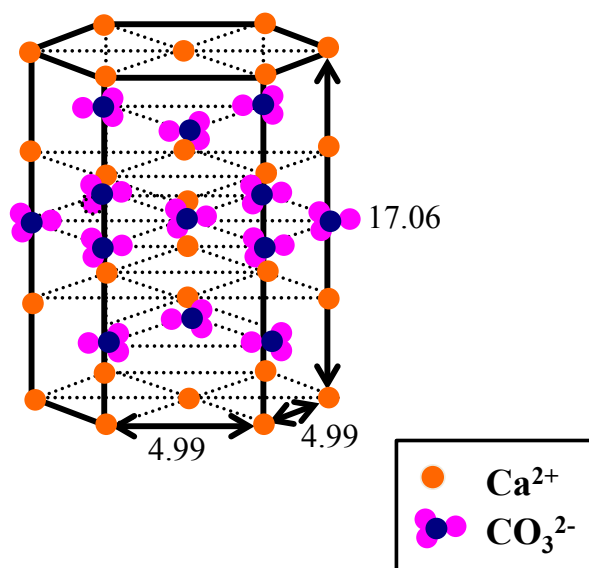


Figure 3-1 Crystalline structure of calcite in rhombic system.

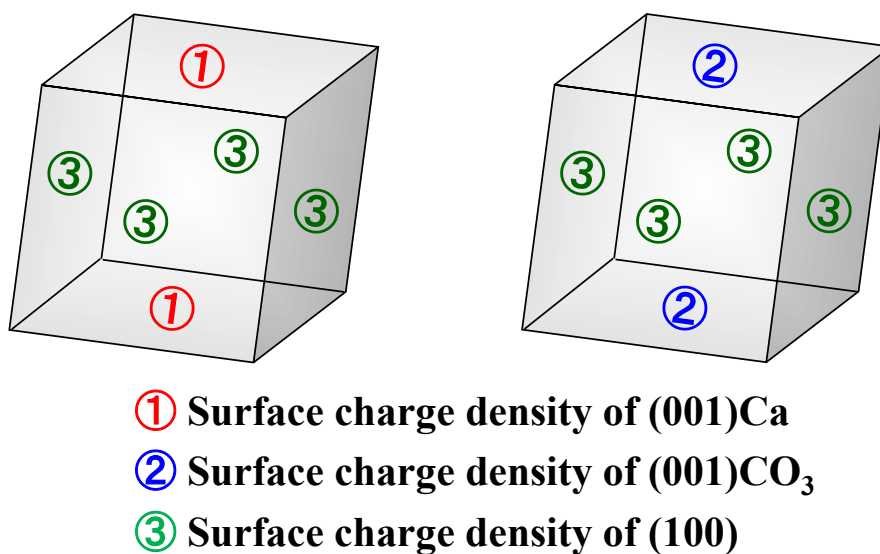


Figure 3-2 Basic cell model for the calculation of MC simulation. The point charges put on the centre of the surface calculated by multiplying surface charge density by area of the surface.

Additionally, Born repulsive potential V_B is adopted to avoid unnatural overlap among particles (Davis et al., 1999).

$$V_B = c_B \exp(-r/\sigma_B) \quad (3-5)$$

where c_B and σ_B are adjustable constants, these values were assumed in order that the minimum value of V_{TOT} is equal to $-20kT$ because a potential barrier of 15-20 kT is sufficient to ensure colloidal stability according to the classical DLVO theory (García et al., 2006). Born repulsive potential is very short range interaction and increasing very sharply as two particles get closer. The total potential of the simulated system V_{TOT} was given by:

$$V_{TOT} = V_A + V_C + V_B \quad (3-6)$$

Angle of the particles is important when the particles have heterogeneous charge. The particles are initially located on the face-centred cubic lattice. Particle size and Particle size distribution were 43 nm and 0.12, respectively, which were determined in the previous experimental result (Kadota et al., 2011).

3.3 Results and discussion

3.3.1 Formation of spindle-shape CaCO_3 by cluster-moving MC simulation

CaCO_3 primary particles were modelled by the cubic particles with surface charge densities obtained from *Chapter 2*. The aggregation structure was analysed using the cluster-moving MC simulation to investigate the aggregation mechanism of CaCO_3 primary particles. Figure 3-3(a) shows a snapshot calculated by means of the cluster-moving MC simulation after equilibrium state. Figure 3-3(b) shows an enlarged view of formed clusters. CaCO_3 clusters with spindle-shape were formed by the aggregation of primary particles as can be seen from Figure 3-3. Matsushita et al. (1993)

revealed that small CaCO_3 particles generated in the early stage of reaction were amorphous and chain-like particles were calcite polymorphs by experimental approaches. These results show that the spindle-shaped structures were formed as calcite particles, not amorphous particles, tend to aggregate in the same direction. Fuji et al. (2000) investigated the surface of colloidal CaCO_3 particles by X-ray diffraction. Since they revealed that the spindle-shaped CaCO_3 clusters were formed by aggregation of colloidal CaCO_3 particles, the surface of colloidal CaCO_3 particles had significant role in forming spindle-shape. The size of clusters formed by the aggregation was calculated in order to comprehend the structure of cluster. The longest distance between particles in the cluster was regarded as the length of clusters. The spindle-shaped clusters were considered as the configuration combined two cones of which the diameter was regarded as the width of clusters. The length and width distribution forming clusters is shown in Figure 3-4(a). The width distribution of clusters had a sharp peak at smaller size than the length distribution of clusters. These results indicate that the growth of clusters proceed in one direction. However, the length and width of clusters simulated by the cluster-moving MC simulation are 176.7 nm and 55.9 nm, respectively, which are smaller than those of experiments because of the small calculated system. On the other hand, the aspect ratio distribution described in Figure 3-4(b) showed that the average aspect ratio 3.07 obtained from a cluster-moving MC simulation was good agreement with the experimental result (Arakawa, 2004; Kadota et al., 2011). The cluster-moving MC simulation is successful in evaluating the aggregation structure of spindle-shaped CaCO_3 clusters. Most primary particles were oriented along with crystallographic direction in calcite, which was consistent with the results measured using electron microscope (Fuji et al., 2000). Figure 3-5 provides the

distribution of the number of particle forming clusters. There are numerous clusters consist of below five particles. This can be explained by the difference in solubility between the different sizes of colloidal CaCO_3 particles. The higher solubility of smaller sized particles and lower solubility of larger sized particles was responsible for creating a concentration gradient, which resulted in Ostwald ripening (Kitamura, 1989). CaCO_3 fine particles generated in the early stage of reaction as described above are amorphous and chain-like particles are calcite polymorphs. The spindle-shaped CaCO_3 clusters grow by repeated creation and extinction of fine particles. Figure 3-6 provides a plot of particle size with length, width and aspect ratio against the number of particles forming clusters. The aspect ratio increased because the major axis increase in length as the number of particles composed of clusters increases. These results indicated that the primary particles aggregated in the same direction.

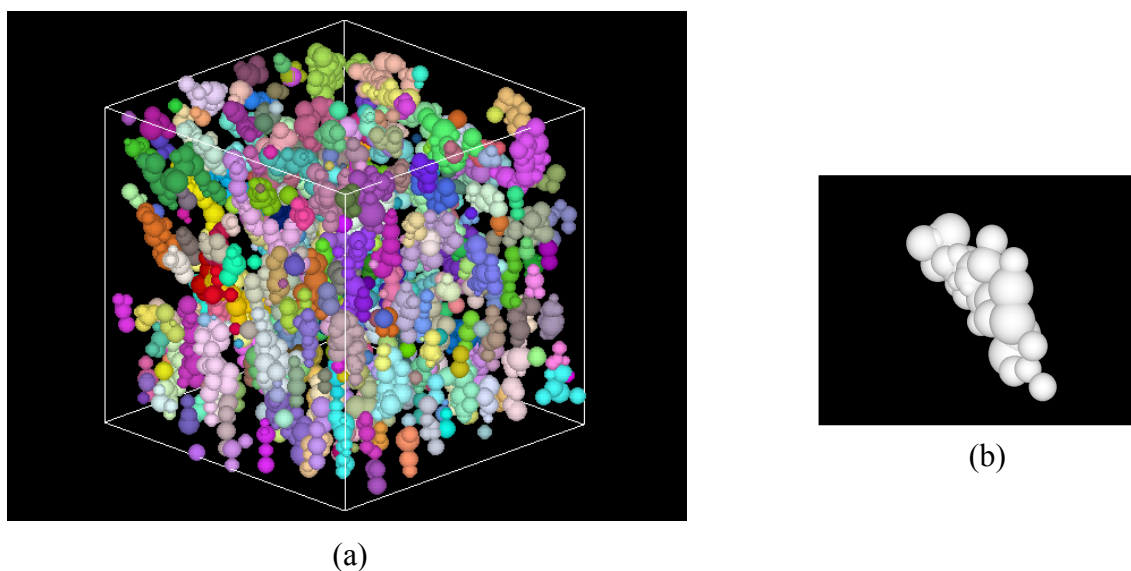


Figure 3-3 Snapshots of aggregate structure of the primary particles. (a) Overview in basic cell (b) A cluster formed by aggregation of the primary particles.

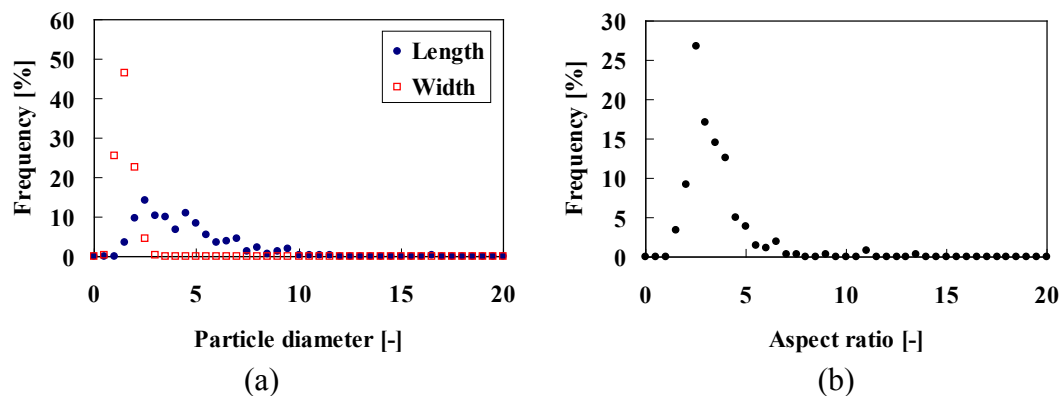


Figure 3-4 Particle size distributions of cluster. (a) Length and width distributions of cluster (b) Aspect ratio distribution of cluster.

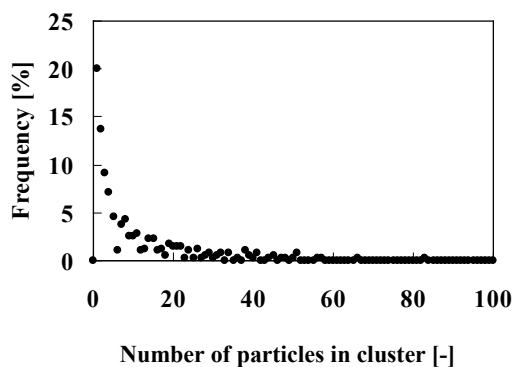


Figure 3-5 Distribution of the number of particles in cluster.

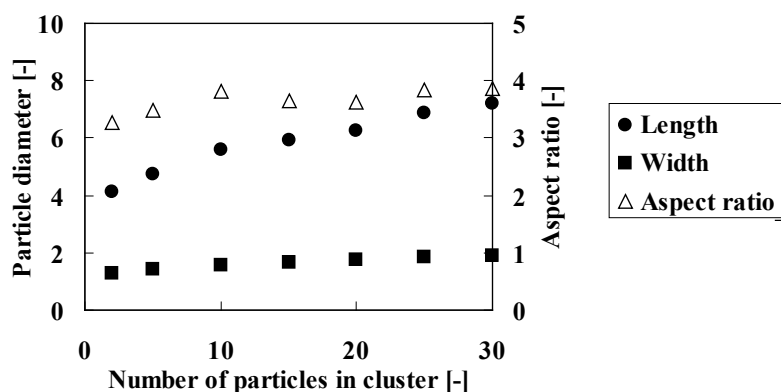


Figure 3-6 Length, width and aspect ratio on different definitions of number of particles in cluster.

3.3.2 Analysis of point charges in the clusters

Figure 3-7 shows snapshots of a cluster, which formed by the primary particles with positive and negative charges. The charge calculated by MD simulations (as shown in Table 3-1) was given on the crystal surface of primary particles. It was found that positive charge on the surface attracted with negative charge on the surface as illustrated in Figure 3-7. As the aggregation of CaCO_3 particles preceded, the CaCO_3 particle grew by attracting each positive and negative charge. The aggregation between colloidal CaCO_3 particles can be approximated as the adhesion of a small particle onto a large cluster. The distance between charges on the particle in all clusters was assessed in Figure 3-8. Figure 3-8 clearly showed that clusters were formed by the connection of positive and negative charges. The calcite crystals have the hexagonal structures because the (104) surface is the most stable surface of calcite crystals. It consists of layers of calcium, carbon and one oxygen atom in a plane with the other two oxygen atoms above and below this plane. In the process of calcite crystal growth, it is concluded that the primary CaCO_3 particles are aggregated in the same direction by connecting the primary particles thorough coulombic force on the surface arising from the existence of high population of (001)Ca and (001)CO₃ in the primary particles.

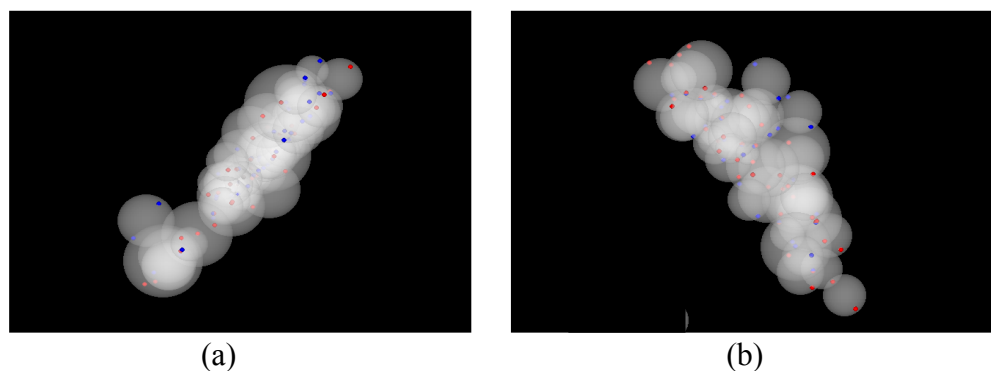


Figure 3-7 Snapshots of cluster with the negative and positive surface charge.

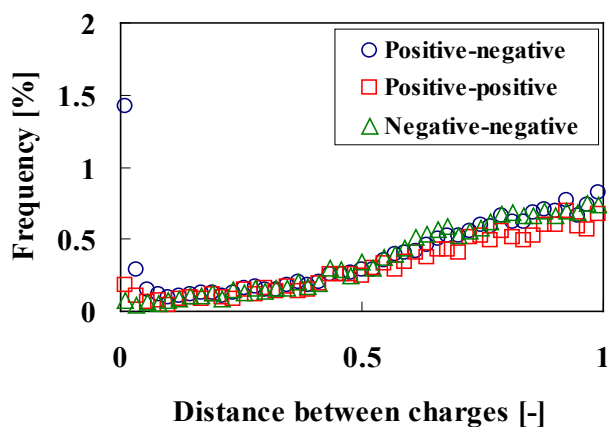


Figure 3-8 Distance between charges in all clusters. Distance between charges is normalised by dividing each distance by the mean primary particle size.

3.4 Conclusion

The formation mechanism of spindle-shaped CaCO_3 has been investigated by a cluster-moving MC simulation. Cubic particles with charge points obtained from MD simulations were modelled as a CaCO_3 primary particle and the aggregation structure was analysed using the cluster-moving MC simulation. I could success in realizing the aggregation process of spindle-shaped CaCO_3 particles by the cluster-moving MC

simulation. The aggregation of primary particles resulted in formation of spindle-shaped CaCO_3 clusters. The width distribution of clusters had a sharp peak at smaller region than the length distribution of clusters. The aspect ratio obtained from cluster-moving MC simulations showed good agreement with the previous experimental result. Many particles forming clusters aggregated with the orientation in the same direction because positive and negative charges attracted each other. Hybrid simulations between MD simulations and cluster-moving MC simulations would give us the promising design methods for aggregation process.

References

- Aoshima, M., Satoh, A., 2004. Two-dimensional Monte Carlo simulations of a polydisperse colloidal dispersion composed of ferromagnetic particles for the case of no external magnetic field. *J Colloid Interface Sci.* 280, 83-90.
- Aoshima, M., Satoh, A., 2006. Two-dimensional Monte Carlo simulations of a colloidal dispersion composed of rod-like ferromagnetic particles in the absence of an applied magnetic field. *J Colloid Interface Sci.* 293, 77-87.
- Arakawa, M., 2004. Nanotechnology in taisho age and characterization in showa age-preparation of nanoparticles of CaCO₃. *J Soc Powder Technol, Jpn.* 41, 25-33.
- Coverdale, G.N., Chantrell, R.W., Hart, A., Parker, D., 1993. A 3-D simulation of a particulate dispersion. *J Magnet Magnetic Mater.* 120, 210-212.
- Coverdale, G.N., Chantrell, R.W., Hart, A., Parker, D., 1994. A computer simulation of the microstructure of a particulate dispersion. *J Appl Phys.* 75, 5574-5576.
- Davis, S.W., McCausland, W., McGahagan, H.C., Tanaka, C.T., Widom, M., 1999. Prediction of stable insulating intermetallic compounds. *Phys Rev E.* 59, 2424-2428.
- Deraguin, B., Landau, L., 1993. Theory of the stability of strongly charged lyophobic sols and of the adhesion of strongly charged particles in solutions of electrolytes. *Prog Surf Sci.* 43, 30-59.
- Dzyaloshinskii, I.E., Lifshitz, E.M., Pitaevskii, L.P., 1961. The general theory of van der Waals forces. *Adv Phys.* 10, 165-209.
- Fuji, M., Kobayashi, H., Takei, T., Watanabe, T., Chikazawa, M., Watanabe, T., Tanabe, K., 2000. Characteristic surface properties of colloidal calcium carbonate. Existing surface hydroxide ion and its properties. *J Soc Inorg Mater, Jpn.* 7, 13-18.
- García, S.G., Jonsson, M., Wold, S., 2006. Temperature effect on the stability of bentonite colloids in water. *J Colloid Interface Sci.* 298, 694-705.
- Israelachvili, J.N., 1991. Intermolecular and surface forces, 2nd edition, Academic Press, New York.
- Kadota, K., Yamamoto, T., Shimosaka, A., Shirakawa, Y., Hidaka, J., Kouzu, M., 2011. Aggregation modeling of calcium carbonate particles by Monte Carlo simulation. *J Nanoparticle Res.* 13, 7209-7218.
- Kitamura, M., 1989. Polymorphism in the crystallization of L-glutamic acid, *J Cryst Growth.* 96, 541-546.
- Kristof, T., Szalai, I., 2003. Magnetic properties and structure of polydisperse ferrofluid models. *Phys Rev E.* 68, 041109.

- Mahanty, J., Ninham, B.W., 1976. Dispersion Forces. Academic Press, New York.
- Matsushita, I., Seikita, T., Suzuki, T., Moriga, T., Ashida, T., Nakabayashi, I., 1993. Effects of Ca^{2+} and OH^- ions on the process of calcium carbonate synthesis and its crystallization. *J Soc Mater Sci, Jpn.* 42, 195-201.
- Satoh, A., 1992. A new technique for metropolis Monte Carlo simulation to capture aggregate structures of fine particles: Cluster-moving Monte Carlo algorithm. *J Colloid Interface Sci.* 150, 461-472.
- Satoh, A., Chantrell, R.W., Kamiyama, S., Coverdale, G.N., 1996a. Two-dimensional Monte Carlo simulations to capture thick chainlike clusters of ferromagnetic particles in colloidal dispersions. *J Colloid Interface Sci.* 178, 620-627.
- Satoh, A., Chantrell, R.W., Kamiyama, S., Coverdale, G.N., 1996b. Three dimensional Monte Carlo simulations of thick chainlike clusters composed of ferromagnetic fine particles. *J Colloid Interface Sci.* 181, 422-428.
- Sinyagin, A.Y., Belov, A., Tang, Z., Kotov, N.A., 2006. Monte Carlo computer simulation of chain formation from nanoparticles. *J Phys Chem B.* 110, 7500-7507.
- Verwey, E.J.W., Overbeek, 1948. J.T.G., Theory of the stability of lyophobic colloids. Elsevier, Amsterdam
- Yamada, H., Hara, N., 1985. Formation process of colloidal calcium carbonate in the reaction of the synthesis of $\text{Ca}(\text{OH})_2\text{-H}_2\text{O-CO}_2$. *Gypsum Lime.* 194, 3-12.

Chapter 4
DEM modelling of granule rearrangement and
fracture behaviours during a closed-die
compaction

4.1 Introduction

Tablets are manufactured by closed-die compaction after a mixture of granules and powders using a rotary tableting machine. Granule properties such as elastic and plastic behaviours would play important roles in manufacturing tablets without a compaction failure. Several researchers reported the assessment of the force-displacement curve of a single granule during a uniaxial compression to comprehend the elastic-plastic behaviour and subsequent failure phenomena (Beekman, et al., 2003; Antonyuk, et al., 2005, 2010; Eckhard and Nebelung, 2011; Sheng, et al., 2004; Muller, et al., 2013; Russell, et al., 2014). The granule deformed elastically in the initial stage of uniaxial compression. After the yield point elastic-plastic deformation would occur until the fracture point, defined by the immediate decline of the compression force. The experimental determination of granule properties is difficult because a granule is too small to capture accurately the deformation and breakage phenomena. To overcome these problems, the DEM is a very effective simulation for capturing the individual granular behaviour under dynamic loading. In a DEM simulation, the design and optimisation of granule properties is particularly important to understand the factors important for compaction. Therefore, although the studies described in *Chapter 1.2.2* have provided more significant results for a single granule fracture than ever before, there still has been a lack of understanding of granule rearrangement and fragmentation during the compaction process. According to the Heckel analysis (Heckel, 1961a, 1961b), in the initial stage of compression, the particles are subjected to rearrangement without any breakage and inter-particulate bonding. As the compression pressure increases, any further movement of the granule would be more difficult. As a result, the fracture of the granule would occur, and subsequent

plastic deformation would be gradually induced (Celik, 1992). Some plastic contact models were adopted for particle compression by DEM to investigate the Heckel plot (Hassanpour and Ghadiri, 2004; Samimi, et al., 2005), Kawakita plot (Persson and Frenning, 2012), tablet strength (Siiria et al., 2011) and the effect of pre-compression (Mehrotra et al., 2009). However, the study of a compaction considering both the rearrangement and fracture of granules calculated by DEM has lacked an understanding of the fundamental mechanisms. DEM modelling of closed-die compaction of aggregated ceramic powders was previously carried out to study the effect of aggregate strength and size on the compaction characteristics (Martin and Bouvard, 2006; Balakrishnan et al., 2010). As for pharmaceutical granules, the compactibility of tablets involving capping and lamination is affected by compaction speed, that is, by the rearrangement and fracture of granules at the beginning of the compaction stage (Garr and Rubinstein, 1991). As mentioned above, there is a lack of understanding of the fundamental granule compaction mechanisms in the tableting process.

In the present work, closed-die compaction of granules was simulated using DEM to investigate the rearrangement and failure behaviour during loading. The modelled granule consisting of primary particles connected by spring bonds represented a granule manufactured by a fluidized-bed granulator. Granules produced by fluidized-bed granulation have a porous and loose structure which consists of primary particles connected by the binder and solidified crystalline bridge bonds (Bika et al., 2005). First, to validate the granule model, a uniaxial compression test of the granule was carried out both experimentally and numerically. Secondly, the modelled granules were compacted in a confined closed die to analyse the granule behaviour and compaction force. A full understanding of the rearrangement and fracture mechanisms

during closed-die compaction could lead to the production of optimal granules for the tableting process.

4.2 Materials and methods

4.2.1. Materials

D-mannitol fine powder and hydroxypropyl cellulose were purchased from B Food Science Co., Ltd. (Aichi, Japan) and Nippon Soda Co., Ltd. (HPC-SL, Tokyo, Japan), respectively. These materials meet the specifications of the Japanese Pharmacopeia (JP). HPC-SL is a low-molecular-weight (~100000) and a low-viscosity grade. Distilled water was used for dissolving HPC-SL powder. A placebo formulation consisting of D-mannitol and HPC-SL was used for the tested granules to simplify the DEM model.

4.2.2. Granulation procedure

Fluidized-bed granulation is a common manufacturing method for preparing granules for a subsequent tableting process because the granules produced by the fluidized-bed granulator have good compactibility and plasticity due to their porous structure, which is achieved by spraying a binder solution. The applied operating conditions are summarized in Table 4-1. After passing through a 710 μm sieve, the D-mannitol powder was fluidized using a fluidized-bed granulator (MP-01, POWREX CORPORATION, Japan) and an 8 wt% aqueous solution of HPC-SL was sprayed as a binder from the top of the granulator. The amount of binder solution was 300 g, that is, the total amount of HPC-SL was 3% based on the total load. After spraying the binder, the granules were dried until the product temperature reached 40°C.

Table 4-1 Process parameters of fluidized bed granulation

Parameter	Value
Bed mass (g)	800
Air flow rate (m ³ /h)	0.6
Spray rate (g/min)	15
Atomizer flow rate (NL/min)	50
Air flow temperature (°C)	70
Binder concentration (w/w%)	8

4.2.3. Characterization of D-mannitol powder and granules

The particle-size distribution of the D-mannitol was measured in liquid medium by laser diffraction using a Mastersizer2000 with a HYDRO 2000SM dispersing unit (Malvern Instruments Ltd., Worcestershire, UK). The samples were dispersed in a saturated solution of the D-mannitol using ultrasonication for 15 seconds to obtain the primary particle size. The particle size distribution of the granules was measured by sieve analysis in accordance with Japanese Pharmacopeia 17. Ten grams of the granular product was placed on the top sieve and it was shaken for 3 minutes using a sieve shaker (SIEVE FACTORY IIDA CO. LTD., Osaka, Japan).

The granules used in the experiment were the sieve fraction between 500 μm and 710 μm . The uniaxial compression tests of the sieved granules were performed using the TA.XT plus Texture Analyser (Stable Micro Systems Ltd., Godalming, UK) to obtain the force-displacement curves. These measurements were repeated 20 times. A granule compression speed was set at 0.2 mm/s with a 10 mm cylindrical tool. After the

load cell (5 kg) detected 10 mN, the force acting on the tool was recorded until a strain of granule was fractured. The variation in the granule shape during the uniaxial compression test was observed using a high-speed digital microscope (VW-9000, KEYENCE Corporation, Osaka, Japan) at a recording speed of 1000 fps.

4.2.4. DEM simulation method

DEM is one of the most popular simulation methods for the numerical analysis of granules (Cundall and Strack, 1979). The contact force between two particles was modelled by the Voigt model, which consists of a spring-dashpot and a slider for the friction in the tangential component. The translational and rotational motions of two particles are calculated by Newton's equations of motion at each step

$$m_i \frac{dv_i}{dt} = \sum_j \mathbf{F}_{ij}^n + \mathbf{F}_{ij}^t + \mathbf{F}_{ij}^k + m_i \mathbf{g} \quad (4-1)$$

$$I_i \frac{d\omega_i}{dt} = \sum_j \mathbf{R}_{ij} \times \mathbf{F}_{ij}^t + \mathbf{M}_{r,i} \quad (4-2)$$

where m_i , \mathbf{v}_i , I_i and ω_i are the mass, the translational velocity, the moment of inertia and the angular velocity of a particle i , respectively. \mathbf{R} and \mathbf{g} represent the vector from the centre of a particle to the particle surface and the gravitational acceleration. The contact forces, \mathbf{F}_{ij}^n and \mathbf{F}_{ij}^t , are calculated by following equations

$$\mathbf{F}_{ij}^n = K_n \mathbf{x}_{ij}^n + \eta_n \mathbf{v}_{ij}^n \quad (4-3)$$

$$\mathbf{F}_{ij}^t = \min[\mu \mathbf{F}_{ij}^n \mathbf{t}_{ij}, \eta_t \mathbf{v}_{ij}^t + K_t \mathbf{x}_{ij}^t] \quad (4-4)$$

The contact model used for the simulation is the non-linear Hertz-Mindlin model. According to the Hertz theory, the normal stiffness K_n between two spherical particles is represented by

$$K_n = \frac{4b}{3\pi} \left(\frac{1}{\delta_i + \delta_j} \right) \quad (4-5)$$

$$\delta_i = \frac{1-\nu_i^2}{\pi E_i} \quad (4-6)$$

where E and ν are Young's modulus and Poisson's ratio, and b is the radius of the contact area. The tangential stiffness K_t is provided by the no-slip Mindlin theory (Mindlin, R.D., 1949).

$$K_t = 8b \left(\frac{2-\nu_i}{G_i} + \frac{2-\nu_j}{G_j} \right)^{-1} \quad (4-7)$$

$$G_i = \frac{E_i}{2(1+\nu_i)} \quad (4-8)$$

The viscous dashpot coefficient of the normal η_n and the tangential η_t are given by

$$\eta_n = 2\gamma\sqrt{m_i K_n} \quad (4-9)$$

$$\eta_t = 2\gamma\sqrt{m_i K_t} \quad (4-10)$$

where γ is the dashpot coefficient which depends on the coefficient of restitution e , which is expressed in the following equation

$$\gamma = -\frac{2 \ln e}{\sqrt{\pi^2 + (\ln e)^2}} \quad (4-11)$$

A spring shows elastic behaviour and a dashpot allows energy dissipation and quasi-static deformation between spherical particles. This model means that particles deform elastically and a repulsive force increases with the increasing overlap distance between the two particles. A method similar to that of Antonyuk et al. (2006) was chosen, but a more simplified model was implemented to reduce the computational costs. The primary particle is assumed that monodisperse in size and that the binder bond had uniform stiffness which is represented by the following equation.

$$\mathbf{F}_{ij}^k = K_r \Delta x \quad (\text{if } \mathbf{F}_{ij}^k < \mathbf{F}_{lim}^k) \quad (4-12)$$

where K_r is a spring constant for the connection between particles, Δx is a distance between surface of particles and \mathbf{F}_{lim}^k is the fracture force of the bond. If the force acting on the bond exceeds the fracture force, the bond breaks and the force is initialized

to zero. Before the bond is broken, the bond provides an attractive force calculated from a linear spring equation. However, when the bond is broken, the attractive force immediately drops to zero and the bond does not form again even if the particles are in contact once again.

4.2.5. Simulation procedure of uniaxial compression and closed-die compaction

The granule was modelled by 500 spherical primary particles. The primary particles were generated randomly without overlap and centripetal force is applied to move primary particles towards the centre of the granule. Then, the granule which has a 500 μm diameter is modelled by connecting the binder bond. To simulate the uniaxial compression test, the modelled granule was put between flat stainless steel platens and the granule was compressed at an upper platen velocity of 0.2 mm/s as illustrated in Figure 4-1(a). Table 4-2 shows the simulation conditions for the uniaxial compression test.

With regard to closed-die compression, 10 granules initially were randomly deposited by gravity into a cylindrical die with a diameter of 3 mm (Figure 4-1(b)). Each granule is composed of 500 primary particles which have a diameter of 50 μm using the DEM parameter validated by the uniaxial compression test. After achieving steady state, an upper punch moved down to compress the granules.

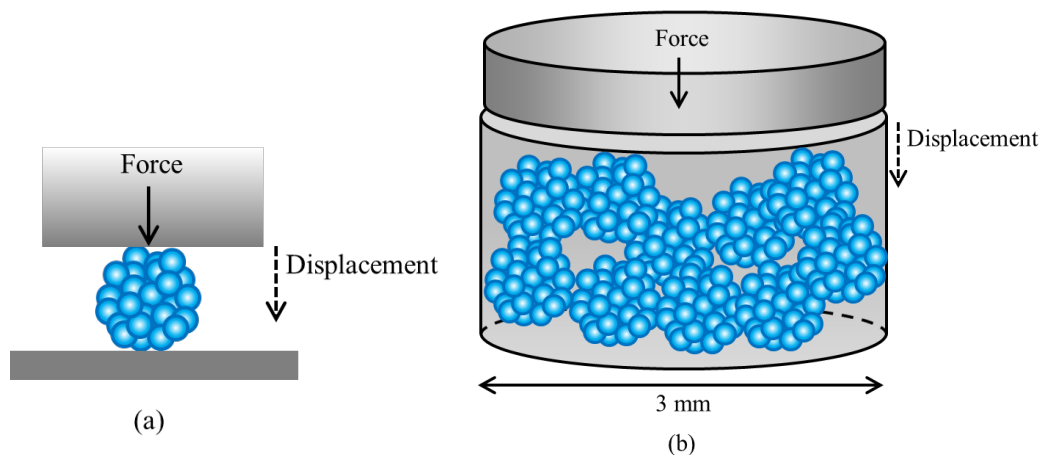


Figure 4-1 Schematic drawing of (a) the uniaxial compression and (b) closed die compaction for DEM simulation

Table 4-2 Simulation conditions for uniaxial compression tests

Parameter	Value
Total time (s)	1.0
Time step (s^{-1})	1.25×10^{-9}
Particle diameter (μm)	50
Particle density (kg/m^3)	1500
Number of particles (-)	500
Young's modulus of particle (GPa)	0.1
Poisson's ratio of particles (-)	0.3
Coefficient of restitution (-)	0.85
Sliding friction coefficient (-)	0.7
Rolling friction coefficient (-)	0.1
Normal spring constant (kN/m)	1.0
Tangential spring constant (kN/m)	0.5
Fracture criteria (N)	3×10^{-3}
Compression velocity (mm/s)	0.2

4.3 Results and discussion

4.3.1 Characterization of the tested granule

Fluidized-bed granulation is frequently used as a manufacturing method in the pharmaceutical industry to improve powder properties including those of the active pharmaceutical ingredient (API) such as its flowability, compactibility and wettability (Davies, 2004). The fluidized-bed granulation process involves fluidized powders in a hot air stream from the bottom of the granulator and spraying a liquid binder from the top of the granulator (top-spray method). D-mannitol fine powder was granulated using the fluidized-bed granulator under the conditions shown in Table 4-1 to prepare a tested granule. The average particle size of the D-mannitol fine powder measured by laser diffraction was 51.0 μm . Based on the results from laser diffraction, the primary particle size used in the DEM simulations was set at 50 μm . Sieve analysis in accordance with the Japanese Pharmacopeia 17 was used to determine the particle size distribution of granules. The granules had an average granule size (D_{50}) of 243 μm . To simplify the simulation model, granules used for the uniaxial compression test were used after sieving between 500 μm and 710 μm as shown in Figure 4-2. The granules had a porous structure and it seemed that the primary particles were connected by a binder bridge and D-mannitol crystalline bridge (Bika et al., 2005). During the spraying process, primary particles agglomerate together by capillary force and the viscous force of the binder solution, which were theoretically modelled to predict a coalescence probability between two particles. After the drying process, porous structured granules with solid binder bridges composed of both the binder and a solidified crystalline bridge formed by recrystallization of the base powder are formed (Ennis et al., 1991; Liu et al., 2000; Iveson et al., 2001; Bika et al., 2005).



Figure 4-2 Optical image of the granule fraction between 500 μm and 710 μm

4.3.2 Comparison between experimental and DEM simulated uniaxial compression tests of a granule

For the calibration of the DEM parameters regarding granule fracture, the Rumpf equation (Rumpf, 1958) regarding granule strength can support an understanding of the relationship among the tensile strength, the bonding force, porosity and particle size.

$$\sigma = \frac{k(1-\varepsilon) F}{\pi D^2} \quad (4-13)$$

where σ is the strength of granule, ε is the granule porosity, k is the coordination number, F is the bonding force and D is the primary particle diameter. The model is based on the assumption that primary particles are monodisperse spherical particles in a random packing, which is the same situation as the DEM model. To fit the experimental results, the bonding force F was estimated by a trial-and-error approach and ε , k and D were

considered to be constant. As seen from the Rumpf equation, when the bonding force F is increased, the strength of the granule is increased. Therefore, the spring constant between primary particles was determined to fit the force-displacement curve obtained experimentally, and then a threshold for the fracture force of the bond was determined (Gröger, T., 2003; Yang, et al., 2008).

The granules tested for all experiments were taken from the sieve fraction between 500 μm and 710 μm . The uniaxial compression test was carried out at a velocity of 0.2 mm/s to measure the compression force until a fracture was identified. The average value (\pm standard deviation) of the fracture force and displacement until fracture as measured by 20 repetitions of the uniaxial compression test were 196.8 ± 55.3 mN and 0.14 ± 0.04 mm, respectively. The fracture forces and displacements until fracture were obtained with relatively large deviations due to the non-homogeneity of the porous fluidized-bed granules. Typical compression forces obtained both experimentally and by numerical simulation as a function of the upper platen displacement are shown in Figure 4-3. The experimental and numerical simulation results of the force-displacement curve were very consistent. Figure 4-3 indicated that a small fluctuation of the compression force was detected until the main fracture occurred at a displacement of approximately 0.15 mm. The fluctuation of the compression force until the main fracture may arise from ductile characteristics and small fractures near the upper platen, which are difficult to implement without a bonding model. High-speed camera observations shown in Figure 4-4 clearly showed that the granule plastically deformed and then a crack was observed. When the crack occurred, the compression force fell immediately and additional secondary fractures were detected. Figure 4-5 shows snapshots of the DEM results of the uniaxial compression test. Grey particles

refer to single particles having no bond and particles in the same colours except for grey and light blue belong to the same fragments. The initial bond breakages were observed near the upper and lower platen (Figure 4-5(b)). This result is consistent with the previous work (Thornton et al., 2004; Schilde et al., 2014). As shown in Figure 4-5(c) and (d), the size of the fragments became smaller as the compaction proceeded. As mentioned above, the DEM results are confirmed quantitatively and qualitatively by the experimental findings, indicating that the DEM simulation could be validated to capture the granule deformation and fracture.

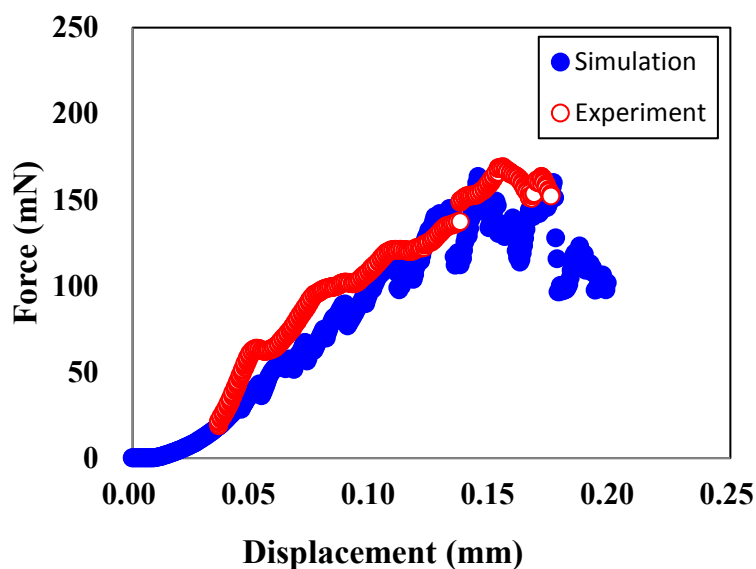


Figure 4-3 Force-displacement curve for a D-mannitol granule of approximately 500 μm diameter

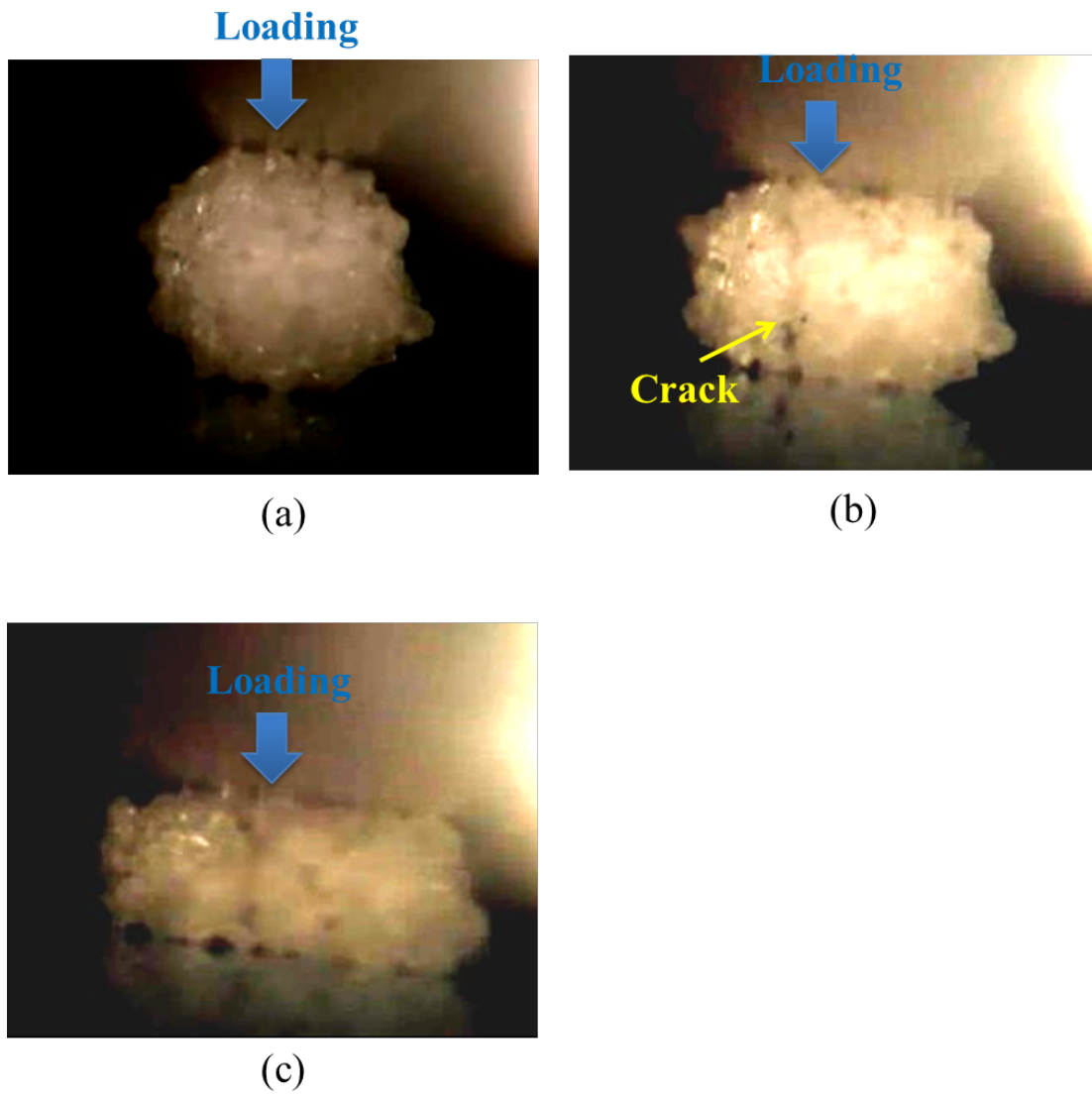


Figure 4-4 High-speed camera observations during the uniaxial compression test at a displacement of (a) 0.00 mm, (b) 0.12 mm and (c) 0.20 mm.

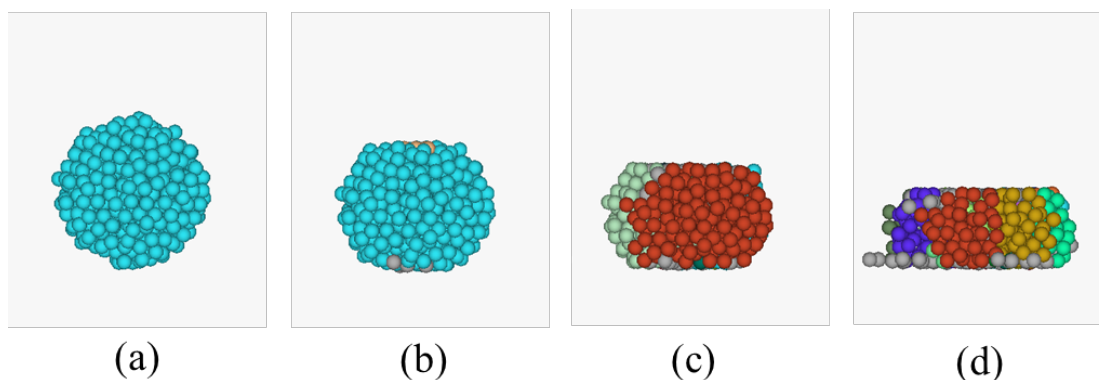


Figure 4-5 Snapshots of fracture behaviour of the granule during uniaxial compression at an upper platen displacement of (a) 0.0 mm, (b) 0.1 mm, (c) 0.175 mm and (d) 0.25 mm. Upper platen velocity was set at 0.2 mm/s. A grey colour represents the particle without bonds and particles in the same colours except for grey and light blue belong to the same fragments.

4.3.3 DEM modelling of granular bed compression

Compaction was simulated at varying upper platen velocities of 0.2, 5 and 50 mm/s to examine the effects of the compaction speed on the granule behaviour. The maximum upper platen velocity was set at 50 mm/s because the upper platen velocity strongly affected compactibility and compaction issues such as capping and lamination. Figure 4-6 shows a snapshot of the compaction of 10 granules in the cylindrical closed die. The snapshots in Figure 4-6 display similar compaction behaviour for all values of upper platen velocity. Granules were not fractured until displacement of 0.15 mm, indicating that rearrangement proceeded as the bonds between particles were gradually broken. Following the rearrangement, fragmentations of granules arising from loading were observed. The number of fragments as a function of displacement as shown in Figure 4-7 varied in a similar manner, however, the number of fragments at a velocity

of 0.2 mm/s was slightly larger. Higher compaction velocity causes a limitation on rearrangement. On the other hand, as the compaction velocity decreases, granules gradually rearranged and the friction due to contact between granules leads to an increase in single-particle fragments. Therefore, the number of single-particle fragments was increasing at a platen velocity of 0.2 mm/s.

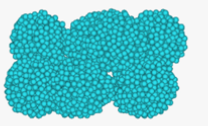
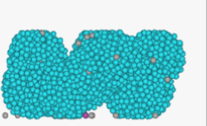
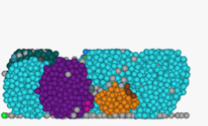
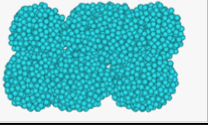
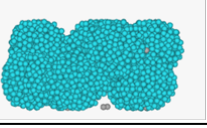
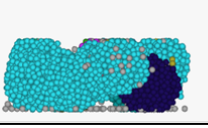
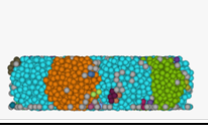
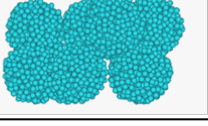
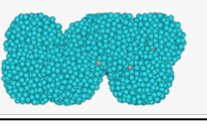
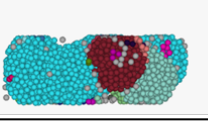
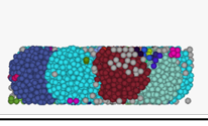
Upper platen velocity	Displacement			
0.2 mm/s				
	0.00 mm	0.15 mm	0.35 mm	0.45 mm
5 mm/s				
	0.00 mm	0.15 mm	0.35 mm	0.45 mm
50 mm/s				
	0.00 mm	0.15 mm	0.35 mm	0.45 mm

Figure 4-6 Snapshots of the compaction process of granules at various upper platen velocities

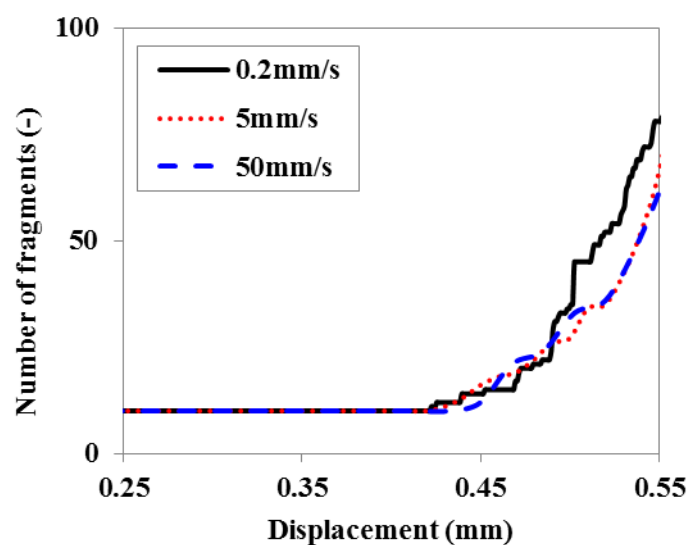


Figure 4-7 Effect of upper platen velocity on the number of granule fragments during closed-die compaction

Figure 4-8 shows the rearrangement behaviour of granules during compaction with the same coloured primary particles belonging to the same initial granule. The pink-coloured granule rearranged towards the bottom of the die at an upper platen velocity of 0.2 mm/s. The rearrangement behaviours of the red granule at various upper platen velocities were slightly different because granule rearrangement was limited at higher velocities. The force-displacement curves obtained at different upper platen velocities are displayed in Figure 4-9. At the beginning of loading the force increased with the increase in displacement due to the elastic deformation of granules corresponding to Hertzian deformation compressed by the upper platen. The force decreased and fluctuated between the displacement values of 0.2 mm and 0.4 mm. In this low-pressure region, the granule rearrangement and fracture are dominant as observed in Figure 4-9, resulting in a fluctuation in the compaction force. After the 0.4

mm displacement, the forces were expected to be similar for the different compaction velocities because rearrangement was limited and plastic deformation took place. It is a well-known fact that compaction velocity has significant effects on the compaction properties such as the compressibility and tableability, that is, tablet strength generally decreases as the tableting velocity increases (Tye et al., 2005). Thus, the limited rearrangement at a higher compaction velocity seems to be caused by compaction failure including capping and lamination.

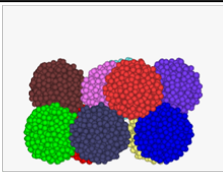
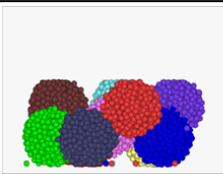
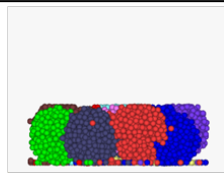
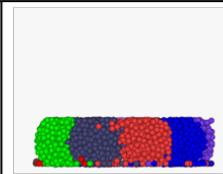
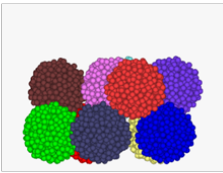
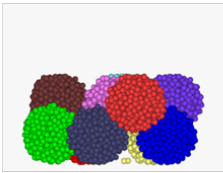
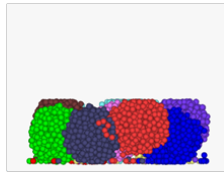
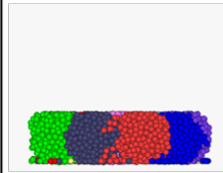
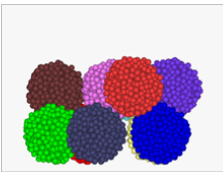
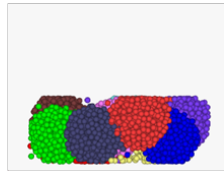
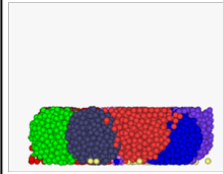
Upper platen velocity	Displacement			
0.2 mm/s				
	0.00 mm	0.15 mm	0.35 mm	0.45 mm
5 mm/s				
	0.00 mm	0.15 mm	0.35 mm	0.45 mm
50 mm/s				
	0.00 mm	0.15 mm	0.35 mm	0.45 mm

Figure 4-8 Snapshots of the compaction process of granules at various upper platen velocities. The same coloured primary particles belong to the same initial granule.

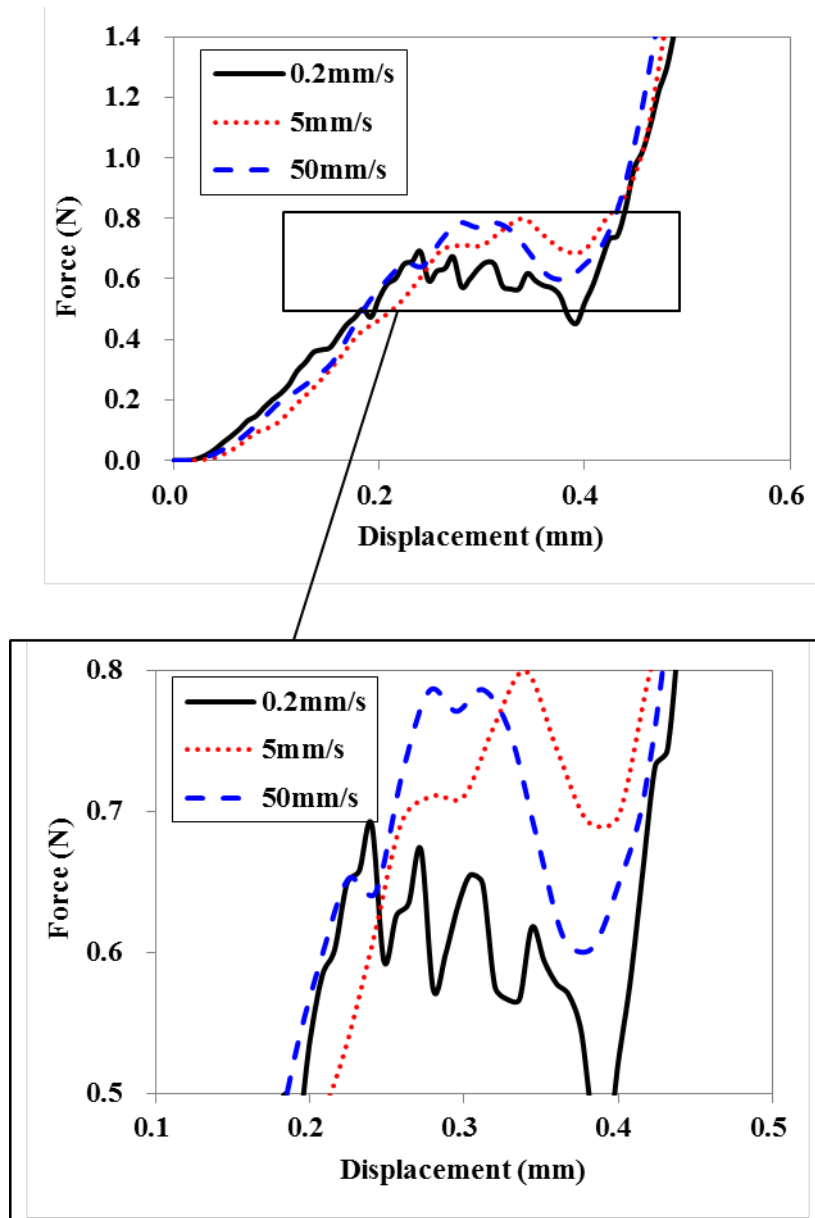


Figure 4-9 Force-displacement curves for DEM-modelled granules during closed-die compaction at an upper platen velocity of 0.2, 5 and 50 mm/s.

The Heckel model is one of the most widely used methods to characterize compressions of a granular bed. This model can calculate a Heckel parameter and a yield pressure of material from the linear region of Heckel plots, which shows an indication of the plasticity or hardness of the granules. The Heckel equation is described as follows.

$$\ln \frac{1}{1-D} = kP + \text{Intercept} \quad (14)$$

where D is the relative density of compaction at applied pressure P and the reciprocal of slope k represents the yield pressure. Heckel plots for the DEM modelled granules at an upper platen velocity of 0.2 mm/s, 5 mm/s and 50 mm/s are given in Figure 4-10, which shows that the Heckel plots in the low-pressure region were bending and fluctuating, which was caused by granule rearrangement and fragmentation. Klevan et al. (2009, 2010) utilized the Shapiro General Compaction Equation (GCE) as an indicator of the powder compression process in the low-pressure region of the Heckel plots and they concluded that the bending of the Heckel plots in the low-pressure region may be used to assess particle fragmentation. They also discussed the major cause of initial bending as being particle rearrangement for particles showing significant rearrangement. In contrast, particle fragmentation is the major cause of the initial bending in the case that particle rearrangement is limited. The DEM results showed that Heckel plots until fluctuation (< 0.1 MPa) mainly represented rearrangement whereas the fluctuation observed at approximately 0.1 MPa was caused by a combination of both rearrangement and fragmentation. Subsequent bending of the Heckel plots (> 0.1 MPa) was assumed to result from both fragmentation and plastic deformation of granules. Plastic deformation of the primary particles occurring in the high-pressure region was not discussed in this paper because the Hertzian contact model was used. Nordström et

al. (2009) found that particle rearrangement is negligible under the critical particle size of approximately 40 μm by the analysis of Kawakita parameters (Kawakita and Ludde, 1971) which represent the incidence of particle rearrangement. In the current work, the modelled granule size is approximately 500 μm , leading to a significant effect on the rearrangement and hence the force fluctuation was clearly observed in the DEM compression profiles. However, the model does not consider the plasticity of the primary particles and non-homogeneous properties such as particle-size distribution and deviation of bonds. Therefore, further work will be needed to design an appropriate granule for closed-die compaction.

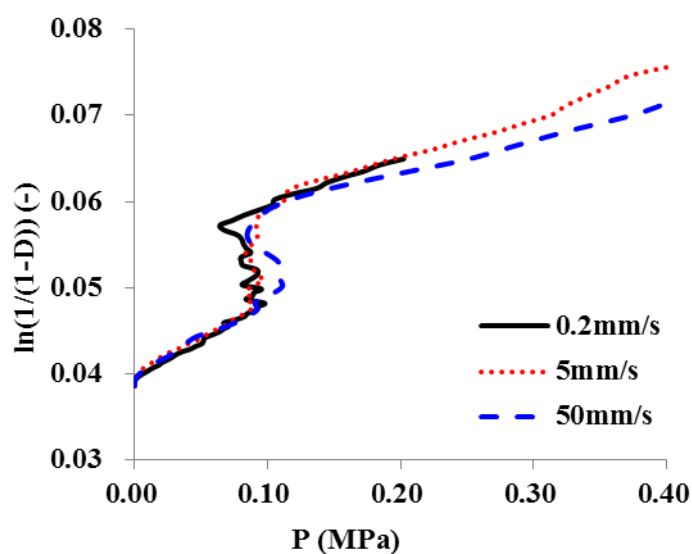


Figure 4-10 Heckel plots for DEM-modelled granules at an upper platen velocity of 0.2, 5 and 50 mm/s up to an applied pressure of 0.4 MPa.

4.4 Conclusion

DEM simulations of a modelled granule were developed to investigate its rearrangement and fracture behaviour during closed-die compaction. The granule was implemented as an agglomerate of the primary particles connected by linear springs, which described the granule prepared by a fluidized-bed granulator. To validate the model, the force applied to the upper platen during the uniaxial compression test of the D-mannitol granule granulated by a fluidized-bed granulator was measured. The experimentally measured uniaxial compression force was in good agreement with the force obtained by DEM simulation. The closed die compactions of the modelled granules were simulated to investigate the effect of compaction velocities on the rearrangement and fracture of modelled granules. Although the snapshots of the behaviour of granules during closed-die compaction seemed to show similar results among various compaction velocities, the force applied to the upper platen fluctuated at the low compaction velocity of 0.2 mm/s. This result was caused by the rearrangement of granules which more easily proceeded at lower compaction velocities. After the rearrangement, granule fractures were dominant as the result of the higher compression force. In addition, Heckel plots also showed that the granule rearrangement occurred in the low-pressure region before plastic deformation occurred. The granule model provides a simulation method that accurately depicts compaction behaviour including granule rearrangement and fracture.

References

- Antonyuk, S., Tomas, J., Heinrich, S., Morl, L., 2005. Breakage behavior of spherical granulates by compression. *Chem. Eng. Sci.* 60, 4031-4044.
- Antonyuk, S., Khanal, M., Tomas, J., Heinrich, S., Morl, L., 2006. Impact breakage of spherical granules: Experimental study and DEM simulation, *Chem Eng Process.* 45, 838-856.
- Antonyuk, S., Heinrich, S., Tomas, J., Deen, N.G., Buijtenen, M.S., Kuipers, J.A.M., 2010. Energy absorption during compression and impact of dry elastic-plastic spherical granules. *Granular Matter.* 12, 15-47.
- Balakrishnan, A., Pizette, P., Martin, C.L., Joshi, S.V., Saha, B.P., 2010. Effect of particle size in aggregated and agglomerated ceramic powders. *Acta Materialia.* 58, 802-812.
- Beekman, W.J., Meesters, G.M.H., Becker, T., Gaertner, A., Gebert, M., Scarlett, B., 2003. Failure mechanism determination for industrial granules using a repeated compression test. *Powder Technol.* 130, 367-376.
- Bika, D., Tardos, G.I., Panmai, S., Farber, L., Michaels, J., 2005. Strength and morphology of solid bridges in dry granules of pharmaceutical powders, *Powder Technol.* 150, 104-116.
- Celik, M., 1992. Overview of compaction data analysis techniques, *Drug Dev Ind Pharm.* 18, 767-810.
- Cundall, P.A., Strack, O.D.L., 1979. A discrete numerical model for granular assemblies, *Geotechnique.* 29, 47-65.
- Davies, P., 2004. Chapter 10: Oral Solid Dosage Forms. In: Gibson, M. (Eds.), *Pharmaceutical Preformulation and Formulation.* Interpharm/ CMC, pp.379-456.
- Eckhard, S., Nebelung, M., 2011. Investigations of the correlation between granule structure and deformation behavior. *Powder Technol.* 206, 79-87.
- Ennis, B.J., Tardos, G., Pfeffer, R., 1991. A microlevel-based characterization of granulation phenomena. *Powder Technol.* 65, 257-272.
- Garr, J.S.M., Rubinstein, M.H., 1991. An investigation into the capping of paracetamol at increasing speeds of compression. *Int. J. Pharm.* 72, 117-122.
- Gröger, T., Tüzünm U., Heyes, D.M., 2003. Modelling and measuring of cohesion in wet granular materials. *Powder Technology.* 133, 203-215.
- Hassanpour, A., Ghadiri, M., 2004. Distinct element analysis and experimental evaluation of the Heckel analysis of bulk powder compression, *Powder Technol.* 141, 251-261.
- Heckel, R.W., 1961a. Density-pressure relationships in powder compaction, *Trans*

- Metall Soc AIME. 221, 671-675.
- Heckel, R.W., 1961b. An analysis of powder compaction phenomena, Trans Metall Soc AIME. 221, 1001-1008.
- Henley, K.J., O'Sullivan, C., Oliveira, J.C., Cronin, K., Byrne, E.P., 2011. Application of Taguchi methods to DEM calibration of bonded agglomerates, Powder Technol. 210, 230-240.
- Henley, K.J., O'Sullivan, C., Byrne, E.P., Cronin, K., 2012. Discrete element modelling of the quasi-static uniaxial compression of individual infant formula agglomerates, Particuology. 10, 523-531.
- Iveson, S.M., Litster, J.D., Hapgood, K., Ennis, B.J., 2001. Nucleation, growth and breakage phenomena in agitated wet granulation processes; a review, Powder Technol. 117, 3-39.
- Kawakita, K., Ludde, K-H., 1971. Some considerations on powder compression equations. Powder. Technol. 4, 61-68.
- Klevan, I., Nordstrom, J., Bauer-Brandl, A., Alderborn, G., 2009. On the physical interpretation of the initial bending of a Shapiro-Konopicky-Heckel compression profile. Euro. J. Pharm. Biopharm. 71, 395-401.
- Klevan, I., Nordstrom, J., Tho, I., Alderborn, G., 2010. A statistical approach to evaluate the potential use of compression parameters for classification of pharmaceutical powder materials. Euro. J. Pharm. Biopharm. 75, 425-435.
- Liu, L.X., Lister, J.D., Iveson, S.M., Ennis, B.J., 2000. Coalescence of deformable granules in wet granulation processes. AIChE J. 46, 529-539.
- Martin, C.L., Bouvard, D., 2006. Discrete Element Simulations of the Compaction of Aggregated Ceramic Powders. J. Am. Ceram. Soc. 89, 3379-3387.
- Mehrotra, A., Chaudhuri, B., Faqih, A., Tomassone, M.S., Muzzio, F.J., 2009. A modeling approach for understanding effects of powder flow properties on tablet weight variability, Powder Technol. 188, 295-300.
- Mindlin, R.D., 1949. Compliance of elastic bodies in contact, Journal of Applied Mechanics. 16, 259-266.
- Muller, P., Seeger, M., Tomas, J., 2013. Compression and breakage behavior of γ -Al₂O₃ granules. Powder Technol. 237, 125-133.
- Nordström, J., Klevan, I., Alderborn, G., 2009. A Particle Rearrangement Index Based on the Kawakita Powder Compression Equation. J. Pharm. Sci. 98, 1053-1063.
- Persson, A.S., Frenning, G., 2012. An experimental evaluation of the accuracy to simulate granule bed compression using the discrete element method, Powder Technol. 219, 249-256.

- Rumpf, H., 1958. Grundlagen und methoden des granulieren. Chem, Ing, Tech. 30, 144-158.
- Russell, A., Muller, P., Shi, H., Tomas, J., 2014. Influences of loading rate and preloading on the mechanical properties of dry elasto-plastic granules under compression. AIChE J. 60, 4037-4050.
- Samimi, A., Hassanpour, A., Ghadiri, M., 2005. Single and bulk compressions of soft granules: Experimental study and DEM evaluation, Chem Eng Sci. 60, 3993-4004.
- Schilde, C., Burmeister, C.F., Kwade, A., 2014. Measurement and simulation of micromechanical properties of nanostructured aggregates via nanoindentation and DEM-simulation, Powder Technol. 259, 1-13.
- Sheng, Y., Briscoe, B.J., Maung, R., Rovea, C., 2004. Compression of polymer bound alumina agglomerates at the micro deformation scale. Powder Technol. 140, 228-239.
- Siiria, S.M., Antikainen, O., Heinamaki, J., Yliruusi, J., 2011. 3D simulation of internal tablet strength during tableting, AAPS PharmSciTech. 12, 593-602.
- Thornton, C., Ciomocos, M.T., Adams, M.J., 2004. Numerical simulations of diametrical compression tests on agglomerates, Powder Technol. 140, 258-267.
- Tye, C.K., Sun, C., Amidon, G.E., 2005. Evaluation of the Effects of Tableting Speed on the Relationships between Compaction Pressure, Tablet Tensile Strength, and Tablet Solid Fraction. J. Pharm. Sci. 94, 465-472.
- Yang, R.Y., Yu, A.B., Choi, S.K., Coates, M.S., Chan, H.K., 2008. Agglomeration of fine particles subjected to centripetal compaction. Powder Technol. 184, 122-129.

Chapter 5

**Size-induced segregation during pharmaceutical
particle die filling assessed by response surface
methodology using discrete element method**

5.1 Introduction

In a rotary tableting machine, mixture of pharmaceutical powders consisting of active pharmaceutical ingredients (APIs), diluents, binders, disintegrants, lubricants and other excipients are transferred from a hopper to the die via a feed shoe during die filling process in a system equipped with a bottom punch that moves down. The tableting of these powders may be associated with segregation, which can severely affect the quality attributes of tablets, such as content uniformity, appearance, hardness and dissolution. Therefore, this manufacturing process needs to be accurately controlled. According to Virtanen et al. (2009) and Lakio et al. (2010, 2012), the particle size distribution in the tablet continuously changed during the tableting process, and segregation arose from the wide size distribution. Xie et al. (2008) examined the segregation tendency between aspirin (ASP) and microcrystalline cellulose (MCC) using the ASTM D 6940-04 segregation tester. They concluded that segregation tendency increased as the particle size ratio between ASP and MCC increased by the analysis of variance (ANOVA) and principal component regression (PCR). In addition, the granulation process and the API properties result in inhomogeneous drug content in different granule size fractions (Dries et al., 2002; Bacher et al., 2008; Poutiainen et al., 2011). This inhomogeneity significantly influences the uniformity of the tablet because granules with relatively high or low drug content undergo a size-induced segregation. In general, particle size affects cohesive forces between particles related to electrostatic, van der Waals and hydrophilic interactions as well as powder compactibility (Davies et al., 2001), leading to tableting issues such as sticking and capping. Several experimental studies have been conducted to quantify the segregation. However, a robust tableting process still requires in-depth understanding of particle flow mechanisms during die

filling.

Several experiments have been performed to investigate powder flow behaviour between hopper and die (Sinka et al., 2004; Jackson et al., 2007; Yaginuma et al., 2007; Sinka et al., 2009; Mills and Sinka, 2013). Jackson et al. (2007) and Sinka et al. (2009) developed a fundamental understanding of pharmaceutical powder particle flow using a suction filling system. They also demonstrated that process parameters, such as shoe velocity and bottom punch motion, played an important role in enhancing tablet weight uniformity and productivity because suction filling efficiently delivered the powder in the die. Mills and Sinka (2013) investigated the powder flow behaviour by gravity and suction filling using microcrystalline cellulose with different particle size and density and found that the critical shoe velocity was more significantly increased by suction than by gravity filling. Furthermore, their experimental evaluation of powder flow during die filling supported the parameter optimisation of rotary tableting. These experimental observations provide useful information on die filling. However, the analysis of single particle behaviour is necessary to understand segregation-related phenomena in more detail.

DEM has proven valuable for assessing the particle flow and segregation during die filling. Its combination with CFD has provided insight into the effect of particle density, particle charge and air on the powder filling behaviour of metal and pharmaceutical particles (Guo et al., 2009a, 2009b, 2011a, 2011b; Nwose et al., 2012; Wu and Guo, 2012). Mateo-Ortiz et al. (2014) investigated the particle size segregation inside a feed frame fitted with two paddle wheels by DEM. Their results revealed that the paddle wheel speed contributed the most to the percolation-induced size segregation. Wu (2008) conducted a die filling simulation using a fixed bottom punch for

pharmaceutical tableting. The effects of particle shape and size distribution on the size-induced segregation during container filling have been analysed by DEM and a percolation process has been evaluated using a screening model (Shimosaka et al., 2013). Although previous studies give support to understand the fundamental knowledge for some filling processes, the characteristic rotary tableting system consisting of moving bottom punch and fixed feed shoe does not fully understand.

This chapter aimed to establish a fundamental understanding of particle flow during die filling by combining moving bottom punch and fixed feed shoe and the segregation of binary particle mixtures during a simple filling process. The effect of die velocity on the filling behaviour and segregation of different sized particles was assessed by simulating the filling process of spherical purified sucrose granules, which have been widely used as core particles for pellets coated with functional films (Narisawa et al., 1996; Shimizu et al., 2003; Palugan et al., 2015). DEM parameters were determined through laboratory experiments, and simulation results were validated by comparison with filling experiments. The filling behaviour of monodisperse particles was evaluated. The segregation of binary particle mixtures was assessed by DEM simulations using the validated DEM parameters and the resulting trend was examined by response surface methodology (RSM). DEM approach considered in RSM clearly revealed the effect of parameters on the segregation in the feed shoe and die.

5.2 Materials and methods

5.2.1. Filling experiments

Purified sucrose spherical granules (NONPAREIL®-103, mean particle size: 850–710 μm , Freund Corporation, Japan) were used as model particles in the investigation of particle filling behaviour in the feed shoe. Pharmaceutical tableting

machines adopt the suction filling system to improve the weight variability. The experimental die-shoe filling system (Figure 5-1) comprised a fixed feed shoe and an actuator (SCLT4-015-300-s, Dyadic Systems Co., Ltd., Japan) that controlled the die and punch velocity. The actuator angle was fixed to achieve a realistic die filling process with the rotary tableting machine. Experimental die and punch velocities (i.e. turret speed of rotary tableting machine) ranged from 100 to 500 mm/s. Particles were added through the feed shoe and their flow behaviour was monitored using a high-speed camera (HAS-L1, DITECT Co. Ltd., Japan). Simulated and experimental particle filling behaviours were compared to validate the proposed model.

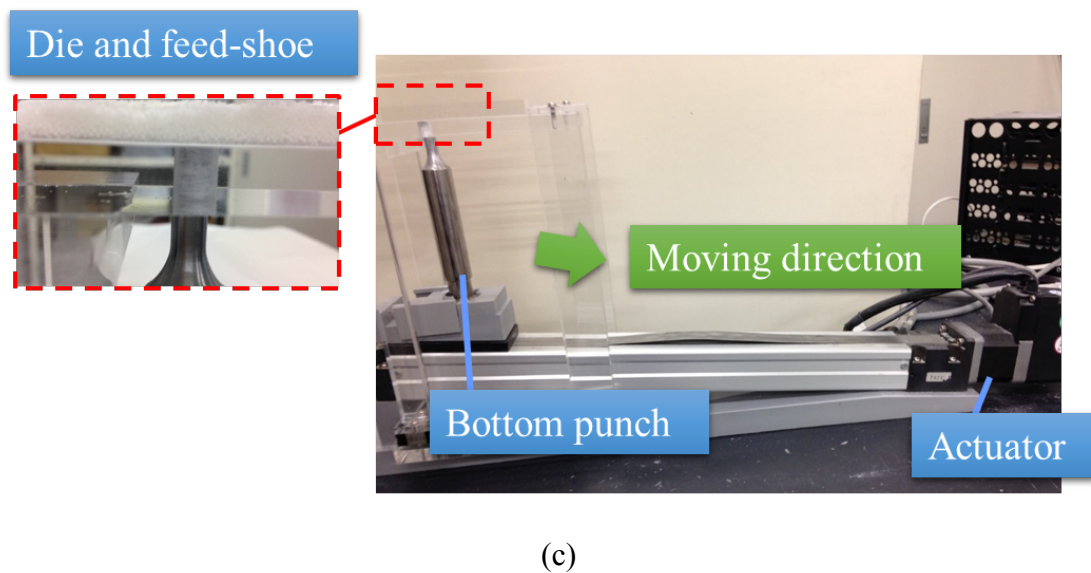
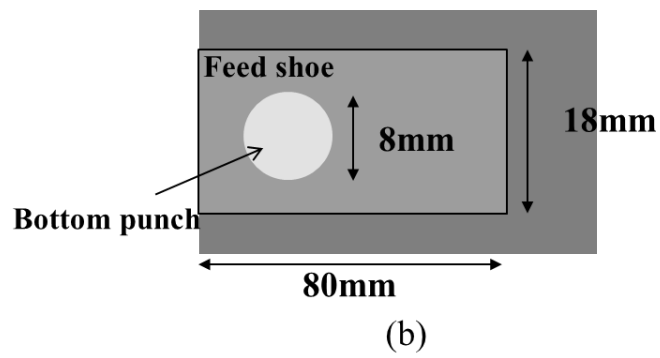
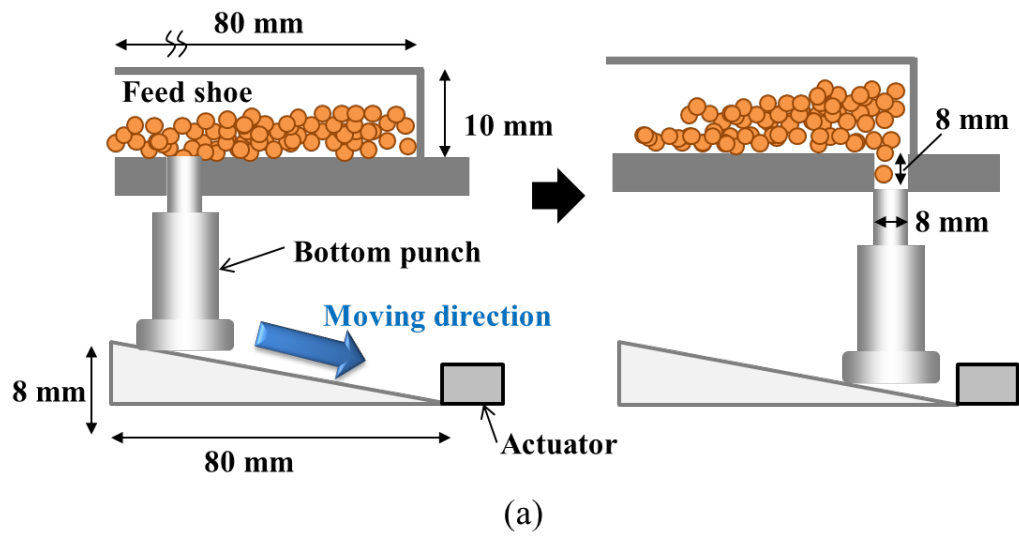


Figure 5-1 Schematic representation of the simulation setup. (a) Side view, (b) top view and (c) overview of experimental system.

5.2.2. Calibration of DEM parameters

Restitution, static friction and rolling friction coefficients were calibrated experimentally for NONPAREIL®-103. The particle-wall restitution coefficient e was determined by measuring the height to which a particle bounces when dropped from a height of 20 cm using a high-speed camera (MotionPro X4Plus, IDT inc.) at a frame rate of 500 fps (Figure 5-2(a)). Therefore,

$$e = \sqrt{\frac{h_2}{h_1}} \quad (5-1)$$

where h_1 is the initial height and h_2 is the bounce height. The particle-particle restitution coefficient was more challenging to evaluate than its particle-wall because the small size of the NONPAREIL® particles hindered the measurement of the relative bouncing of particles suggested in the literature (Wong et al., 2009; Bharadwaj et al., 2010; Gonzalez-Montellano et al., 2012). The NONPAREIL® samples were softly compacted at 7 MPa to produce a flat surface and a NONPAREIL® particle was dropped onto this surface for bounce height measurements. Static and rolling friction coefficients were obtained by measuring the angle of repose and rolling distance from a slope, respectively. The rolling distance was evaluated by letting the particles travel down from a plate inclined at 20° (Figure 5-2(b)). To measure the angle of repose, particles were randomly piled in a square-shaped box (3 cm × 3 cm × 10 cm) and allowed to roll by removing one of the box walls (Figure 5-2(c)). Bounce heights and rolling distances were measured ten times while angles of repose were determined three times. These obtained parameters were applied to differently-sized particles.

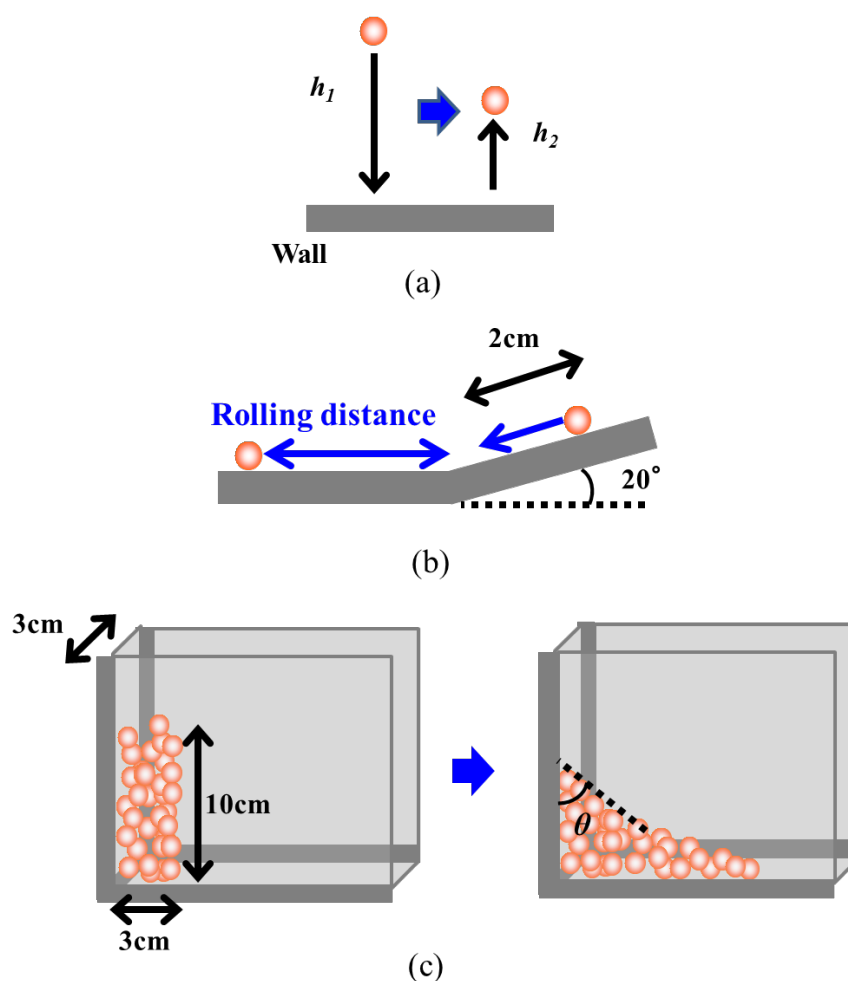


Figure 5-2 Calibration methods for DEM parameters. (a) Bounce height, (b) rolling distance and (c) angle of repose.

5.2.3. DEM simulations

The three-dimensional particle filling behaviour in the tableting process was simulated using the DEM approach (Cundell and Strack, 1979) implemented in the commercial EDEM software (DEM Solutions, Ltd.). In these simulations, all forces acting on particles are calculated during each time step and translational and rotational motions of all individual particles are subsequently updated by integrating Newton's equation of motion. For the i th particle,

$$m_i \frac{d\mathbf{v}_i}{dt} = \sum_j^n (\mathbf{F}_{c,n,ij} + \mathbf{F}_{c,t,ij}) - m\mathbf{g} \quad (5-2)$$

$$I_i \frac{d\boldsymbol{\omega}_i}{dt} = \sum_j^n (\mathbf{R}_{ij} \times \mathbf{F}_{c,t,ij} - \mathbf{M}\mathbf{r}_{ir}) \quad (5-3)$$

where \mathbf{v}_i is the translational velocity, $\boldsymbol{\omega}_i$ is the angular velocity, m_i is the mass, I_i is the moment of inertia, and \mathbf{R}_i is the radius. Normal and tangential forces ($\mathbf{F}_{c,n,ij}$ and $\mathbf{F}_{c,t,ij}$, respectively) between two particles are defined as

$$\mathbf{F}_{c,n,ij} = k_n \boldsymbol{\delta}_{n,ij} + c_n \dot{\boldsymbol{\delta}}_{n,ij} \quad (5-4)$$

$$\mathbf{F}_{c,t,ij} = \min \left\{ k_t \boldsymbol{\delta}_{t,ij} + c_t \dot{\boldsymbol{\delta}}_{t,ij}, \mu \mathbf{F}_{c,n,ij} \frac{\boldsymbol{\delta}_{t,ij}}{|\boldsymbol{\delta}_{t,ij}|} \right\} \quad (5-5)$$

where k_n is the normal stiffness coefficient, k_t is the tangential stiffness coefficient, c_n is the normal damping coefficient, c_t is the tangential damping coefficient, $\boldsymbol{\delta}_n$ is the normal overlap between particles, $\boldsymbol{\delta}_t$ is the tangential overlap between particles and μ is the coefficient of sliding friction. The DEM approach usually assumes that particles are spherical and accounts for the effect of particle shape by setting the rolling friction as

$$\mathbf{M} = -\mu_r |\mathbf{F}_{c,n,ij}| r_i \frac{\boldsymbol{\omega}_i}{|\boldsymbol{\omega}_i|} \quad (5-6)$$

where μ_r is the coefficient of rolling friction, r_i is the distance of contact point and $\boldsymbol{\omega}_i$ is the vector of angular velocity.

Simulation conditions are listed in Table 5-1. Feed shoe and filling die simulated geometries conformed to the experimental setup shown in Figure 5-1. Particles were randomly positioned in the feed shoe without overlapping and allowed to fall by gravity. At steady state, the die was activated while the bottom punch moved downward.

Table 5-1 DEM parameters and conditions

Parameters	Value
Young's modulus (GPa)	
Particle	0.1
Wall	210
Poisson's ratio (-)	
Particle	0.3
Wall	0.3
Particle density (kg/m ³)	1500
Simulation condition for monodisperse particles	
Time step (s)	1.0×10 ⁻⁶
Particle diameter (μm)	800
Number of particles (-)	30000

5.2.4. Quantification of segregation of binary particle mixtures

DEM simulations involving binary particle mixtures were performed to investigate the effect of small particle size (400, 300 and 200 μm), die velocity (500, 1000, 1500 and 2000 mm/s), and cell inside the die on the segregation index. Cells were created by dividing the die into three horizontal (Positions: -1, 0 and 1) and three vertical positions (Positions: -1, 0 and 1), as shown in Figure 5-3. Simulation conditions are described in Table 5-2. The die velocity was increased to 2000 mm/s because it appeared to correspond to the angular velocity of commercial tableting machines. The segregation index I_s (Zigan et al., 2008), which represents the homogeneity of the binary mixture in the die, was calculated as

$$I_s = \sqrt{\sum_i \frac{V_i}{V_L} \times \left[\frac{c_i - c_L}{c_L} \right]^2} \quad (5-7)$$

where c_i is the volume fraction of small particles in cell i , c_L is the mean volume fraction of small particles over all cells in the initial system, V_i is the volume occupied by

particles in cell i and V_L is the total volume occupied by all particles. The segregation index I_s equals zero when particles in cell i and overall exhibit the same volume fraction, which corresponds to the absence of segregation. In contrast, this index increases with enhanced segregation.

The effect of horizontal position (x_1), vertical position (x_2), particle size (x_3) and die velocity (x_4) on the segregation index I_s was assessed by RSM. Second order regression coefficients, which comprised main, interaction and quadratic effects as represented by equation (5-8), and p-values for individual input parameters were statistically analysed using JMP[®] 12 software (SAS Institute Inc., USA).

$$I_s = a_0 + \sum_i a_i x_i + \sum_i a_i x_i^2 + \sum_i \sum_j a_{ij} x_i x_j \quad (5-8)$$

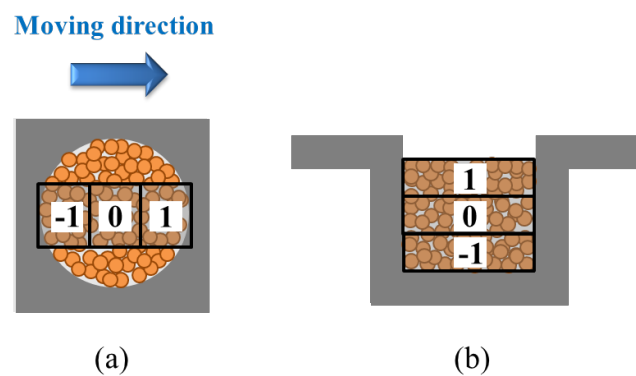


Figure 5-3. Compartmentalisation of the die. (a) Top view (horizontal position) and (b) side view (vertical position).

Table 5-2 Simulation conditions for binary particle mixtures

Parameters		Value			
Time step (s)		1.0×10 ⁻⁷			
Large particle size (μm)		500			
Number of large particles (-)		15788			
Small particle size (μm)	400	300	200		
Number of small particles (-)	30836	73093	246690		
Variables					
Horizontal position (-) ¹⁾	-1	0	1		
Vertical position (-) ¹⁾	-1	0	1		
Small particle size (μm)	400	300	200		
Die velocity (mm/s)	500	1000	1500	2000	

1) Detailed positions are described in Figure 5-3

5.3 Results and discussion

5.3.1 Material parameter calibration for DEM simulations

The accurate simulation of a dynamic particle flow system rests on the calibration of DEM parameters. The experimental bounce height, rolling distance, and angle of repose of NONPAREIL[®]-103 particles were measured (Table 5-3) to determine restitution, static friction and rolling friction coefficients (Table 5-4), respectively. The particle-wall restitution coefficient was about twice as high as its particle-particle counterpart because of the hardness and shock absorption ability of the wall. The particle-wall rolling friction coefficient was small, indicating that the particle rolled over a long distance on the stainless steel plate. In contrast, the particle-particle rolling friction coefficient reached a relatively high value of 0.112 because of friction or adhesive force between particles. The simulated angle of repose amounted to about 64°, in good agreement with the experimentally obtained value. These results were

consistent with parameters measured by Sibanc et al. (2013) for pharmaceutical pellets, which support the validity of parameters in this study. Obtained DEM parameters were used to substantiate the simulated particle flow behaviour.

Table 5-3 Experimental bounce height, rolling distance and angle of repose

Bounced height (cm) ¹⁾		
	Particle-Particle	2.362 ± 1.111
	Particle-Wall	9.238 ± 1.543
Rolling distance (cm) ¹⁾		
	Particle-Particle	4.19 ± 0.54
	Particle-Wall	6.03 ± 1.65
Angle of repose (degree) ²⁾		
		64 ± 1

1) Mean ±standard deviation (n = 10)

2) Mean ±standard deviation (n = 3)

Table 5-4 Summary of experimental DEM parameters

Coefficient of restitution (-)		
	Particle-Particle	0.336
	Particle-Wall	0.677
Coefficient of rolling friction (-)		
	Particle-Particle	0.112
	Particle-Wall	0.075
Coefficient of static friction (-)		
	Particle-Particle	0.4
	Particle-Wall	0.2

5.3.2 Comparison between experimental and simulated NONPAREIL[®] particle flow behaviours

Experimental and simulation results were compared qualitatively and quantitatively to validate the proposed DEM model. Figures 5-4(a) and (b) show high-speed camera snapshots of the die filling process. These snapshots revealed that the particles were gradually transferred into the die at a velocity of 100 mm/s, which led to low weight variation (Figure 5-4(a)). A velocity of 500 mm/s resulted in particle flow stream and cavity (Figure 5-4(b)). This cavity may induce high weight variations because of the unstable particle flow. During the post-filling compaction, capping, which corresponds to the cone-shaped failure of tablets, tends to occur because of air entrapment in the cavity. Figures 5-4(c) and (d) show numerical results obtained under the same conditions as experiments. These simulations demonstrated that a small cavity formed while the particles gradually filled the die at a velocity of 100 mm/s. On the other hand, a continuous bulk flow, consistent with the behaviour identified by Schneider et al. (2007), was associated with a cavity at a die velocity of 500 mm/s. Therefore, experimental results strongly agreed with simulations from the qualitative viewpoint (Figure 5-4).

To quantify the filling behaviour, the filling ratio δ was calculated as

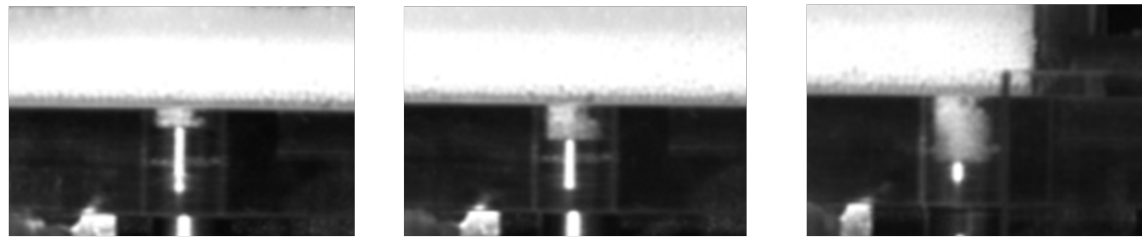
$$\delta = \frac{\sum V_p}{V} \quad (5-9)$$

where $\sum V_p$ is the sum of the volume occupied by all particles in the die and V is the volume of the die. Figure 5-5 compares the experimental and simulated filling ratios at the end of the filling process for various die velocities. Each experimental run was repeated three times and error bars on the plots represent the standard deviation. The filling ratio decreased with increasing die velocity, consistent with the decrease in the

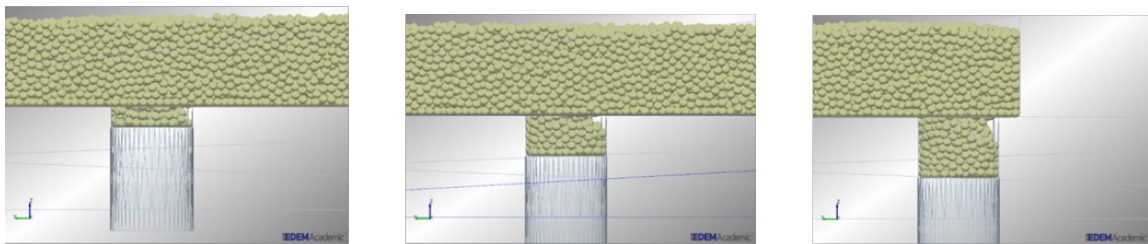
time needed by the particles to go through the feed shoe. Although the effect of air (i.e. negative pressure occurred by suction) was considered negligible, experiment and simulation showed reasonable agreement. In the current model, air impacted particle flow to a small extent because it escaped from the die during the filling process and particles were sufficiently large. This observation is consistent with a study by Guo et al. (2011b) stating that air does not hinder particle transfer from a moving feed shoe to a fixed die because it escapes from the die before completion of the powder coverage. In contrast, the filling ratio obtained by experiment was slightly larger than the simulated one. This is because the diameter of Nonpareil[®] particles is within a range of 710 - 850 μm (i.e. Nonpareil[®] is not monodispersed particle) (Figure 5-6). Since a packing behaviour of particles is highly affected by the distribution of particles, the filling ratio of experiment could be larger than that of simulation. Nevertheless, experimental and simulated results reasonably agreed with qualitatively and quantitatively. This model would be sufficient to simulate the filling behaviour accurately.



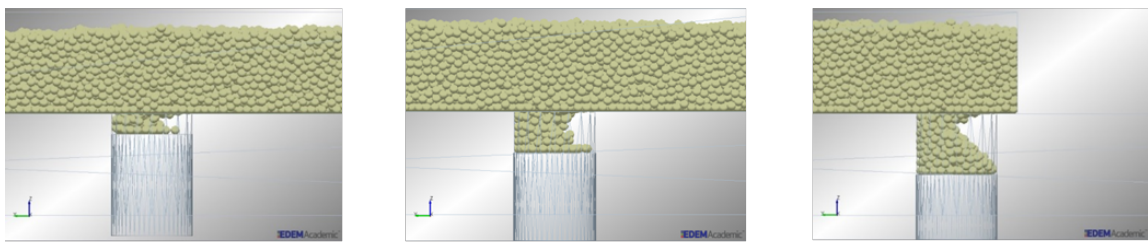
(a)



(b)



(c)



(d)

Figure 5-4 High-speed camera observations and simulated snapshots during filling process at different die velocities: (a) and (c) 100 mm/s and (b) and (d) 500 mm/s.

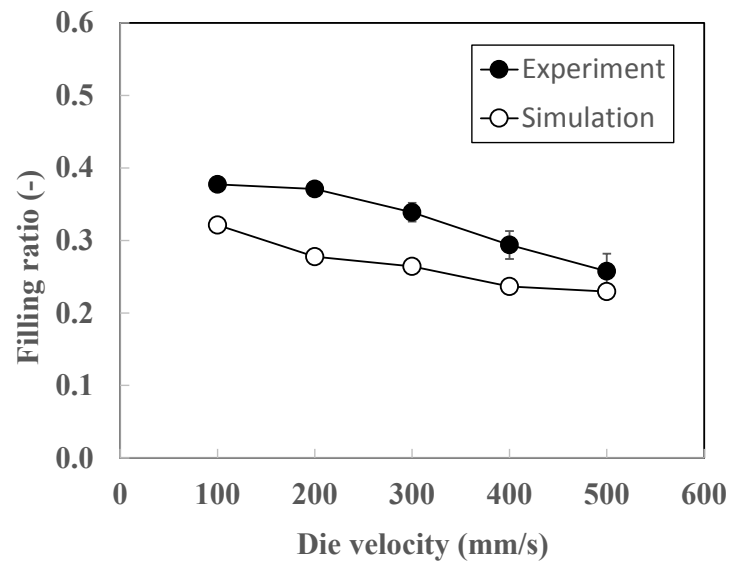


Figure 5-5 Experimental and simulated filling ratios as a function of die velocity. Error bars represent a standard deviation ($n = 3$).

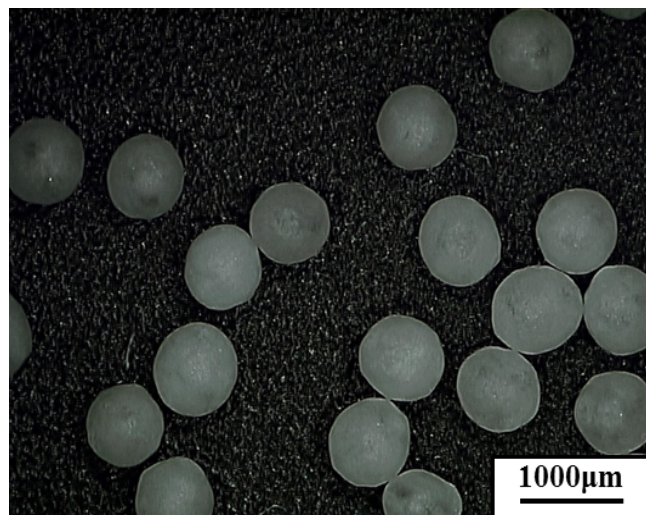


Figure 5-6 Optical micrograph of Nonpareil[®]

5.3.3 Segregation of binary particle mixtures

Pharmaceutical tableting involves a mixture of powders and granules exhibiting different properties. In the tableting machine, this mixture tends to segregate during 1) hopper discharge, 2) residence in the feed shoe and 3) die filling. Hopper discharge-related segregation has been extensively studied by experimental (Engblom et al., 2012) and numerical approaches (Ketterhagen et al., 2007). The influence of residence time and flow behaviour in the feed shoe has also been investigated to optimise paddle rotation and feed shoe shape (Mateo-Ortiz and Mendez, 2015). Segregation during die filling affects tablet quality but remains poorly understood, especially when the bottom punch simultaneously moves forwards and downwards.

The effects of die velocity and particle size on the segregation of binary mixtures, which greatly influences tablet content uniformity and compressibility, were assessed in detail through DEM simulations. Although the maximum die velocity in *section 5.3.2.* was set at 500 mm/s by the limitation of experimental apparatus, the range from 500 to 2000 mm/s were chosen for DEM simulation of binary mixture filling in order to investigate the filing behaviour including die velocity of commercial scale tableting machine, which typically achieves approximately 2000 mm/s. Figure 5-7 shows the typical powder flow behaviour at a die velocity of 500 mm/s for large (500 μm , blue) and small particles (200–400 μm , red). The particles flowed into the left side of the die (backward), similarly to the patterns observed in Figure 5-4. The segregation index was calculated over 108 points (Figure 5-8). Horizontal position 1 and vertical position -1 tended to display high I_s values, indicating that small particles flowed toward the bottom corner of the die and in the moving direction. Vertical position 1 consistently presented low I_s values, suggesting the absence of segregation in the

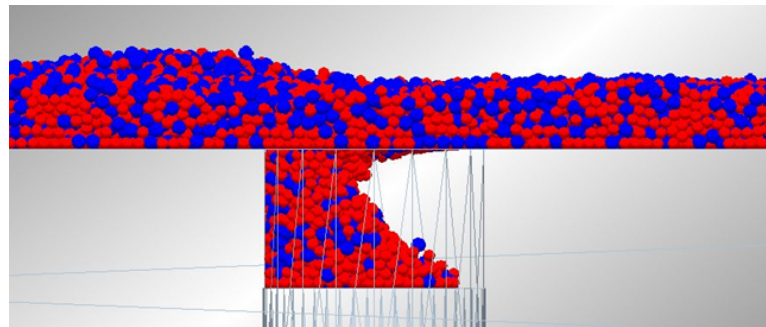
uppermost region of the die. The segregation index increased from horizontal position -1 to horizontal position 1 for $200\ \mu\text{m}$ particles in vertical positions -1 and 0 .

A statistical analysis was conducted regarding the effects of simulation conditions and positions on the segregation index (Table 5-5). In Table 5-5, p-values are listed in descending order, i.e. arranged from smallest to largest values. Conventionally, p-value less than 0.05 is regarded as statistically significant. The adjusted R -squared value (R^2) represents the proportion of the variation in the dependent variable and it is appropriate to evaluate the model for a multiple regression model. Figure 5-9 compares predicted and actual segregation indices. The adjusted R^2 value 0.74 indicated that the model fitted the data relatively well. Additionally, the 95% confidence interval curves (red dotted line) were not cross the mean of actual data (blue dotted line), indicating the overall regression model was statistically significant. Horizontal position (p-value < 0.0001), vertical position (p-value < 0.0001) and particle size (p-value < 0.0001) exhibited statistically significant effects for segregation index. Figure 5-10 shows response surface plots of the segregation index as a function of horizontal and vertical positions for different particle sizes at a die velocity of $500\ \text{mm/s}$. The Horizontal position and the Vertical position were selected for the horizontal axes of contour plot because these factors had more significant effect on the segregation index among all factors and interactions. In addition, the effect of small particle size which also significantly affected on the segregation index was illustrated in Figure 5-10(a) – (c). Predicted segregation index was calculated using all factors and their interactions. All response surfaces showed similar trends. Specifically, the segregation index reached a maximum at horizontal position 1 and vertical position -1 . This maximum increased with decreasing particle size at that position. The location of the particle in the die also

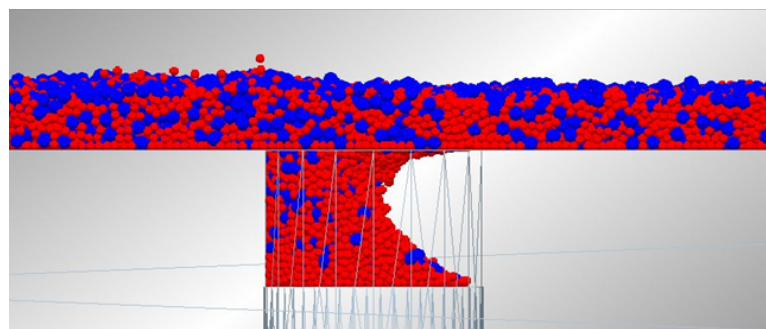
impacted the segregation index. During the die filling involving binary particle mixtures, small particles percolated between large particles in the feed shoe (Figure 5-11(a)) before flowing towards a corner of the die (Figure 5-11(b)). In addition, particle size affected the segregation index to a great extent. A decrease in small particle size enhanced percolation. For small particles measuring 300 and 400 μm in size and a die velocity of 500 mm/s, the segregation indices reached high values at horizontal position -1 , indicating that small particle segregation in this horizontal position may occur in some cases because of percolation (Figure 5-11(c)). The percolation-induced size segregation of finer particles during gravity filling of a container has been previously observed on the left-hand side of a container by DEM simulations (Shimosaka et al., 2013). The die velocity exhibited little influence on the segregation index (p-value = 0.5318). In addition, interaction and quadratic effects of the die velocity were statistically negligible. Small particle percolation, which progressed in the feed shoe before particles flowed into the die, impacted the segregation to a far greater extent than die velocity.

Previous experimental studies characterised a bulk flow of pharmaceutical powders without precisely analysing the movement of individual particles and segregation phenomena. Achieving control over segregation is important for the pharmaceutical tableting process because tablets comprise several powders with different properties, which may cause tableting issues such as capping and sticking. This study revealed that homogeneous particle sizes may prevent segregation. Moreover, die velocity had little effect on segregation. These results provide fundamental knowledge for enhancing the production efficiency and operation speed of tableting machine. In future work, it is suggested that the effects of granule shape, granule size

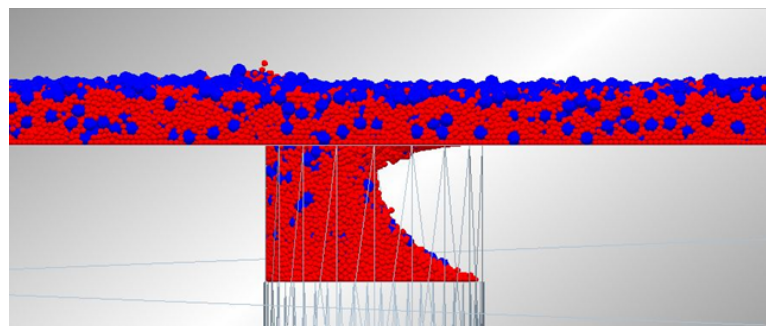
distribution and surface properties (e.g., electrostatic property and surface roughness) should be considered.



(a)



(b)



(c)

Figure 5-7 Snapshots of binary particle mixtures during die filling at a die velocity of 500 mm/s for different small particle sizes. (a) 400 μm , (b) 300 μm and (c) 200 μm . Large and small particles appear in blue and red, respectively.

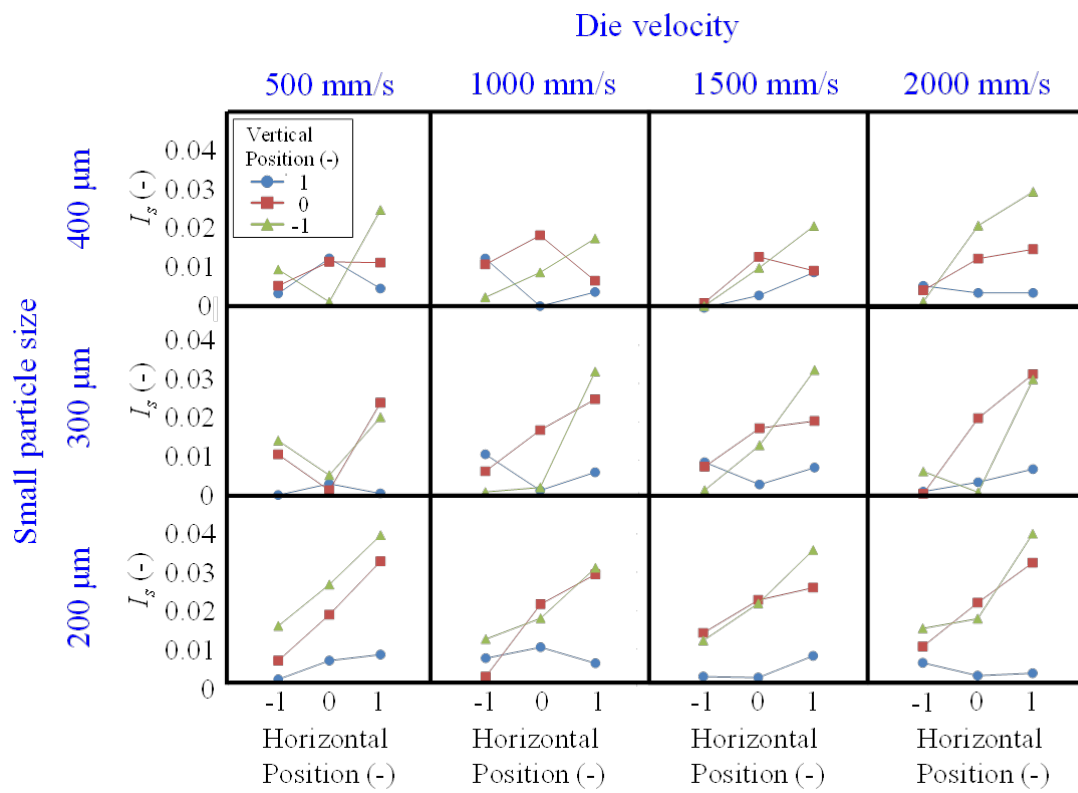


Figure 5-8 Effects of die velocity and small particle size on the segregation index for each of the horizontal and vertical positions.

Table 5-5 Multiple regression analysis of the segregation index

Factor	Segregation index I_s (-)	
	Coefficient	p -value
Horizontal position, x_1	0.0063426	<0.0001
Vertical position, x_2	-0.005786	<0.0001
$x_1 * x_2$	-0.005338	<0.0001
Small particle size, x_3	-3.286e-5	<0.0001
$x_2 * x_2$	-0.004299	0.0001
$x_2 * (x_3-300)$	-2.835e-5	0.0003
$x_1 * (x_3-300)$	-1.835e-5	0.0176
$x_1 * x_1$	0.0018149	0.0942
$x_1 * (x_4-1250)$	1.7533e-6	0.1172
$(x_3-300) * (x_3-300)$	1.4467e-7	0.1810
Die velocity, x_4	5.6811e-7	0.5318
$x_2 * (x_4-1250)$	-6.779e-7	0.5424
$(x_4-1250) * (x_4-1250)$	1.1734e-9	0.5635
$(x_4-1250) * (x_3-300)$	3.7872e-9	0.7334
Constant	0.0216114	<0.0001

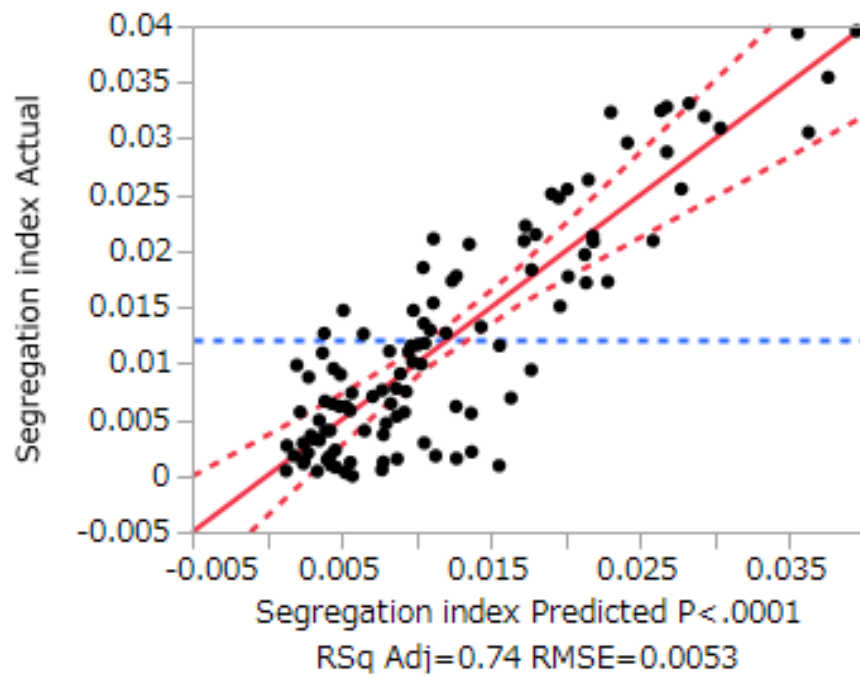
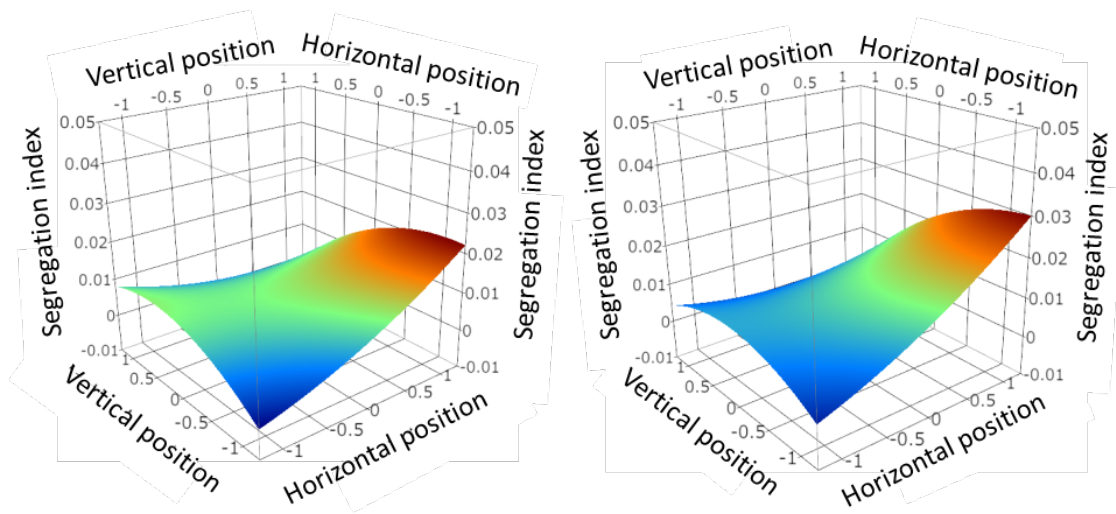
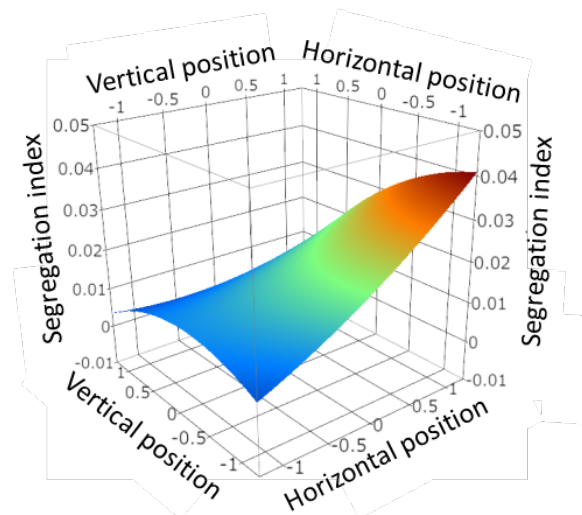


Figure 5-9 Predicted and actual segregation indices. Red line, red dotted lines and blue dotted line represents the fitted regression line, the 95% confidence curves and the mean of actual data, respectively.



(a) Small particle size: 400μm

(b) Small particle size: 300μm



(c) Small particle size: 200μm

Figure 5-10 Response surface plots of the segregation index as a function of horizontal and vertical positions at a die velocity of 500 mm/s for different small particle sizes.

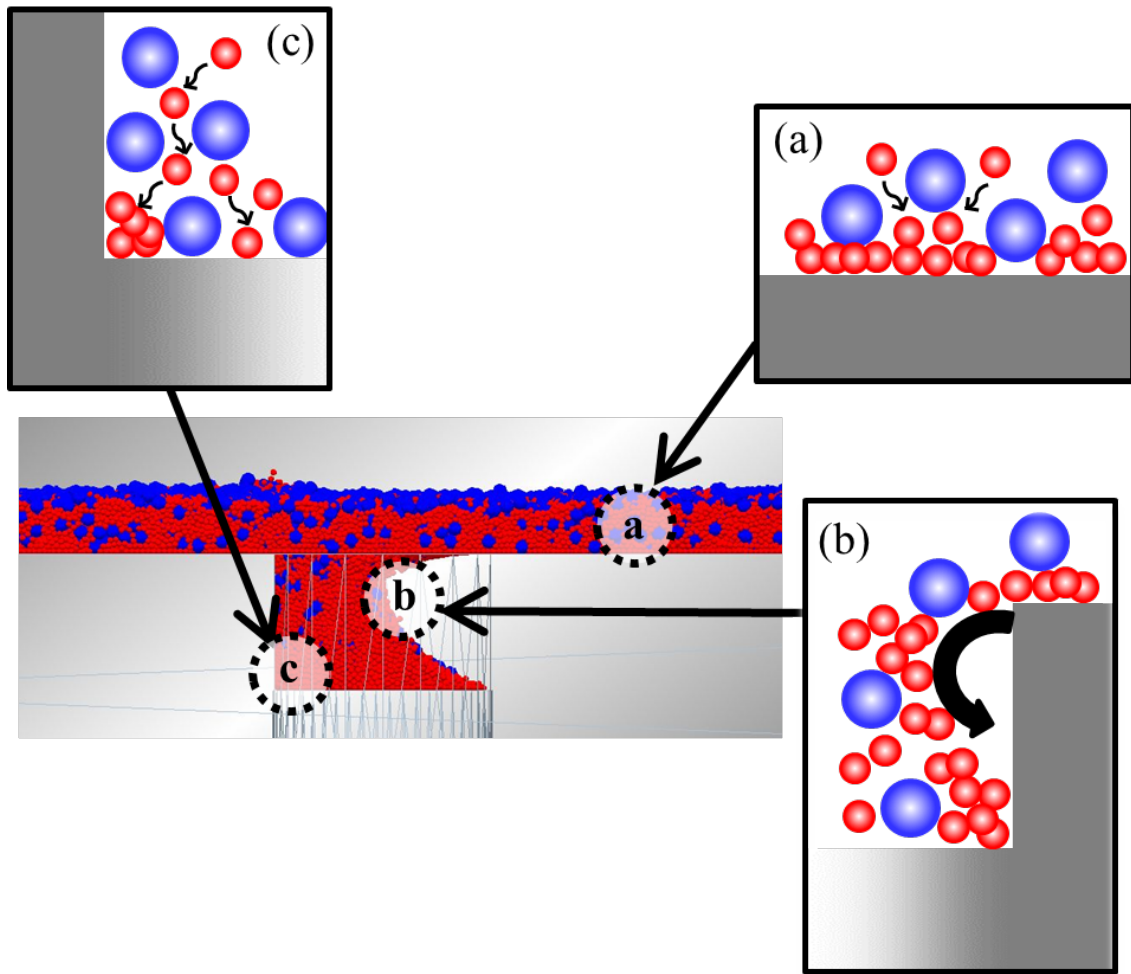


Figure 5-11 Schematic representation of small particle segregation. (a) Small particle percolation in the feed shoe. (b) Small particle flow leading to segregation at the bottom front corner of the die. (c) Small particle percolation of at the bottom back corner of the die.

5.4 Conclusion

The particle flow pattern and size-induced segregation during die filling were investigated by the DEM and the results were statistically analysed using RSM. DEM parameters, including restitution, rolling friction and static friction coefficients, were experimentally calibrated to capture the accurate particle filling behaviour. The resulting DEM model was validated by comparing experimental and simulated results obtained for monodisperse particles. Particles were gradually delivered into the die at a low die velocity. In contrast, particle flow stream was observed concomitant with cavity formation when the die velocity increased. In addition, numerical filling ratios agreed well with the experimental results. This comparison substantiated the ability of the model to describe particle flow.

The behaviour of binary particle mixtures during die filling was also investigated by DEM simulations with RSM to assess the effects of particle size, die velocity and position in the die on segregation. Unlike particle size and position in the die, die velocity had little impact on the segregation. A detailed monitoring of the filling behaviour revealed that small particles percolated between large particles in the feed shoe before reaching the die and flowing towards its corner. The use of DEM combined with RSM approach has a potential to be a powerful method to capture the segregation behaviour effectively and it is useful for optimizing the process parameters.

References

- Bacher, C., Olsen, P.M., Bertelsen, P., Sonnergaard, J.M., 2008. Granule fraction inhomogeneity of calcium carbonate/sorbitol in roller compacted granules, *Int. J. Pharm.* 349, 19-23.
- Bharadwaj, R., Smith, C., Hancock, B.C., 2010. The coefficient of restitution of some pharmaceutical tablets/compacts, *Int. J. Pharm.* 402, 50-56.
- Cundell, P.A., Strack, O.D.L., 1979. A discrete numerical model for granular assemblies, *Geotechnique*, 29, 47-65.
- Davies, P., 2001. Oral Solid Dosage Forms, in: Gibson, M. (Eds.), *Pharmaceutical Preformulation and Formulation*. CRC Press LLC., Florida, pp. 379-458.
- Engblom, N., Saxen, H., Zevenhoven, R., Nylander, H., Enstad, G.G., 2012. Effects of process parameters and hopper angle on segregation of cohesive ternary powder mixtures in a small scale cylindrical silo, *Adv. Powder Technol.* 23, 566-579.
- Gonzalez-Montellano, C., Fuentes, J. M., Ayuga-Tellez, E., Ayuga, F., 2012. Determination of the mechanical properties of maize grains and olives required for use in DEM simulations, *J. Food Eng.* 111, 553-562.
- Guo, Y., Wu, C-Y., Kafui, K. D., Thornton, C., 2009a. Numerical analysis of density-induced segregation during die filling, *Powder Technol.* 197, 111-119.
- Guo, Y., Kafui, D., Wu, C-Y., Thornton, C., Seville, J.P.K., 2009b. A coupled DEM/CFD analysis of the effect of air on powder flow during die filling, *AIChE J.* 55, 49-62.
- Guo, Y., Wu, C-Y., Thornton, C., 2011a. The effect of air and particle density difference on segregation of powder mixtures during die filling, *Chem. Eng. Sci.* 66, 661-673.
- Guo, Y., Wu, C-Y., Kafui, K.D., Thornton, C., 2011b. 3D DEM/CFD analysis of size-induced segregation during die filling, *Powder Technol.* 206, 177-188.
- Jackson, S., Sinka, I.C., Cocks, A. C. F., 2007. The effect of suction during die fill on a rotary tablet press, *Eur. J. Pharm. Biopharm.* 65, 253-256.
- Ketterhagen, W.R., Curtis, J.S., Wassgren, C.R., Kong, A., Narayan, P.J., Hancock, B.C., 2007. Granular segregation in discharging cylindrical hoppers: A discrete element and experimental study, *Chem. Eng. Sci.* 62, 6423-6439.
- Lakio, S., Siiria, S., Raikkonen, H., Airaksinen, S., Narvanen, T., Antikainen, O., Yliruusi, J., 2010. New insights into segregation during tableting, *Int. J. Pharm.* 379, 19-26.
- Lakio, S., Hatara, J., Tervakangas, H., Sandler, N., 2012. Determination of segregation tendency of granules using surface imaging, *J. Pharm. Sci.* 101, 2229-2238.

- Mateo-Ortiz, D., Muzzio, F. J., Mendez, R., 2014. Particle size segregation promoted by powder flow in confined space: The die filling process case, *Powder Technol.* 262, 215-222.
- Mateo-Ortiz, D., Mendez, R., 2015. Relationship between residence time distribution and forces applied by paddles on powder attrition during the die filling process, *Powder Technol.* 278, 111-117.
- Mills, L. A., Sinka, I. C., 2013. Effect of particle size and density on the die fill of powders, *Eur. J. Pharm. Biopharm.* 84, 642-652.
- Narisawa, S., Nagata, M., Hirakawa, Y., Kobayashi, M., Yoshino, H., 1996. An Organic Acid-Induced Sigmoidal Release System for Oral Controlled-Release Preparations. 2. Permeability Enhancement of Eudragit RS Coating Led by the Physicochemical Interactions with Organic Acid, *J. Pharm. Sci.* 85, 184-188.
- Nwose, E. N., Pei, C., Wu, C-Y., 2012. Modelling die filling with charged particles using DEM/CFD, *Particuology*, 10, 229-235.
- Palugan, L., Cerea, M., Zema, L., Gazzaniga, A., Maroni, A., 2015. Coated pellets for oral colon delivery, *J Drug Deliv. Sci. Tech.* 25, 1-15.
- Poutiainen, S., Pajander, J., Savolainen, A., Ketolainen, J., Jarvinen, K., 2011. Evolution of granule structure and drug content during fluidized bed granulation by X-ray microtomography and confocal raman spectroscopy, *J. Pharm. Sci.* 100, 5254-5269.
- Schneider, L.C.R., Sinka, I.C., Cocks, A.C.F., 2007. Characterisation of the flow behaviour of pharmaceutical powders using a model die-shoe filling system, *Powder Technol.* 173, 59-71.
- Shimizu, T., Nakano, Y., Morimoto, S., Tabata, T., Hamaguchi, N., Igari, Y., 2003. Formulation study for Lansoprazole Fast-disintegrating Tablet. I. Effect of Compression on Dissolution Behavior, *Chem. Pharm. Bull.* 51, 942-947.
- Shimosaka, A., Shirakawa, Y., Hidaka, J., 2013. Effects of Particle Shape and Size Distribution on Size Segregation of Particles, *J. Chem. Eng. Jpn.* 46, 187-195.
- Sibanc, R., Kitak, T., Govedarica, B., Srcic, S., Dreu, R., 2013. Physical properties of pharmaceutical pellets, *Chem. Eng. Sci.* 86, 50-60.
- Sinka, I.C., Schneider, L.C.R., Cocks, A.C.F., 2004. Measurement of the flow properties of powders with special reference to die fill. *Int. J. Pharm.* 280, 27-38.
- Sinka, I. C., Motazedian, F., Cocks, A. F. C., Pitt, K. G., 2009. The effect of processing parameters on pharmaceutical tablet properties, *Powder Technol.* 189, 276-284.
- Van den Dries, K., Vromans, H., 2002. Relationship between inhomogeneity phenomena and granule growth mechanisms in a high-shear mixer, *Int. J. Pharm.*

247, 167-177.

- Virtanen, S., Antikainen, O., Raikonen, H., Yliruusi, J., 2009. Granule size distribution of tablets, *J. Pharm. Sci.* 99, 2061-2069.
- Wong, C., Daniel, M., Rongong, J., 2009. Energy dissipation prediction of particle dampers, *J. Sound Vib.* 319, 91-118.
- Wu, C-Y., 2008. DEM simulations of die filling during pharmaceutical tableting, *Particuology*, 6, 412-418.
- Wu, C-Y., Guo, Y., 2012. Numerical modelling of suction filling using DEM/CFD, *Chem. Eng. Sci.* 73, 231-238.
- Xie, L., Wu, H., Shen, M., Augsburg, L.L., Lyon, R.C., Khan, M.A., Hussain, A.S., Hoag, S.W., 2008. Quality-by-Design (QbD): Effect of testing parameters and formulation variables on the segregation tendency of pharmaceutical powder measured by the ASTM D 6940-04 segregation tester, *J. Pharm. Sci.* 97, 4485-4497.
- Yaginuma, Y., Ozeki, Y., Kakizawa, M., Gomi, S.I., Watanabe, Y., 2007. Effects of powder flowability on die-fill properties in rotary compression, *J Drug Deliv. Sci. Tech.* 17, 205-210.
- Zigan, S., Thorpe, R.B., Tuzun, U., Enstad, G.G., Battistin, F., 2008. Theoretical and experimental testing of a scaling rule for air current segregation of alumina powder in cylindrical silos, *Powder Technol.* 183, 133-145.

Chapter 6

Numerical evaluation of the capping tendency of microcrystalline cellulose tablets during a diametrical compression test

6.1 Introduction

The tableting process is well-known to have many problems, including sticking, capping, lamination, chipping and binding. Capping (also known as cone-shaped failure), the separation of a tablet into two parts: cap and body, is one of the most common tableting issues. Preventing capping during the entire tableting process is highly desired because the capped tablets have a severe influence on the tablet quality during the subsequent coating, handling, packaging and transport processes. To prevent capping, many research studies have been conducted on the factors that cause capping, such as the local stress concentration due to elastic recovery (Dwivedi et al., 1992; Han et al., 2008), high residual die wall pressure (Sugimori et al., 1989a, 1989b), air entrapment (Tanino et al., 1995), and weak binding strength between granules (Sugimori et al., 1989b). In general, the capping tendency is considered to decrease with reducing tableting speed, adding pre-compression, applying low compaction forces, improving the formulation and optimising the blending process. However, a detailed understanding of the capping mechanism is important for the development of a robust process, as recommended by the ICH Q8(R2). Therefore, several novel prediction methods of the capping tendency have been investigated. Nakamura et al. (2011, 2012) proposed that the capping tendency could be evaluated using the energy of elastic recovery and plastic deformation. Kuppuswamy et al. (2001) predicted the capping tendency using a static indentation test. Akseli et al. (2013) developed predictive tools of the capping tendency using an ultrasonic measurement and proposed a capping index that is the ratio of the sum of the number of capped tablets during ejection and strength test (diametrical compression test) divided by the total number of tested tablets. The capping occurring during strength test serves as a warning of the capping during the

tableting process; consequently, as a useful and simple method to predict the capping tendency, the strength test was chosen as a prediction tool for the capping tendency.

The continuum approach, known as the finite element method (FEM), regards the powder as a mechanical continuum. Although pharmaceutical powders in the tablet are not a continuous medium at the particle level, the useful information, such as distributions of density, stress and strain, can be obtained when the powder is small and dense enough. The Drucker-Prager Cap model (DPC model), which considers shear failure and the plastic yielding, has been used as a constitutive model of FEM to determine the local mechanical properties of pharmaceutical powder during powder compactions (Michrafy et al., 2002; Sinka et al., 2003; Cunningham et al., 2004; Wu et al., 2005, 2008; Han et al., 2008; Klinzing et al., 2010; Sinha et al., 2010a, 2010b; Diarra et al., 2013; Hayashi et al., 2013; Kadiri and Michrafy, 2013; Sinka et al., 2013). Using the FEM, Michrafy et al. (2002) simulated the relative density distribution and the stress distribution within a lactose tablet. Sinka et al. (2003) applied FEM to a microcrystalline cellulose (MCC) tablet compaction process and obtained a surface density map based on an indentation tests to validate their FEM simulation results. MCC is one of the powders most frequently used in the pharmaceutical industry, with many researchers having investigated the compaction properties of MCC tablets in the die during the tableting process. Regarding capping, several previous FEM studies also reported that stress concentration at the upper edge of a tablet under the process of ejection during tableting may lead to capping (Wu et al., 2005, 2008; Han et al., 2008; Kadiri and Michrafy, 2013). Comparing the FEM results of the stress concentration with the X-ray Computed Tomography results of the characterisation of an internal crack in tablet, Wu et al. (2008) suggested that capping occurs due to the stress

concentration in the tablet due to the forces applied by the dies during the ejection process. All of these research studies help to understand the capping mechanism scientifically; however, a more convenient method must be developed to determine whether the capping tendency will occur. Therefore, in this study, I attempted to develop such an estimation method to enable a robust tableting process.

Capping typically occurs during compression, unloading or ejection from the die and subsequent coating and packaging, or physical testing (Akseli et al., 2014). It will be highly desired if one can know the changes of mechanical properties or mechanical state under the loading conditions and the correlations between these changes inside the tablet and capping. The objective of this study is to explore possible approach to estimate capping tendency by investigation on the mechanical behaviour of pharmaceutical powder. In this paper, using the simple diametrical compression test (i.e., strength test), the effects of double-radius and single-radius concave punch shapes on the capping tendency were investigated by the 3D FEM simulations without introduction of complex failure criteria into the constitutive model. MCC is one of the most frequently used powders in the pharmaceutical industry as the excipient added to a pharmaceutical formulation, and the mechanical behaviours during the powder compaction have been investigated by many researchers. To compare with previous studies, in this paper MCC is chosen as the study objective. The density-dependent DPC model was implemented using ABAQUS software with a user subroutine. Pharmaceutical powder compactions were simulated firstly; subsequently, the diametrical compression analysis of the tablets generated with prior FEM compaction simulations were conducted for further analysis. During the diametrical compression simulation of the tablets, the variation in the plastic strain within tablets was

investigated and visualised using the AC YIELD output of ABAQUS as a possible estimation method of the capping tendency.

6.2 Materials and Methods

6.2.1. Materials

The powder material examined in this study was microcrystalline cellulose (MCC, CEOLUS PH-101, Asahi Kasei Chemicals, Japan). The average particle size for this MCC were determined by laser diffraction using a Mastersizer2000 with a dry powder feeder Scirocco 2000 (Malvern Instruments Ltd., UK) and the bulk density was determined using a 100 mL cylindrical vessel according to Japanese pharmacopoeia (XVI). These measurements were conducted three times. The average particle size and the bulk density were 62.9 μm and 0.29 g/cm^3 respectively. The die wall and punches were lubricated with a magnesium stearate (NOF Corporation, Japan) to reduce the friction between the die wall and the powder.

6.2.2. Tableting and diametrical compression testing

MCC powder was compacted using a single tableting machine with a 20 kN load cell and an instrumented die (TK-TB20kN, TOKUSHU KEISOKU co., ltd, Japan) set at 1 mm/s compaction speed and 1 mm/s ejection speed. The parameters of the upper punch displacement, lower punch displacement, upper punch force, lower punch force and die wall stress were recorded every 0.2 ms. Force and displacement transducers are accurately-calibrated every year by a manufacturer to ensure the reliability of experimental data. Force and displacement transducers have an accuracy of ± 0.01 kN and ± 10 μm , respectively. The die wall and punches were lubricated with a small amounts of magnesium-stearate by brushing before each compaction. Single-radius (R:

12 mm, Cup depth: 0.65 mm, Figure 6-1(a)) and double-radius (R1: 11 mm, R2: 3.75 mm, Cup depth: 1.02 mm, Figure 6-1(b)) concave 8 mm diameter punches (I Holland Ltd., UK) were used to prepare tablets containing 200 mg MCC powder. The MCC powder was manually filled into the die and was compacted on the punch forces varied from 1 kN to 10 kN without pre-compression. Punches and die were cleaned and wiped using a cloth and ethanol after each compaction. Prior to strength testing, the weight and thickness were measured by an analytical balance (AB104, METTLER TOLEDO International Inc., Switzerland) and a micrometer (PK-1012, Mitutoyo, Japan), respectively. Failure load of tablets were measured immediately after weight and thickness measurements using a strength tester (Dr. Schleuniger Pharmatron, Model 6D, USA). A high-speed camera (VW-9000, KEYENCE Corporation, Japan) was used to observe fracture initiation and propagation during the diametrical compression test at a recording speed of 1,000 fps.

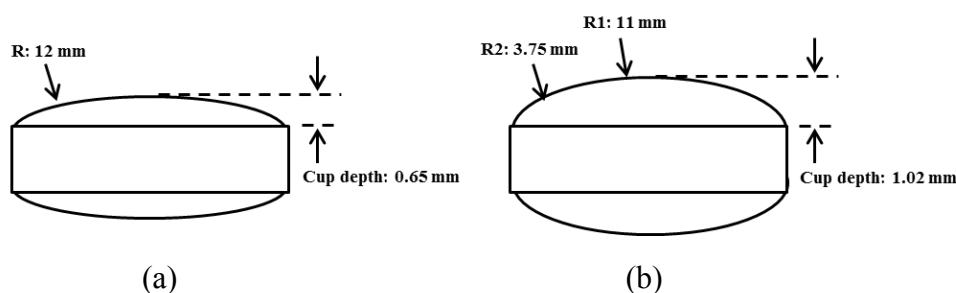


Figure 6-1 Schematic drawings of tablet shapes. (a) Single-radius, (b) Double-radius.

6.2.3. Evaluation of the capping tendency

Capping is a common defect in pharmaceutical compression processes, in which the cap of a tablet splits from the body parts. A friability test is often used to determine whether capping occurs via visual inspection after tumbling using a

friabilator. In this study, the capping tendency was evaluated using the diametrical compression test because this test can be simulated easily by the FEM. During diametrical compression testing, tablets are placed horizontally between the flat platens; after the test, the fracture pattern of the tablet was determined. A tablet splitting into halves along the loading direction (as shown in Figure 6-2) was defined as having no capping tendency. On the other hand, a delaminated tablet that split not only along the loading direction but also in the direction perpendicular to the loading direction (shown in Figure 6-3) was defined as having a capping tendency (Lennartz and Mielck, 1998; Akseli et al., 2013; Bozic et al., 2008).

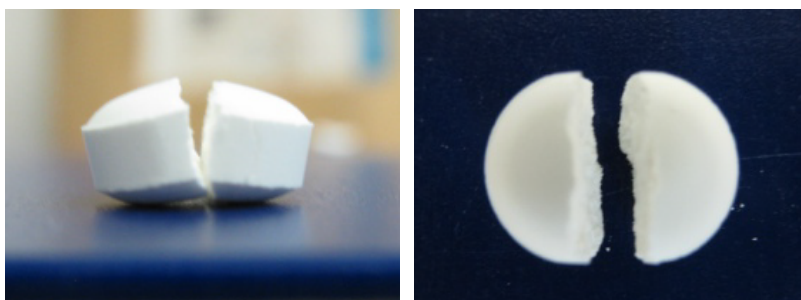


Figure 6-2 Failure patterns of tablets without a capping tendency after the diametrical compression test.



Figure 6-3 Failure patterns of tablets with a capping tendency after the diametrical compression test.

6.2.4. Numerical simulation

The DPC model (Drucker and Prager, 1952) used in this study has been widely used and has been described in detail in many previous reports in the literature (Sinka and Cocks, 2007). Figure 6-4 presents a family of 2D Drucker-Prager cap surfaces corresponding to different densities, where p and q are the hydrostatic pressure and the von-Mises equivalent stress, respectively. Briefly, the yield surface of the DPC model consists of the shear failure surface F_s , the cap surface F_c and the transition surface F_t , as given below (Wu et al., 2005):

$$F_s = q - p \tan \beta - d = 0 \quad (6-1)$$

$$F_c = \sqrt{(p - p_a)^2 + \frac{R^2 q^2}{\left(1 + \alpha - \frac{\alpha}{\cos \beta}\right)^2}} - R(d + p_a \tan \beta) = 0 \quad (6-2)$$

$$F_t = \sqrt{(p - p_a)^2 + \left[q - \left(1 - \frac{\alpha}{\cos \beta}\right)(d + p_a \tan \beta) \right]^2} - \alpha(d + p_a \tan \beta) = 0 \quad (6-3)$$

where d is the cohesion of the powder, β is the friction angle, and R and α are a parameter that determining the shape of the cap segment and a small number that defines the transition surface F_t between the shear failure face and the cap face, respectively. p_a is an evolution parameter that represents the volumetric plastic strain driven hardening/softening. Assuming that the model is isotropic, to define the yield surface of the DPC model, a total of five parameters, i.e., d , β , R , α and p_a , are required; all of these parameters are functions of the relative density (RD) which is defined as

$$RD = \frac{\rho}{\rho_{app}} \quad (6-4)$$

where ρ is the current density and the density of apparent fully densified particle ρ_{app} is 1.577 g/cm^3 (Kumar and Kothari, 1999; Shang et al., 2013a) measured using a helium pycnometer.

The DPC parameters (d , β , R and p_a) and elastic parameters (Young's modulus and Poisson's ratio) were obtained using a previously published method (Cunningham et al., 2004; Sinka and Cocks, 2007; Han et al., 2008). Because the 2D shear failure surface is a straight line, the 2D shear failure surface can be determined by diametrical compression test and uniaxial compression test (Figure 6-4). A diametrical compression and a uniaxial compression tests of MCC compacts were carried out using the single tableting machine the same as describe by Han et al. (2008). From the radial tensile strength of tablet σ_d measured from diametrical compression test, defined as $\sigma_d = \frac{2F_d}{\pi Dt}$ (where F_d is the maximum crush force, D is the diameter of the tablet and t

is the thickness of tablet), and the uniaxial strength σ_c , defined as $\sigma_c = \frac{2F_y}{\pi D^2}$ (where F_y is the uniaxial yield force), obtained from uniaxial compression test, d and β can be determined as follows (Han et al., 2008):

$$d = \frac{\sigma_c \sigma_d (\sqrt{13} - 2)}{\sigma_c - 2\sigma_d} \quad (6-5)$$

$$\tan \beta = \frac{3(\sigma_c - d)}{\sigma_c} \quad (6-6)$$

The state of stress (p_A , q_A) produced by an instrumented die compression test at the cap surface (Figure 6-4) can be used to deduce the parameters p_a and R as follows (Doremus,

2007):

$$p_a = (-B + \Delta^{1/2}) / 2A \quad (6-7)$$

where $\Delta = B^2 - 4AC$, $A = 2[(1 + \alpha - \alpha/\cos \beta)\tan \beta]^2$, $B = 3q_A + 4d(1 + \alpha - \alpha/\cos \beta)\tan \beta$, and $C = 2d^2 - 3p_A q_A - 2q_A^2$

$$R = \sqrt{\frac{2(1 + \alpha - \alpha/\cos \beta)^2}{3q_A}}(p_A - p_a) \quad (6-8)$$

The parameter α , which determines the transition face, is usually set between 0.01 and 0.05. In this study, α was set as 0.02 (Han et al., 2008).

The Young's modulus and Poisson's ratio can be determined from the unloading curve of a die compaction experiment. The Young's modulus and Poisson's ratio were also obtained as a function of the relative density. The die-wall friction coefficient was calculated from the Janssen-Walker equation, which was based on the differential slice method (Janssen, 1895; Walker, 1966; Cunningham et al., 2004). Because the die wall was adequately lubricated, a small die-wall friction coefficient of 0.08 was obtained from the experiments, which was similar to values published in the literature (Cunningham et al., 2004; Han et al., 2008). The die-wall friction coefficient was applied on the powder/wall and powder/punch interfaces.

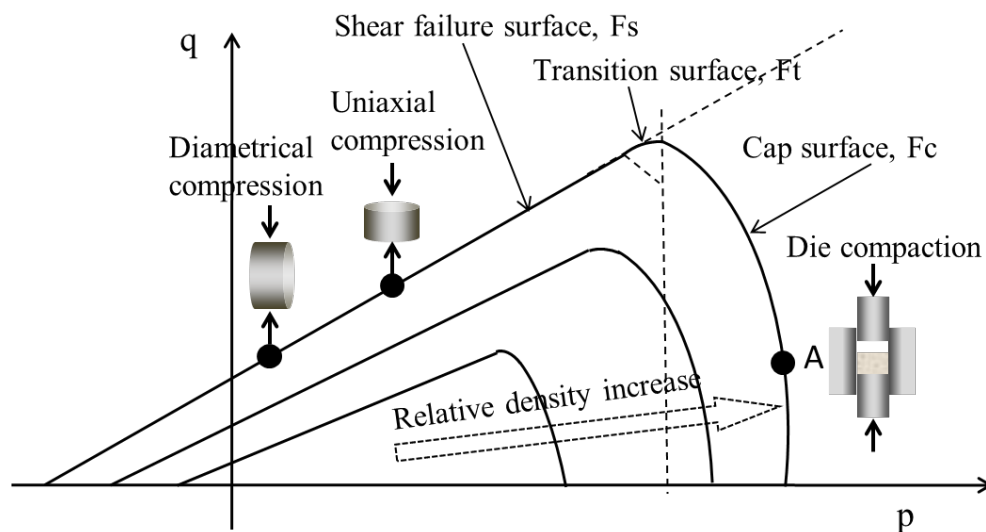


Figure 6-4 A schematic illustration of the density-dependent Drucker-Prager Cap model.

FEM simulations of powder compactions and diametrical compression of the whole 3D model were performed using ABAQUS/standard (version 6.11), and the density-dependent DPC model was implemented via user subroutines (USDFLD). Figure 6-5 shows only half of the 3D finite element model and the simulation procedure. The die wall and the upper/lower punches were modelled as discrete rigid bodies by 4-node 3-D bilinear rigid quadrilateral elements (R3D4) with element size of 0.3 mm. The cylindrical die was modelled 8 mm in diameter and 15 mm in height with 1 mm radius fillet on the top edge of the die. Two types of punches were employed, dingle-radius (R: 12 mm, Cup depth: 0.65 mm) and double-radius (R1: 11 mm, R2: 3.75 mm, Cup depth: 1.02 mm) concave with 8 mm in diameter. The 3D eight-node brick elements with reduced integration (C3D8R) was used for modelling the powders. The powder model of initial volume of 307.2 mm^3 (200 mg weight, relative density of 0.42

resulting from the minimum relative density which can be calibrated) before powder compaction was modelled by elements produced by sweeping technique in element size of 0.2 mm. To investigate the internal change during the powder compaction and the tablet diametrical compression in more detail, the refined elements with 0.12 mm in element height were used in the middle part of powder model (Figure 6-5). In the simulation, first, the lower punch was fixed, and the upper punch was applied the displacement boundary condition to compress the powder to a specified thickness (compaction thickness), then the upper punch was removed and the lower punch was moved upwards by applying a displacement boundary condition of 14 mm to eject the tablets. After being ejected from the die completely, the FEM model with the density distribution and stress distribution produced in powder compaction analysis was used in the diametrical compression simulation to determine the subsequent pattern of fractures. The powder model was compressed in diametrical direction by two rigid plates modelled by R3D4 elements with the element size of 0.25 mm. One of the rigid plate was fixed and the other plate (Figure 6-5) was applied displacement boundary conditions. During the simulation the interaction between the powder, die wall, upper/lower punches and rigid plates was modelled by finite sliding contact with the friction coefficient determined from experiments. The reaction force of the upper punch at the end of powder compaction was recorded as the compaction force, and the largest distance between the upper surface and lower surface of the powder after the ejection was defined as the thickness (Figure 6-5).

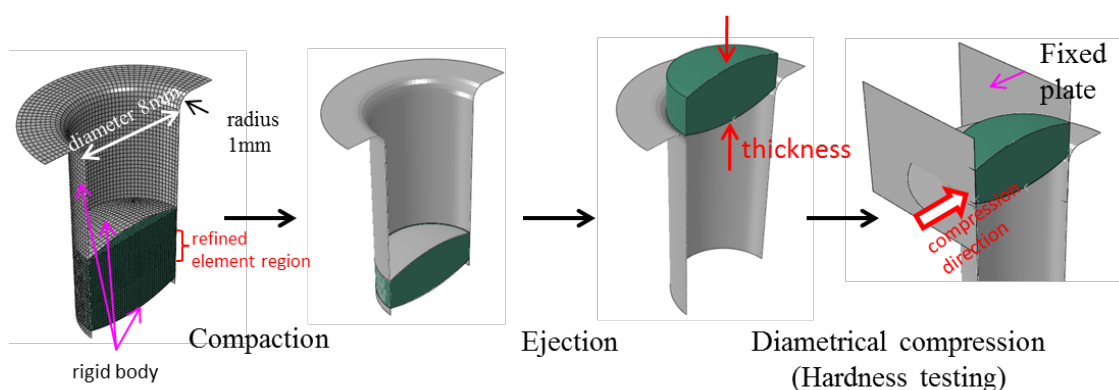


Figure 6-5 FEM simulation procedure of compaction and of the diametrical compression test.

6.3 Results and discussion

6.3.1. Compaction and strength test of microcrystalline cellulose tablets

The effects of double-radius and single-radius concave punch shapes on the capping tendency during diametrical compression test were investigated. Table 6-1 lists the weight, the thickness and the failure load at various compaction forces, and the relationship between the compaction force and the failure load of the tablets in both double-radius and single-radius shapes are shown in Figure 6-6. The open symbols represent the cases in which the capping tendency was observed. The failure load of both types of shaped tablets exhibited the same increasing trend with the compaction force; however, the capping tendency of the double-radius tablet occurred at a lower compaction force. Because the curvature of the punch is one of the factor that influence the capping tendency, development of a method to estimate the capping tendency when the curvature of the tablet changes is necessary to design a better tablet shape.

Table 6-1 Physical properties of tablets obtained on various compaction forces.

	Compaction Force (kN)	Weight (mg)	Thickness (mm)	Failure load (N)	Capping tendency
Double radius concave	0.97 ± 0.03	200.8 ± 0.9	5.77 ± 0.01	48 ± 2	No
	2.14 ± 0.03	200.7 ± 1.0	4.74 ± 0.01	124 ± 3	No
	3.74 ± 0.05	200.9 ± 1.1	4.27 ± 0.01	199 ± 5	No
	5.29 ± 0.14	200.6 ± 0.9	3.98 ± 0.01	269 ± 6	Yes
	7.12 ± 0.22	201.0 ± 1.1	3.83 ± 0.01	333 ± 11	Yes
	9.30 ± 0.18	200.9 ± 1.2	3.72 ± 0.01	384 ± 12	Yes
Single radius concave	1.33 ± 0.02	201.3 ± 0.9	5.11 ± 0.02	72 ± 2	No
	3.56 ± 0.05	200.6 ± 1.6	4.10 ± 0.02	188 ± 7	No
	5.05 ± 0.07	200.9 ± 1.4	3.87 ± 0.01	253 ± 6	No
	7.06 ± 0.16	200.9 ± 1.7	3.68 ± 0.01	312 ± 10	No
	8.58 ± 0.19	200.4 ± 1.0	3.57 ± 0.01	359 ± 10	No
	10.64 ± 0.21	200.9 ± 1.6	3.54 ± 0.01	397 ± 10	Yes

Mean ± standard deviation (n=10)

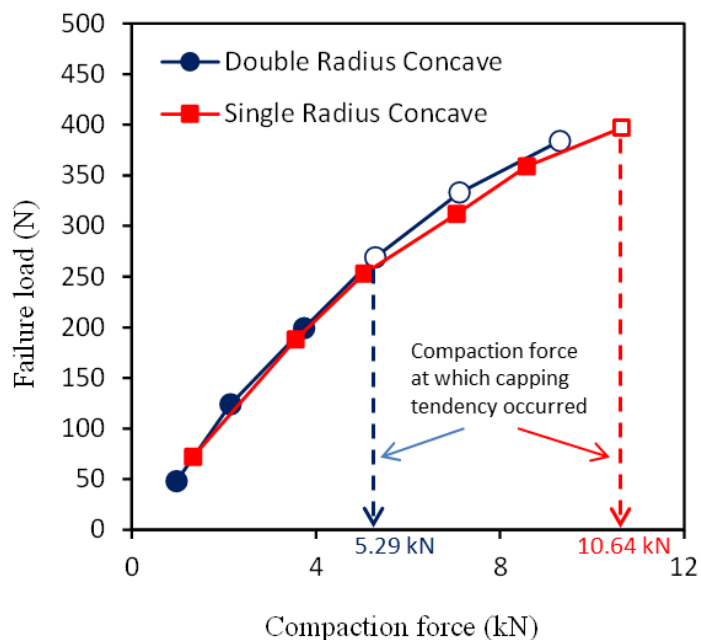
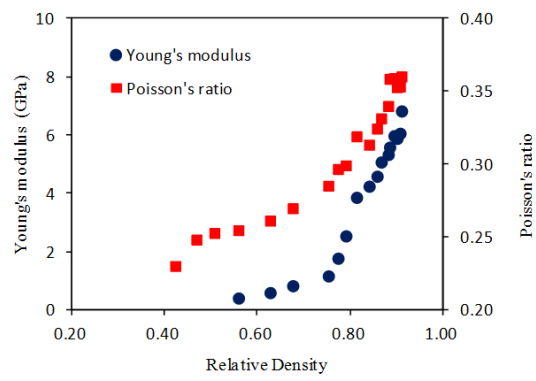


Figure 6-6 The effect of the tablet concavity on the failure load and capping tendency.

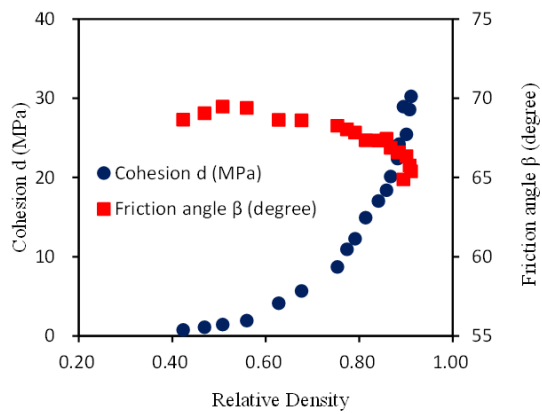
Open symbols represent the capping tendency.

6.3.2. Calibration of the material parameters of the DPC model

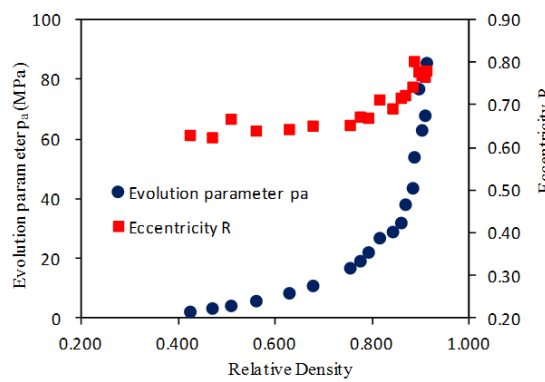
The two elastic parameters (Young's modulus and Poisson's ratio) and the four DPC parameters (d , β , R and p_a) measured by experiments as functions of relative density are summarized in Figure 6-7. The Young's modulus and Poisson's ratio both increase with the relative density (Figure 6-7(a)); these results are comparable with those obtained by Cunningham et al. (2004). Furthermore, the relative-density dependent Young's modulus values measured via our powder compaction test are consistent with those obtained using a four-point beam bending technique (Bassam et al., 1990). Figure 6-7(b) illustrates the cohesion d and friction angle β determined from the uniaxial and diametrical compression tests. The cohesion d increases exponentially, while the friction angle β gradually decreases as the powder densifies. The evolution parameter p_a and the eccentricity R determined from the instrumented die compression tests are shown Figure 6-7(c). All of these measured DPC parameters are in good agreement with those published in the literature (Cunningham et al. 2004; Han et al., 2008). With all these parameters, the DPC model can be defined.



(a)



(b)



(c)

Figure 6-7 Elastic parameters and DPC parameters as a function of the relative density.

(a) Young's modulus and Poisson's ratio. (b) Cohesion d and friction angle β . (c)

Evolution parameter p_a and eccentricity R .

6.3.3. FEM results of the tablet thickness and the density distribution

To validate the FEM simulation used in this study, the tablet thickness values estimated via the FEM under different powder compaction forces were compared with the experimental values. As MCC is well-known to undergo elastic recovery following compression, the obtained tablet thickness after ejection is notably different from the compaction thickness. In practical application, the thickness of tablet is important not only in ensuring that each tablet is identical in appearance but also for subsequent processing, such as coating, printing and packing. For example, tablet thickness sometimes causes trouble when the tablets are fed in the pockets of blister packages. The elastic recovery in the thickness was reported to possibly influence the results of near-infrared spectroscopy (NIR) (Macias et al., 2011). Therefore, accurate prediction of the thickness of a tablet as the shape of the tablet changes is important. The thickness of the tablets after ejection obtained via the FEM with the material parameters determined by *section 6.3.1*, and the experiments are plotted as a function of the compaction force in Figure 6-8. The thickness of both single-radius and double-radius tablets after elastic recovery were found to be accurately estimated using FEM; this result can be of use in a robust manufacturing process.

Figure 6-9 shows the relative density distribution change of the two different shape tablets with final average value of 0.874 during the tableting process. The powder is first densified by the upper punch at the top corner. At the small compact distance, because of the large cap depth, double-radius concave punch compacts the powder in more local area than single-radius concave punch. With the processing of the compaction distance, the densified region of powder enlarges due to increasing contact

area with the punch. At the end of compaction, the highest density region stays at the top corner of single-radius tablet, while for the double-radius tablet, the most densified region is pushed into the cap part. Removing the upper punch, the elastic recovery of MCC powder shifts the density distribution profile of both two shape tablets to a small value. During the ejection from the die, the friction of the die wall makes the density distribution profile of single-radius tablet shift to large value. Different from the single-radius tablet, the friction uniformed the density distribution within the double-radius tablet slightly. Comparing the density distributions of these two shaped tablet observes that the single-radius tablet have a more uniform density distribution than the double-radius tablet. Moreover, the lowest density region of the single-radius tablet is in the centre of the tablet, while the lowest density of double-radius tablet appears in the periphery region. As mentioned above, because the mechanical properties of the tablet are density dependent, the differences in density distribution imply the different distribution of the mechanical properties in these two differently shaped types of tablets, which may have effects on the fracture process during diametrical compression. Akseli et al. (2013, 2014) measured a ratio of Young's modulus in axial and radial directions of tablets using ultrasonic technique and they found that as the ratio deviated from unity, tablets expected to be more heterogeneous and this approach revealed that heterogeneities in the tablet lead to capping. In our research, double-radius tablet has more heterogeneous density than single-radius tablet as described in Figure 6-9 and this indicates that heterogeneity may lead to capping during diametrical compression.

Prior studies measuring the MCC tablet density distribution in a single-radius tablet were conducted using X-ray computed tomography (Sinka et al., 2004; Klinzing

et al., 2010) and NMR imaging (Djemai and Sinka, 2006); both density measurements clearly presented high density regions located at the upper edge of the tablet and low density regions located in the middle of the tablet, which agree well with the results in Figure 6-10 (b). Kadiri et al. (2013) predicted the density distribution within the single-radius MCC tablets using FEM and also obtained similar results to this report. The comparison of the density distribution obtained to those published in previous papers also provides support for the validity of our simulation methods.

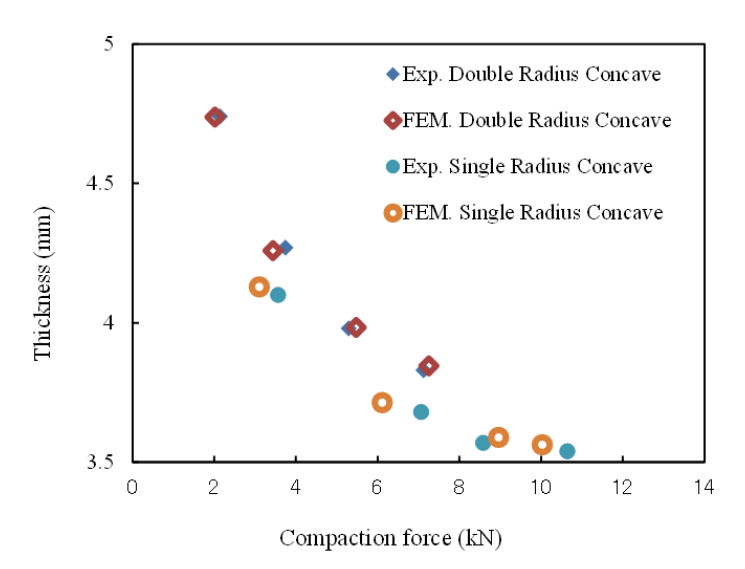


Figure 6-8 Comparison of the FEM predictions and the experimental results: tablet thickness vs. compaction force.

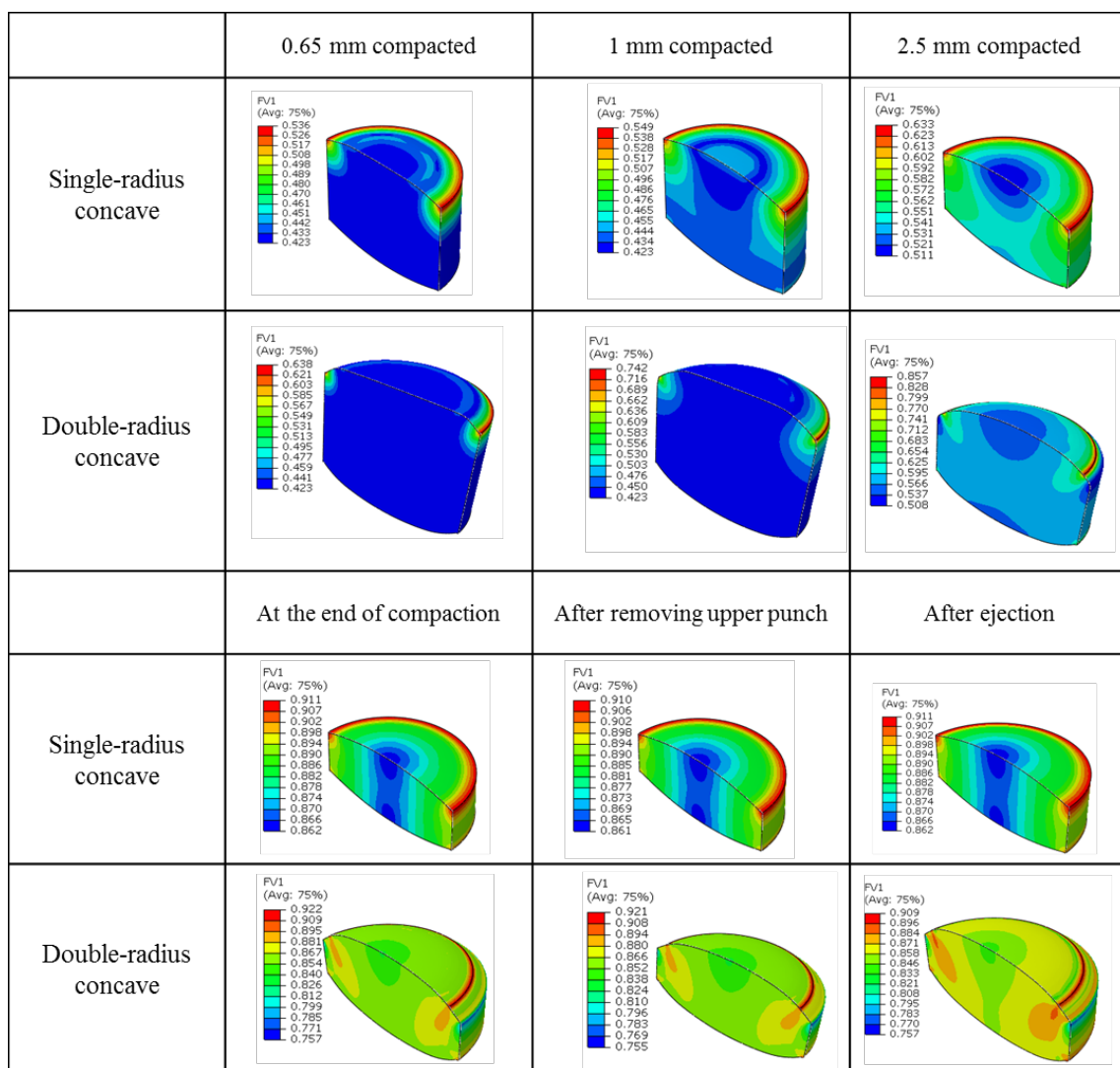


Figure 6-9 Variation of the density distribution during the compaction for double-radius and single-radius tablets.

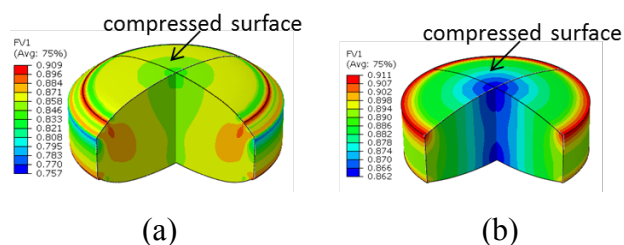


Figure 6-10 Density distribution within the two types of tablets: (a) double-radius concave (b) single-radius concave.

6.3.4. Estimation of the capping tendency during the diametrical compression test via the actively yielding (AC YIELD) output of ABAQUS

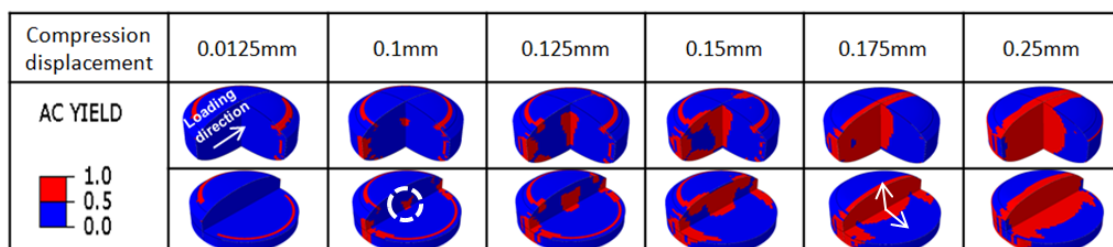
In the field of engineering, stress-based and strain-based criteria are usually used to as the failure criteria. Several studies have been attempted to predict the capping tendency during powder compaction by focusing on the von Mises stress; such FEM studies have suggested that the stress concentration appeared inside of the tablet caused crack and capping (Wu et al., 2005, 2008; Han et al., 2008; Kadiri and Michrafy, 2013). Regarding the failure criteria of tablets, Procopio et al. (2003) performed the diametrical compression test of flat shaped MCC tablets to investigate the effect of plasticity of materials. These researchers' FEM and experimental results demonstrated that MCC tablets deform plastically at the contact region with the compression test plate and that this deformation (i.e., plasticity) affected the position of the maximum stress generated, resulting in initiation of the crack. Shang et al. (2013b) and Podczeczek et al. (2013) simulated the diametrical compression test of a homogeneous density tablet and used the assumed critical value in stress-based criteria to estimate the tensile strength. Since the relative density depended Young's modulus and Poisson ratio, a heterogeneous density distribution inside the tablet produced by the friction between powder and die-wall during the powder compaction (Figure 6-10 (a)) has an important role in capping tendency. Also under the diametrical compression, the density distribution changes dramatically, which affects the mechanical properties states inside the tablets and capping tendency (Nystrom et al., 1978; Mullarney and Hancock, 2006). So the localized stress/strain must be quite different from the nominal applied stress/strain. It is very hard to determine the critical failure values usually used in the stress-based or strain-based failure criteria. Therefore, the estimation of capping tendency by using the

simple stress-based or strain-based failure criteria is apparently not so convenient for the heterogeneous tablet.

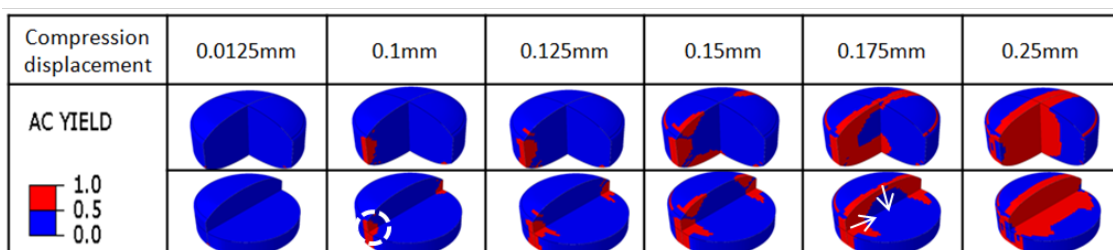
In this study, the variation in plastic strain of a heterogeneous tablet during the diametrical compression test was focused to investigate the fracture pattern. The tablet has a plastic strain distribution produced by prior powder compaction before being diametrical compressed. To remove the effect of the initial plastic strain and investigate the variation in plastic strain inside tablets, the output variable AC YIELD of ABAQUS was chosen, which is a scalar quantity denoting whether the plastic strain of the materials has changed or not. A value of 0 indicates that the plastic strain did not change and that the material did not yield, while a value of 1 indicates that the plastic strain did change and the material did yield (ABAQUS User's Manual).

Figure 6-11 illustrates the variable AC YIELD distribution within the tablet produced by different compaction force during diametrical compression tests. Figures 6-11(a) and (c) show the change of the AC YIELD distribution under the continuous diametrical compression of the double-radius tablet and the single-radius tablet with the capping tendency examined in experiments, respectively. Both figures indicate the variation in plastic strain, that is AC YIELD equal to 1, began from the centre of the tablets and then extended to the periphery region. In contrast, in the case of tablets without the capping tendency (Figures 6-11(b) and (d)), the variation in plastic strain started from the periphery of the tablets and propagated to the central region. These results indicate that if the variation in plastic strain starts from the central region during the diametrical compression, then capping will occur; on the contrary, if the material yielding starts from the periphery region, then the tablet will split into halves along the loading direction without capping. A crack initiating inside the tablet and its

propagation direction are important to understand the mechanism of the capping tendency, and a variation in plastic strain plays a significant role in the fracture behaviour. Plotting the contour of AC YIELD, which shows the place where yield begins, together with the experiment results in Figure 6-12. The use of the criterion of the AC YIELD starting location to predict the capping tendency is confirmed the experimentally observed phenomena. In addition, Figure 6-13 illustrates the isometric photo of the capped tablet under the diametrical compression test, it is interesting to find that the simulated contour of AC YIELD under the certain continuous diametrical compression shows that the fragment on tablet edge produced a similar shape to that of observed in experiments and the yielding region occurred inside the tablet has a tendency to propagate horizontally.

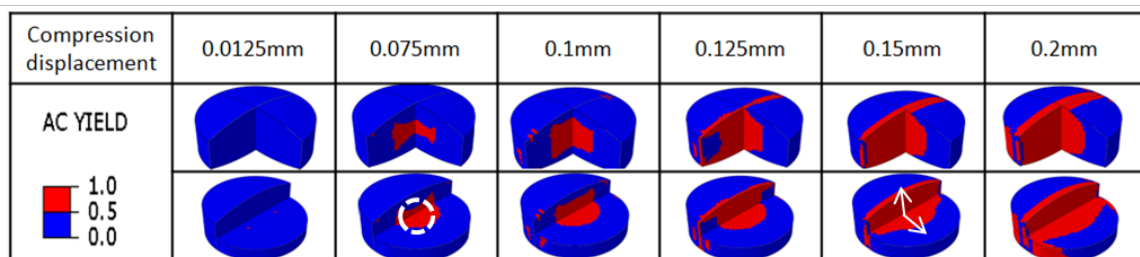


(a) Double radius concave, compaction force 7.2 kN

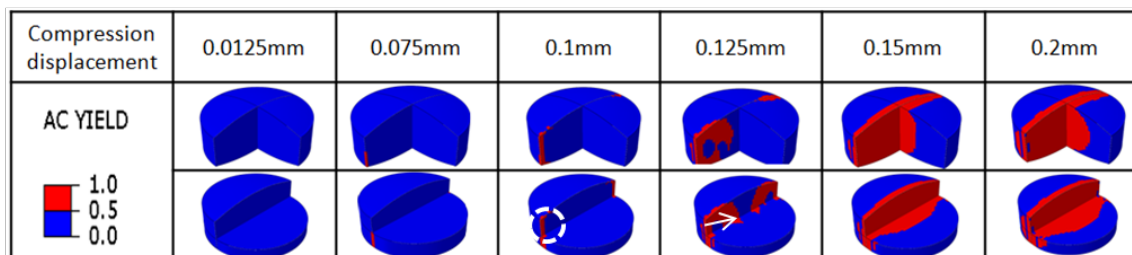


(b) Double radius concave, compaction force 3.4 kN

Figure 6-11 Contour plot of the variable AC YIELD during the diametrical compression test (red regions indicate that the MCC has already yielded, and blue regions indicate that the MCC has not yielded). (a) A double-radius concave tablet with a capping tendency (thickness 3.85 mm, compaction force 7.2 kN). (b) A double-radius concave tablet without a capping tendency (thickness 4.26 mm, compaction force 3.4 kN).



(c) Single radius concave, compaction force 10.0 kN



(d) Single radius concave, compaction force 6.1 kN

Figure 6-11 (Continued)

(c) A single-radius concave tablet with a capping tendency (thickness 3.56 mm, compaction force 10.0 kN). (d) A single-radius concave tablet without a capping tendency (thickness 3.71 mm, compaction force 6.1 kN)

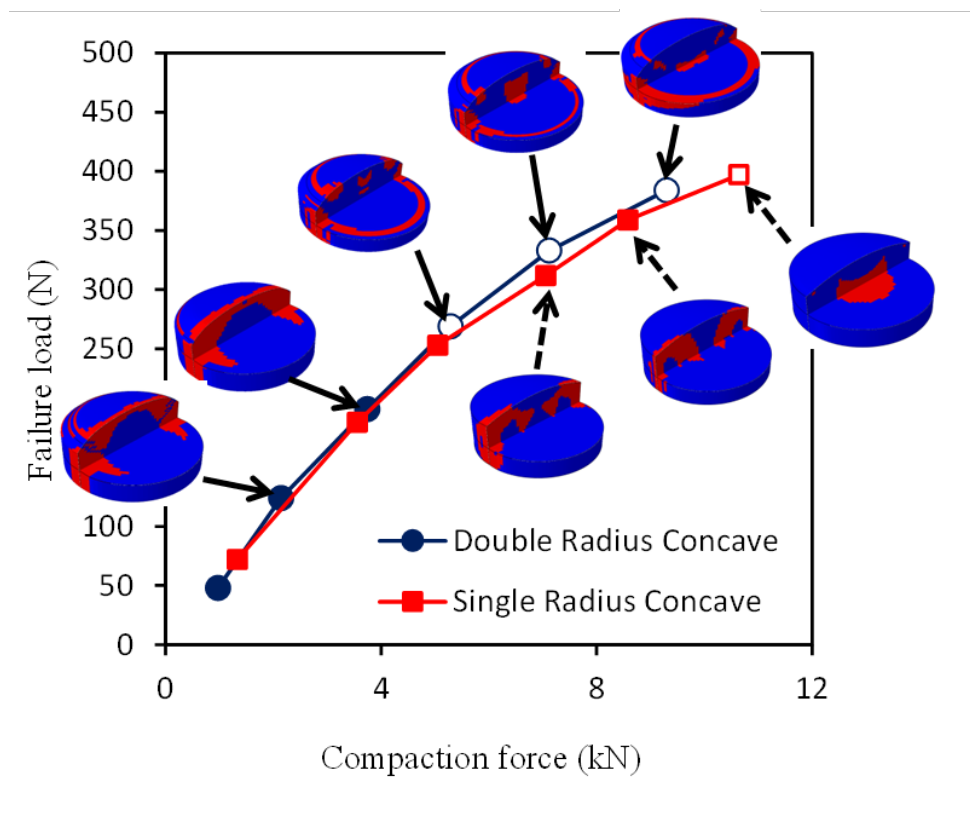


Figure 6-12 The AC YIELD start location of tablets obtained via different compaction forces during the diametrical compression test. Open symbols represent the capping tendency.

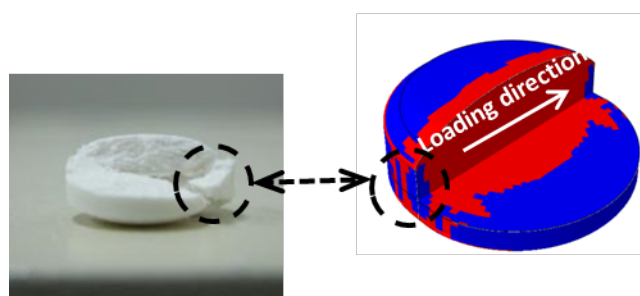


Figure 6-13 Comparison of the numerical result to the capping image of a tablet obtained by experiment after the diametrical compression test.

To investigate the exact fracture behaviour of a tablet with capping tendency during the diametrical compression test, a high-speed camera was used at the speed of 1,000 fps. Figure 6-14(a) shows the high-speed camera observations of a double-radius tablet with capping tendency. After the tablet split into halves along the loading direction and the crack propagated, the laminated crack (i.e., capping tendency) was detected on the side face. From the high-speed camera observations, these results imply that defects due to a variation in the plastic strain inside the tablet can promote crack propagation to the side of the tablet after normal diametrical crack, as described in Figure 6-14(b). Under continuous diametrical compression, if the material failure (or yielding) first occurs in the centre of the tablet, then the failure area will tend to propagate both along the loading direction and perpendicular to the loading direction, as shown in Figure 6-11. Along the loading direction, the powder is compressed and densified, which increased the amount of material with the larger yielding face (Figure 6-4). In contrast, in the direction perpendicular to the loading direction, the powder undergoes the tensile stress due to the volume expansion, which weakens the material by decreasing the powder density. Therefore, the failure area propagates more easily in the direction perpendicular to the loading direction, which leads to delamination of the tablet. On the other hand, if the failure originates from the periphery region, it propagates along the path of the minimum solid cross-sectional area (Roberts and Rowe, 1989), which is the symmetrical plane perpendicular to the diameter and along the loading direction. Such a fracture process results in the normal splitting of a tablet. Although the tablets were produced by the same powder weight and the same shape punch but different compaction force, the yielding inside the tablet began in difference

region, i.e. yielding began in the centre of the tablet made under high compaction force and in periphery region under low compaction force, during the diametrical compression simulation which leads to different fracture patterns still requires further investigation. In our future work, more detailed discussion about the relationship between failure mechanism and Drucker Prager yield surface is need. Nevertheless, by comparing the AC YIELD distribution to our experimental observation, it was found that our numerical results reasonably described the experimentally observed phenomena.

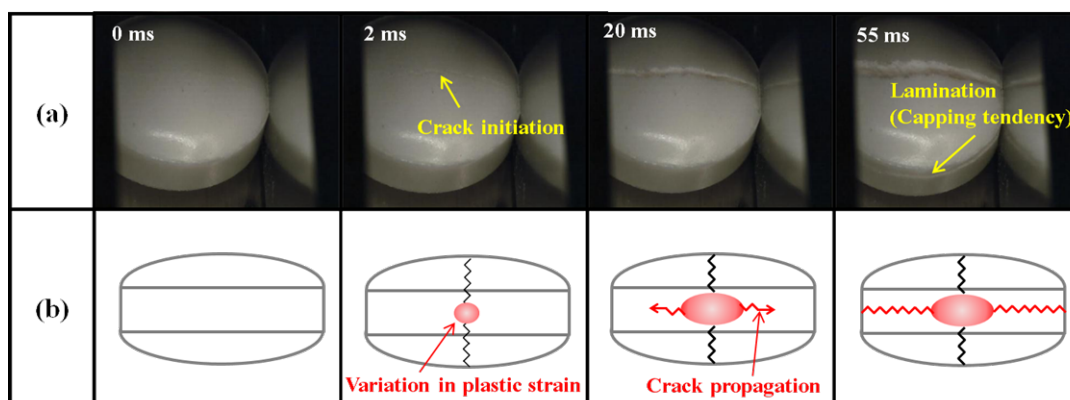


Figure 6-14 Fracturing process of a MCC tablet during diametrical compression: (a) High-speed camera observation during the hardness test and (b) schematic representation of the fracturing process inside a tablet.

6.4 Conclusion

This study evaluated the capping tendency of MCC tablets of both single-radius and double-radius via the diametrical compression test. The relationship between the failure load of the tablet and compaction force were investigated. The failure load values of both shapes of tablets were found to exhibit the same trend, but the capping tendency of the double-radius tablet occurred at a lower compaction force compared to that of the single-radius tablet. A 3D finite element analysis using the density-dependent Drucker-Prager Cap model was performed to simulate powder compaction and diametrical compression. To avoid introducing a complex failure criterion into the constitutive model, I focused on the variation in plastic strain of tablet during the diametric compress and visualised the variation in plastic strain using the AC YIELD output of ABAQUS. It was found that subsequently capping occurred if the variation in plastic strain started from the central region during the diametrical compression; in contrast, if material yielding initiated from the periphery region, then capping did not occur. These results indicate that the variation in plastic strain inside a tablet is an origin of cracking and it is a cause of the capping tendency (i.e., lamination) during the diametrical compression test. These results provide me a simple method to estimate the capping tendency. This estimation method is useful for optimising the tablet shape and the operational conditions in the tableting process.

References

ABAQUS, User's Manual, version 6.11

Akseli, I., Ladyzhynsky, N., Katz, J., He, X., 2013. Development of predictive tools to assess capping tendency of tablet formulations. *Powder Technol.* 236, 139-148.

Akseli, I., Stecula, A., He, X., Ladyzhynsky, N., 2014. Quantitative correlation of the effect of process conditions on the capping tendencies of tablet formulations. *J. Pharm. Sci.* 103, 1652-1663.

Bassam, F., York, P., Rowe, R. C., Roberts, R. J., 1990. Young's modulus of powders used as pharmaceutical excipients. *Int. J. Pharm.* 64, 55-60.

Bozic, D. Z., Dreu, R., Vrečer, F., 2008. Influence of dry granulation on compactibility and capping tendency of macrolide antibiotic formulation. *Int. J. Pharm.* 357, 44-54.

Cunningham, J. C., Sinka, I. C., Zavaliangos, A., 2004. Analysis of tablet compaction. I. Characterization of mechanical behavior of powder and powder/tooling friction. *J. Pharm. Sci.* 93, 2022-2039.

Diarra, H., Mazel, V., Busignies, V., Tchoreloff, P., 2013. FEM simulation of the die compaction of pharmaceutical products: Influence of visco-elastic phenomena and comparison with experiments. *Int. J. Pharm.* 453, 389-394.

Djemai, A., Sinka, I.C., 2006. NMR imaging of density distributions in tablets. *Int. J. Pharm.* 319, 55-62.

Doremus, P., 2007. Chapter 10: Calibration of compaction models. In: P.R.Brewin, O.Coube, P.Doremus, J.H.Tweed (Eds.), *Modelling of Powder Die Compaction*. Springer, pp.151-163.

Drucker, D.C., Prager, W., 1952. Soil mechanics and plastic analysis of limit design. *Quart. Appl. math.* 10, 157-165.

Dwivedi, S.K., Oates, R.J., Mitchell, A.G., 1992. Estimation of elastic recovery, work of decompression and Young's modulus using a rotary tablet press. *J. Pharm. Pharmacol.* 44, 459-466.

Han, L.H., Elliott, J.A., Bentham, A.C., Mills, A., Amidon, G.E., Hancock, B.C., 2008. A modified Drucker-Prager Cap model for die compaction simulation of pharmaceutical powders. *Int. J. Solids Struct.* 45, 3088-3106.

Hayashi, Y., Miura, T., Shimada, T., Onuki, Y., Obata, Y., Takayama, K., 2013. Prediction of tablet characteristics from residual stress distribution estimated by the finite element method. *J. Pharm. Sci.* 102, 3678-3686.

ICH Guideline: Pharmaceutical Development Q8(R2), http://www.ich.org/fileadmin/Public_Web_Site/ICH_Products/Guidelines/Quality

/Q8_R1/Step4/Q8_R2_Guideline.pdf

- Janssen, H.A., Versuche über Getreidedruck in Silozellen. 1895. Zeitschr. d. Vereines deutscher Ingenieure, 39, 1045-1049.
- Kadiri, M. S., Michrafy, A., 2013. The effect of punch's shape on die compaction of pharmaceutical powders. Powder Technol. 239, 467-477.
- Klinzing, G. R., Zavaliangos, A., Cunningham, J., Mascaro, T., Winstead, D., 2010. Temperature and density evolution during compaction of a capsule shaped tablet. Comput. Chem. Eng. 34, 1082-1091.
- Koynov, A., Akseli, I., Cuitino, A. M., 2011. Modeling and simulation of compact strength due to particle bonding using a hybrid discrete-continuum approach. Int. J. Pharm. 418, 273-285.
- Kruggel-Emden, K., Simsek, E., Rickelt, S., Wirtz, S., Scherer, V., 2007. Review and extension of normal force models for the Discrete Element Method. Powder Technol. 171, 157-173.
- Kumar, V., Kothari, S. H., 1999. Effect of compressional force on the crystallinity of directly compressible cellulose excipients. Int. J. Pharm. 177, 173-182.
- Kuppuswamy, R., Anderson, S. R., Augsburger, L. L., Hoag, S. W., 2001. Estimation of capping incidence by indentation fracture tests. AAPS PharmSci. 3, 1-12.
- Lennartz, P., Mielck, J. B., 1998. Minitableting: improving the compactability of paracetamol powder mixture. Int. J. Pharm. 171, 75-85.
- Macias, K., Jayawickrama, D., McGeorge, G., 2011. The impact of elastic recovery on Near-Infrared tablet prediction. Am. Pharm. Rev. 14, <http://www.americanpharmaceuticalreview.com/Featured-Articles/37317-The-Impact-of-Elastic-Recovery-on-Near-Infrared-Tablet-Predictions/>
- Michrafy, A., Ringenbacher, D., Tchoreloff, P., 2002. Modelling the compaction behavior of powders: application to pharmaceutical powders. Powder Technol. 127, 257-266.
- Mullarney, M.P., Hancock, B.C., 2006. Mechanical property anisotropy of pharmaceutical excipient compacts. Int. J. Pharm. 314, 9-14.
- Nakamura, H., Sugino, Y., Iwasaki, T., Watano, S., 2011. Development of a Novel Tablet Machine for a Tiny Amount of Powder and Evaluation of Capping Tendency. Chem. Pharm. Bull. 59, 1518-1522.
- Nakamura, H., Sugino, Y., Watano, S., 2012. In-Die Evaluation of Capping Tendency of Pharmaceutical Tablets Using Force-Displacement Curve and Stress Relaxation Parameter. Chem. Pharm. Bull. 60, 772-777.
- Nystrom, C., Malmqvist, K., Mazur, J., Alex, W., Holzer A.W., 1978. Measurement of

- axial and radial tensile strength of tablets and their relation to capping. *Acta Pharm. Suec.* 15, 226-232.
- Podczec, F., Drake, K.R., Newton, J.M., 2013. Investigations into the tensile failure of doubly-convex tablets under diametral loading using finite element methodology. *Int. J. Pharm.* 454, 412-424.
- Procopio, A. T., Zavaliangos, A., Cunningham, J. C., 2003. Analysis of the diametrical compression test and the applicability to plastically deforming materials. *J. Mater. Sci.* 38, 3629-3639.
- Roberts, R. J., Rowe, R. C., 1989. Determination of the critical stress intensity factor (KIC) of microcrystalline cellulose using radially edge-cracked tablets. *Int. J. Pharm.* 52, 213-219.
- Shang, C., Sinka, I. C., Jayaraman, B., Pan, J., 2013a. Break force and tensile strength relationships for curved faced tablets subject to diametrical compression. *Int. J. Pharm.* 442, 57-64.
- Shang, C., Sinka, I. C., Pan, J., 2013b. Modelling of the break force of tablets under diametrical compression. *Int. J. Pharm.* 445, 99-107.
- Siiria, S. M., Antikainen, O., Heinamaki, J., Yliruusi, J., 2011. 3D simulation of Internal Tablet Strength During Tableting. *AAPS PharmSciTech.* 12, 593-603.
- Sinha, T., Curtis, J. S., Hancock, B. C., Wassgren, C., 2010a. A study on the sensitivity of Drucker-Prager Cap model parameters during the decompression phase of powder compaction simulations. *Powder Technol.* 198, 315-324.
- Sinha, T., Bharadwaj, R., Curtis, J. S., Hancock, B. C., Wassgren, C., 2010b. Finite element analysis of pharmaceutical tablet compaction using a density dependent material plasticity model. *Powder Technol.* 202, 46-54.
- Sinka, I. C., Cunningham, J. C., Zavaliangos, A., 2003. The effect of wall friction in the compaction of pharmaceutical tablets with curved faces: a validation study of the Drucker-Prager Cap model. *Powder Technol.* 133, 33-43.
- Sinka, I. C., Burch, S. F., Tweed, J. H., Cunningham, J. C., 2004. Measurement of density variations in tablets using X-ray computed tomography. *Int. J. Pharm.* 271, 215-224.
- Sinka, I.C., Cocks, A.C.F., 2007. Chapter 14: Modeling die compaction in the pharmaceutical industry. In: P.R.Brewin, O.Coube, P.Doremus, J.H.Tweed (Eds.), *Modelling of Powder Die Compaction*. Springer, pp.223-242.
- Sugimori, K., Mori, S., Kawashima, Y., 1989a. Characterisation of die wall pressure to predict capping of flat- or convex-faced drug tablets of various sizes. *Powder Technol.* 58, 259–264.

- Sugimori, K., Mori, S., Kawashima, Y., 1989b. The role of binders in the prevention of capping within a tablet. *Chem. Pharm. Bull.* 37, 1064-1067.
- Tanino, T., Aoki, Y., Furuya, Y., Sato, K., Takeda, T., Mizuta, T., 1995. Occurrence of capping due to insufficient air escape during tablet compression and a method to prevent it. *Chem. Pharm. Bull.* 43, 1772–1779.
- Thornton, C., Ning, Z., 1998. A theoretical model for the stick/bounce behavior of adhesive, elastic-plastic, spheres. *Powder Technol.* 99, 154-162.
- Walker, D.M., An approximate theory for pressures and arching in hoppers. 1966. *Chem. Eng. Sci.* 21, 975-997.
- Wu, C. Y., Ruddy, O. M., Bentham, A. C., Hancock, B. C., Best, S. M., Elliott, J. A., 2005. Modelling the mechanical behavior of pharmaceutical powders during compaction. *Powder Technol.* 152, 107-117.
- Wu, C. Y., Hancock, B. C., Mills, A., Bentham, A. C., Best, S. M., Elliott, J. A., 2008. Numerical and experimental investigation of capping mechanisms during pharmaceutical tablet compaction. *Powder Technol.* 181, 121-129.

Chapter 7 Concluding remarks

There is no doubt that tableting process is key process to decide fundamental tablet qualities, therefore, it is quite important to control and understand the tableting process by the numerical simulations. Therefore, a numerical study of pharmaceutical tableting has been presented in this thesis to further understanding of fundamental phenomena in terms of the material properties, filling and compaction behaviours.

Investigation of the formation mechanism of spindle CaCO_3 are presented in Chapter 2 and 3 for the sake of understanding the fundamental material properties, which seems to affect tablet qualities. MD simulations were carried out to analyse the differences of surface properties among four types of CaCO_3 surfaces; (001)Ca, (001) CO_3 , (100) and (104). Both (001)Ca and (001) CO_3 represent Ca^{2+} terminated and CO_3^{2-} terminated surface, respectively. Four different separation distances, 3.3, 2.3, 1.5 and 0.7 nm were used to calculate the behaviour of water molecules, charge density, diffusion and grain boundary energy. Water molecules were adsorbed and layer water structure formed near CaCO_3 interfaces on the all types of CaCO_3 surface, by contrast, water molecules were strongly oriented on the (001)Ca and (001) CO_3 surfaces due to the force by polar surface made from ionic configuration. The calculation of charge density found that (001)Ca and (001) CO_3 surfaces charged positively and negatively, respectively. On the other hand, both (100) and (104) surfaces charged almost neutral because of being consisted of both Ca^{2+} and CO_3^{2-} . These confined water molecule behaviours lead to difference of dielectric constant among four types of surfaces. In addition, the grain boundary energy of interface between (001)Ca and (001) CO_3 was the lowest among five types of interface. It indicates that the aggregation of (001)Ca and (001) CO_3 surface is the easiest among all types of interfaces. Furthermore, the cluster moving MC simulations were carried out to investigate the aggregation process of

primary particles of CaCO_3 . From the results of the Cluster-moving MC simulations by introducing cubic model with the charge densities calculated from MD simulations, the aggregation of primary particles resulted in formation of spindle shaped CaCO_3 clusters. Length and width were calculated to investigate the shape of clusters formed by a aggregation of primary particles. Aspect ratio of spindle-shape CaCO_3 calculated by MC simulation agreed well with the aspect ratio obtained by experiment. Considering from the distance between charges on the particle about all of CaCO_3 clusters, most of primary particles agglomerated in the same direction since positive and negative charges attracted to each other. It concluded that CaCO_3 particles formed non-spherical CaCO_3 particles like spindle-shape for being aggregated in the same direction. As summarised above, MD and MC simulations could become potential tools for a prediction of material properties in future.

In Chapter 4, the closed-die compaction behaviour of D-mannitol granules were simulated by the DEM to investigate the granule rearrangement and fracture behaviour during compaction which affects the compactibility of the tablet. The D-mannitol granules produced in a fluidized bed are modelled as agglomerates of primary particles connected by linear spring bonds. The validity of the model granule used in the DEM simulation was demonstrated by comparing the experimental results of a uniaxial compression test. During uniaxial compression, the numerical results of the force-displacement curve corresponded reasonably well to the experimental data. The closed-die compaction of the modelled granules was carried out to investigate the rearrangement and fracture behaviours of the granule at different upper platen velocities. The forces during closed-die compaction calculated by DEM fluctuated in the low-pressure region due to the rearrangement of granules. A Heckel analysis showed

that the force fluctuation occurred at the initial bending region of the Heckel plot, which represents the granule rearrangement and fracture. Furthermore, the upper platen velocity affected the trend of compaction forces, which can lead to compaction failure due to capping. These results could contribute to designing the appropriate granules during closed die compaction.

DEM simulations for investigating the segregation behaviour of binary particles during die filling consisted of a horizontally moving die equipped with a vertically moving bottom punch are given in Chapter 5. In order to achieve accurate particle flow simulations, parameters of the pharmaceutical spherical granules were calibrated using experimental bounced height, rolling distance and angle of repose. These parameters were implemented in the die filling DEM simulations and compared with experimental results of high-speed camera observations and the filling ratio. Simulations and experimental results showed reasonable qualitative and quantitative agreement, validating the simulation model. The validated model was employed to evaluate the segregation of binary particle mixtures. The RSM analysis revealed that, unlike the die velocity, small particle size, horizontal position and vertical position affected the segregation index significantly. The segregation resulted from percolation of small particles between large particles in the feed shoe and bottom back corner of the die. DEM combined with RSM approach will become significantly efficient method to understand the process for implementing the quality by design approach.

In Chapter 6, the numerical evaluation of capping tendency can be performed by FEM with application of AC Yield analysis. Capping tendency was evaluated using a tablet strength tester, that is, the fracture pattern of the tablet during diametrical compression testing was checked. The density-dependent DPC model was employed for

a microcrystalline cellulose and DPC parameters were obtained from experiments using the single tableting machine. The AC Yield observation was used as an indication to judge whether the capping tendency will occur or not. The FEM study revealed that the initial position of variation in plastic strain affect the capping tendency. This chapter provided an effective method for evaluating the capping tendency during diametrical compression test using the FEM.

Further investigation should be performed to develop robust tableting process. For instance, the effects of particle shape, size distribution, cohesive force between particles and presence of excipients on die filling process have not yet been addressed. In case of the compaction process, plastic deformation behaviour of granules and primary particles should be implemented by combining DEM-FEM or plastic contact model in the current numerical model in high-pressure region.

Numerical simulations are attractive for pharmaceutical companies because of its potential contribution to the construction of efficient, robust and optimised manufacturing process. In addition, these models also can contribute to quality risk assessment and establishment of control strategies to endure the tablet quality. In the near future, the knowledge obtained from numerical simulations will be essential to design the overall pharmaceutical process including tableting process following the QbD approach.

List of publications

Chapter 2:

Kazunori Kadota, Ryoichi Furukawa, Yoshiyuki Shirakawa, Atsuko Shimosaka, Jusuke Hidaka, 2014. Effect of surface properties of calcium carbonate on aggregation process investigated by molecular dynamics simulation. *Journal of Materials Science*. 49, 1724-1733.

Chapter 3:

Kazunori Kadota, Ryoichi Furukawa, Yuichi Tozuka, Atsuko Shimosaka, Yoshiyuki Shirakawa, Jusuke Hidaka, 2014. Formation mechanism of non-spherical calcium carbonate particles in the solution using cluster-moving Monte Carlo simulation. *Journal of Molecular Liquids*. 194, 115-120.

Chapter 4:

Ryoichi Furukawa, Kazunori Kadota, Tetsuro Noguchi, Atsuko Shimosaka, Yoshiyuki Shirakawa, DEM modelling of granule rearrangement and fracture behaviours during a closed-die compaction. *AAPS PharmSciTech*, accepted.

Chapter 5:

Ryoichi Furukawa, Yuki Shiosaka, Kazunori Kadota, Keisuke Takagaki, Tetsurou Noguchi, Atsuko Shimosaka, Yoshiyuki Shirakawa, 2016. Size-induced segregation during pharmaceutical particle die filling assessed by response surface methodology

List of publications

using discrete element method. *Journal of Drug Delivery Science and Technology*. 35, 284-293.

Chapter 6:

Ryoichi Furukawa, Yuan Chen, Akio Horiguchi, Keisuke Takagaki, Junichi Nishi, Akira Konishi, Yoshiyuki Shirakawa, Masaaki Sugimoto, Shinji Narisawa, 2015. Numerical evaluation of the capping tendency of microcrystalline cellulose tablets during a diametrical compression test. *International Journal of Pharmaceutics*. 493, 182-191.

Acknowledgements

First of all, I would like to thank my supervisor, Prof. Yoshiyuki Shirakawa, for his invaluable guidance and support. This thesis would not have been able to accomplish without his supervision. I would also like to thank my committee members, Prof. Yasushige Mori and Prof. Hideki Ichikawa, for their thoughtful feedback and comments. Prof. Jusuke Hidaka and Dr. Atsuko Shimosaka are acknowledged for their valuable comments and great supports.

I am thankful to Dr. Kazunori Kadota for providing me the support and helpful discussion. I would like to express my sincere gratitude to Dr. Hiroshi Mio, Mr. Takenobu Yamamoto, Dr. Shinya Yamanaka and Dr. Masatoshi Akashi for their experimental and programming supports. I also thank Mr. Akira Kitayama, Mr. Yuto Deki and Mr. Yuki Shiosaka for grateful supports of my research.

I sincerely thank to my colleagues, Dr. Shinji Narisawa, Mr. Tetsuro Noguchi, Dr. Masaaki Sugimoto, Mr. Akira Konishi, Mr. Junichi Nishi and Mr. Keisuke Takagaki for their constructive comments for my research. I want to thank Mr. Akio Horiguchi and Dr. Chen Yuan (MCHC R&D Synergy Center, Inc.) for the scientific discussions and their supports with the use of finite element method.

Finally, I am extremely thankful to my parents, wife, and daughter for their unconditional supports towards my studies throughout the years. Thank you.